Detection of Cardiac Troponin I in circulation using Raman Spectroscopy; An Approach to Prediction of Myocardial Infarction

by

Amir Pasha Tashakor

B.Sc. (Hons.), Simon Fraser University, 2010

Thesis Submitted in Partial Fulfillment
of the Requirements for the Degree of

Master of Applied Sciences

in the
School of Engineering Science
Faculty of Applied Sciences

SIMON FRASER UNIVERSITY

Spring 2012

Approval

Name: **Pasha Tashakor**

Degree: **Master of Applied Science**

Title of Thesis: ***Detection of Cardiac Troponin I in Circulation Using Raman Spectroscopy; An Approach to Prediction of Myocardial Infarction***

Examining Committee:

Chair: Dr. Parvaneh Saeedi, P.Eng., Assistant Professor

Dr. Andrew Rawicz, P. Eng.
Senior Supervisor
Professor, School of Engineering Science

Dr. Glen Tibbits
Supervisor
Professor and chair, Department of Biomedical Physiology and Kinesiology

---

Mr. Bruno Jaggi, P. Eng.
External Examiner
Adjunct Professor, Department of Biomedical Engineering, University of British Columbia

Date Defended/Approved: April 2, 2012

Partial Copyright Licence

Abstract

Myocardial infarction (MI) pertains to cardiac tissue death, secondary to prolonged inadequate perfusion to myocardial cells. Despite medical advances, MI remains a global leading cause of mortality and morbidity. Minute and subclinical physiological changes occur hours prior to a symptomatically appreciable 'attack'. These well-established phenomena involve the release of specific cardiac biomarkers into systemic circulation. Quantitative measurement of systemic cTnI concentrations is widely and routinely implemented in the diagnosis of MI. However, current technology is limited to detection of 'post-attack' concentrations, which often indicates irreversible damage. Consequently, we aimed to noninvasively detect concentrations of cTnI through biophotonic technology. For the first time in literature, we characterized and repeatedly verified unique Raman signature of mouse cTnI in water and BSA. Further, we investigated concentration changes, optimized integration durations, and proposed a conceptual design. This project potentially begets preclinical detection of biomarkers, earlier diagnosis, prompt medical intervention, and enhanced overall prognosis.

Keywords: Raman Spectroscopy; Cardiac Troponin; Myocardial Infarction; Biophotonics; cTnI

Acknowledgements

Foremost, I would like to express my sincere gratitude to my senior supervising Professor, Andrew Rawicz, whom for the past three years has supported and encouraged me in my research, my knowledge in engineering as well as other aspects of life. I would like to thank Professor Glen Tibbits and his research team. This project was simply impossible without his help and contribution. Further, I would like to thank Professor Bruno Jaggi who has greatly enriched my knowledge with his exceptional insights into engineering. I would also like to thank Professor Edward Grant as well as my senior colleague, Sara Moghaddamjoo, who made this possible with her unconditional support.

Lastly, I would like to thank my beloved parents for their support and patience. I am greatly indebted to my brother; this dissertation is simply impossible without him.

Table of Contents

List of Tables

List of Figures

List of Acronyms

ACS	Acute Coronary Syndrome
AMI	Acute Myocardial Infarction
APD	Avalanche photo diode
ATP	Adenosine triphosphate
BP	Bandpass Filter
BS	Beam Splitter
BSA	Bovine Serum Albumin
CCD	Charged Coupled Device
cSLO	Confocal Scanning Laser Ophthalmoscopy
cTnC	Cardiac Troponin C
cTnI	Cardiac Troponin I
cTnT	Cardiac Troponin T
CW	Continuous Wavelength
DG	Diffraction Grating
DM	Dichroic Mirror
ECG	Electrocardiogram
ELISA	Enzyme-Linked Immunosorbent Assay
F	Phenylalanine
FIR	Finite Impulse Response
Glu	Glutamine
HCl	Hydrochloric Acid
KOH	Potassium Hydroxide
LPDF	Long Pass Dichroic Filter
NaOH	Sodium Hydroxide
NSTEMI	Non-ST segment elevation myocardial infarction
PCB	Printed Circuit Board
PLS	Partial least-squares
PMT	Photo Multiplier Tube
SG	Savitzky–Golay (SG)
SLO	Scanning Laser Ophthalmoscopy

SNR	signal-to-noise Ratio
STEMI	ST segment elevation myocardial infarction
TMB	Tetramethyl benzidine
ULRR	Upper Limit of Reference Range
W	Tryptophan
Y	Tyrosine

Executive Summary

International health authorities consistently report Coronary Heart Disease (CHD) as a global leading cause of mortality and significant morbidity. These statistics have been recurrent over the past decade, despite interdisciplinary public health measures, aimed at prevention and early treatment of heart disease. Within the spectrum of CHD, Myocardial Infarction (MI), or heart attack, is one of the leading etiological causes of morbidity and mortality, with nearly 20% of patients dying within one month of a diagnosis. Heart attacks are typically regarded as the onset of an acute set of symptoms, with chest pain representing the most classic. However, minute and subclinical physiologic changes are known to occur, hours prior to externally appreciable symptoms. Extensive research report the release of specific cardiac biomarkers into the systemic circulation, secondary to prolonged inadequate perfusion of myocardial cells initiating the MI. A recognition of these physiological changes institutes current diagnostic guidelines. Consequently, a serum concentration of Cardiac Troponin I (cTnI), a protein cardiac biomarker, is widely and routinely quantified in emergency departments. Elevated cTnI concentrations, in addition to recognizable symptoms and an abnormal ECG reading, collectively suggest a diagnosis of MI. However, current medical technology limits detection of cTnI concentrations to 'post attack' levels, despite existence of low biomarker concentrations within the circulation several hours prior. Unfortunately, these comparatively high concentrations often indicate prolonged durations of malperfusion and irreversible cardiac tissue damage. An early diagnosis and

prompt medical intervention is the cornerstone of management in acute MI. Therefore, while the current implemented apparatus are of critical importance, they are suboptimal in that their limitations in concentration detection leads to a worse overall prognosis as compared to potentially more sensitive technology. In addition, currently implemented assays for cTnI measurement are not universally standardized, imposing considerable variation in the threshold at which a sample is considered deemed abnormal. This lack of standardization imposes particular disadvantages as measurement on assays from different manufacturers is not accurately comparable, inducing confusion between clinicians at different institutions. Studies report that biomarker concentrations vary by as much as 100 folds in assays manufactured by different companies.

Recognizing these limitations, and the substantial burden of disease MI places on the health care system, we aimed to quantitatively measure circulating cTnI concentrations through biophotonics. Therefore, limitations faced by the ELISA apparatus such as lack of standardization can be resolved. Furthermore, we aimed to conceptualize a device for continuous and non-invasive biomarker detection, ideal for high risk patients; accordingly, early medical intervention can be sought with arguably better overall prognosis.

Our first biophotonic approach was through florescence as since the Typtophan amino acid on the cTnI protein renders it a suitable candidate for detection by this technology. However, since florescence spectroscopy signalling is dominated by

Typtophan activity, the abundant presence of other blood proteins containing larger numbers of this aromatic amino acid overwhelms the overall signalling from cTnI. Furthermore, inherent structural alteration of the cTnI protein within the circulation makes it difficult for florescence signalling to accurately quantify its concentrations. Therefore, we adapted Raman Spectroscopy, which is capable of studying the quantum changes in the mouse cTnI protein.

The goal of this project was to design and calibrate a real-time miniaturized Raman spectroscope detection apparatus, capable of noninvasively detecting subclinical concentrations of cardiac biomarkers in the circulation. Successful implementation of this device theoretically leads to early knowledge of pathology by patients, earlier medical assessment and intervention, and hence minimal tissue damage and a better overall prognosis. In the long term, this small device will be attached to spectacle frames worn by patients as a modality for continuous monitoring for circulatory biomarkers. The human retina is an anatomically strategic site for our purposes as the unique visibility of dense vasculature provides a detection “window”, representative of the general circulatory status.

With the collaboration with the National Research Council at the University of British Columbia, Grant Group Laboratory at the Department of Chemistry at University of British Columbia, and Cardiac Physiology Group Laboratory at Simon Fraser University, to our knowledge, we are the first group that has successfully observed, defined, and documented the unique Raman signature of mouse cTnI protein. The

current project served as the next step in the progression of this concept. Herein, the cTnI Raman signature is reproduced and validated. Further, the experiment was conducted within a new environment, namely Bovine Serum Albumin (BSA) which is more physiologically similar to intact human blood as compared to the previous experiments utilizing the cTnI protein solution. The Raman signature of cTnI was also successfully and consistently characterized in BSA. Further, through this project, we enhanced our assay sensitivity by implementing new techniques and redefined our concentration limits. As discussed, the extremely low physiological concentration of cardiac biomarkers in the subclinical setting is the major challenge of this project. While we are still unable to accurately measure cTnI serum concentrations in intact human blood at physiological levels, we have significantly improved our sensitivity compared to previous findings. Lastly, the conceptual design of apparatus implementation within spectacle frames was improved.

In conclusion, our results thus far reinforce the potential feasibility of this project given future improvements in assay sensitivity as well as device optimization. While this project is in its early stages, detection of cTnI through Raman signal acquisition could be the future approach for early and non-invasive diagnosis of cardiac tissue damage with substantial life-saving potential.

1. Introduction and background information

1.1. Introduction

Despite recent medical advances in cardiovascular care, myocardial infarction remains a leading cause of death worldwide [1]. Myocardial infarction (MI) is a serious life threatening condition, caused by inadequate perfusion to the cardiac cells. The critical role of the heart as a vital organ as well as the relative sensitivity of cardiac cells to periods of malperfusion translates into significant hypoxic injury of the heart muscle, and consequently considerable morbidity and mortality, in the setting of myocardial infarction. Common etiology of suboptimal perfusion include an acute blockage in one or more of the cardiac arteries, irregular and dysrhythmic cardiac contraction, as well as a general state of hypovolemia within the systemic circulation.

According to the American Heart Association, more than 930,000 cases of myocardial infarctions occur in the United States annually [2]. In the United States alone, about 8.5 million individuals had previously experienced a heart attack while 17.6 million people had been diagnosed with the disease. Moreover, more than 900,000 Americans die of heart disease annually, with more than 140,000 deaths attributed directly to heart attack. Acute myocardial infarction is reported to have a 30% mortality rate with approximately 50% of the deaths happening prior to patient arrival at the

hospital. Such statistics highlight the significant burden placed on the quantity and quality of lives of patient with coronary disease, as well as its considerable negative financial implications on the health care system. [3]

Heart attacks are typically regarded as an acute series of symptoms with chest pain being the most classic. Despite this acute presentation of symptoms, subtle physiological changes have been described which onset several hours prior to the often clinically distinct “attack”. The most clinically applicable of these changes is the diminutive release of well described cardiac biomarkers. These fairly specific biomarkers are released into the circulation secondary to myocardial tissue death, and this process is initiated well before the onset of the attack. [4]

Cardiac Troponin I (cTnI) is considered to be one of the most specific and widely used of these cardiac biomarkers. [5] Blood concentrations of this biomarker is known to exponentially rise from hours prior to the attack, peaking at approximately 24 hours post attack and gradually decreasing over the next few days. While cTnI concentrations are routinely used to confirm the diagnosis of a heart attack (Figure 1), current medical technology limits physicians to detection of “post-attack” biomarker concentrations in the circulation. Unfortunately, at this point physiological damages are often irreversible. Considering the fact that early medical intervention during ischemic attacks to the heart is of paramount importance and can prevent further tissue damage, early detection of such biomarkers can be lifesaving.

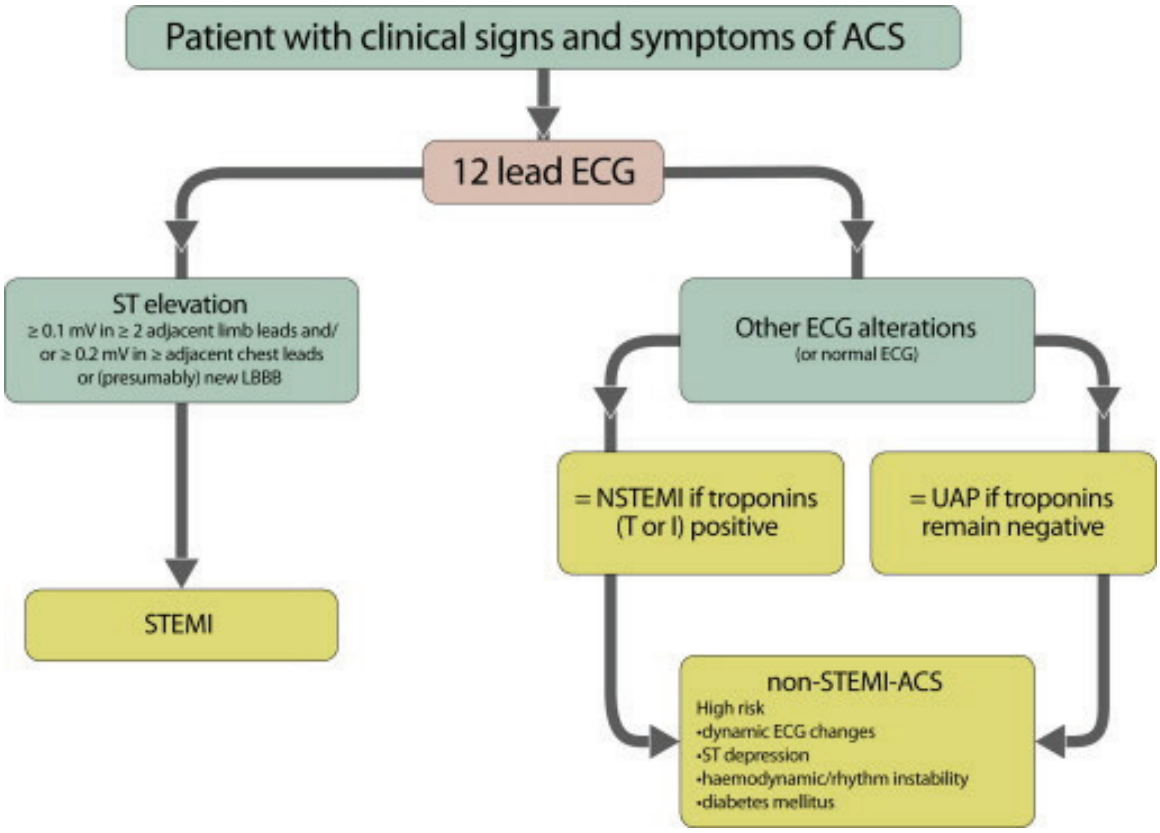

Figure 1: Admission Charts of Patients with Suspected Cardiac Damage [6]

Only a few cardiac biomarker measurements are routinely used by physicians. Currently, the most widely implemented biomarker measurement, used for clinical diagnosis of heart damage is cardiac troponin. Other cardiac biomarkers are less specific and may be elevated in skeletal muscle injury, liver disease, or kidney disease. [7]

1.2. Background

1.2.1. Heart Attack

Myocardial Infarction, also known as heart attack, is the death of cardiac myocytes due to prolonged and severe ischemia. While this may happen at any age, the incidence of this condition significantly and proportionally increases with advancing age. [8] The classic sequence of pathophysiological events in a typical MI is as follows:

- Sudden change in accumulation and swelling in artery walls due to macrophages
- Release of granule content and aggregation to form microthrombi
- Vasopasm
- Coagulation pathway activation by tissue factors which adds to the bulk of thrombus (Figure 2)
- Blockage of the lumen of the vessel by the thrombus and obstruction of blood supply (Figure 3)
- Ischemia, which if prolonged may lead to Myocyte necrosis

Due to the high dependency of myocardial function on oxygen, severe ischemia induces loss of contractility within one minute.

Based on clinical studies, early changes are potentially reversible. In fact, only severe ischemia lasting 20 minutes or more leads to necrosis. [9] The following table shows the approximate time of onset of key events in MI.

Table 1: Approximate onset of key events in myocardial infarction.

Feature	Time
Onset of ATP depletion	Seconds
Loss of Contractility	< 2 min
ATP Reduced: To 50% of Normal To 10% of Normal	 10 min 40 min
Irreversible Cell injury	>20 min

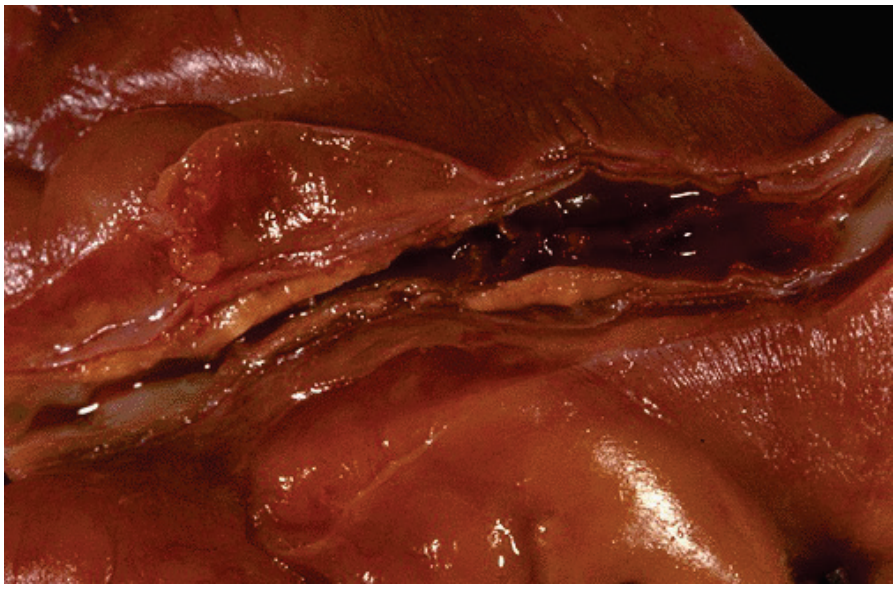

Figure 2: Thrombosis in a Coronary Artery [10]

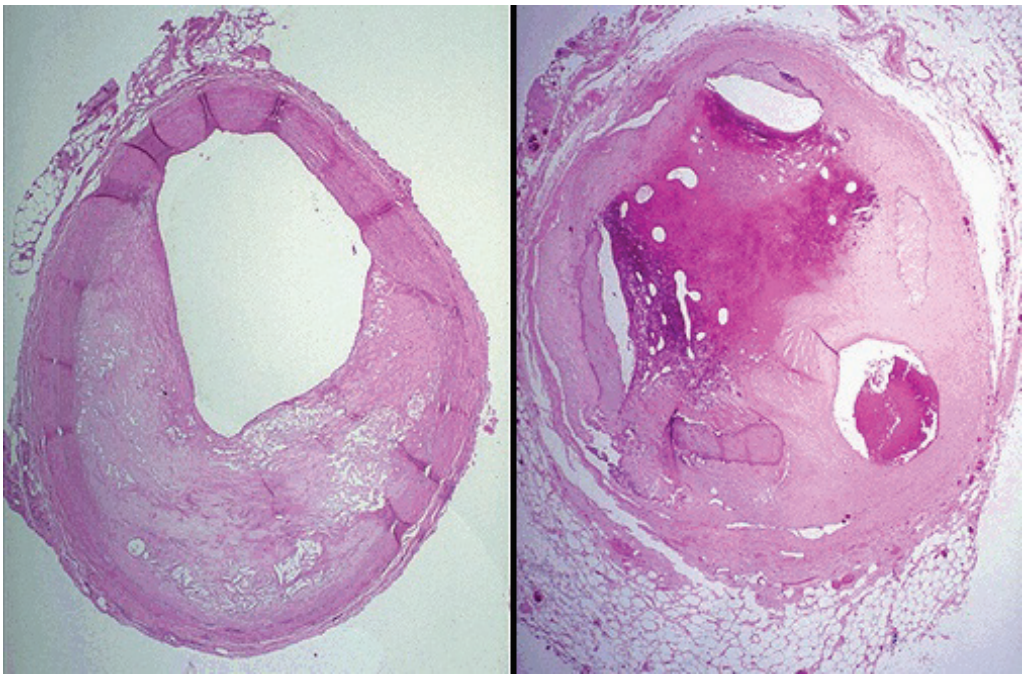

Figure 3: The left figure represents a cross section of coronary artery with a 50% occlusion. The right figure shows thrombosis with only three small lumens remaining. [10]

Without pathology, Cardiac Troponin I and T are not detectable in circulation; however, following MI, serum concentration of both of these biomarkers begins to rise by 2 to 4 hours with peak concentrations at 24 hours. Initially these Troponin complexes are released within the cytoplasm of myocytes from actin filaments, and subsequently they leak extracellularly and into the circulation. [11]

1.2.2. Mechanism of Troponin release in cytoplasm

Adenosine-5'-triphosphate (ATP) depletion is triggered by reduction in supply of oxygen, either secondary to an acute thrombotic obstruction the vessels, systemic hypovolemia, or cardiac electrical irregularities. Cellular respiration is an oxygen dependant mechanism which takes place within the mitochondria of the cells and

produces ATP as resultant product. ATP serves as a global energy "currency" within the body. Absence of oxygen leads to ATP depletion, which consequently has widespread effects. [12] More specifically, the activity of ATP-dependant plasma membrane energy-dependent pumps is attenuated, causing an osmotically imbalanced intercellular atmosphere which leads to cell swelling secondary to inflow of isomotic water. Further, much of the cellular metabolism and functioning is altered due to ATP deficiency.

Prolonged ATP depletion, results in protein misfoldings and structural disruptions. Moreover ATP dependant Ca^{2+} active pumps fail to function, leading to an influx of Ca^{2+}. This results in the loss of calcium homeostasis, activating many inherently destructive proteins in the cell such as proteases and ATPases. Also, intracellular accumulation of Ca^{2+} alters the mitochondrial permeability. Ultimately, high concentrations of Ca^{2+} results in direct activation of caspases leading to cell apoptosis. Free radicals, created from an attempt by the hypoxic cells to generate energy anaerobically diminish the cell's restricted permeability and contribute to its death. [13] [14] Therefore, due to the depletion of ATP and alteration in membrane permeability, as well as the activity of proteases and free radicals, the troponin complex dissociates and leaks into the circulation.

1.2.3. Cardiac Troponin I (cTnI) Measurement

The hospital gold standard for detection of myocardial infarction in patients presenting with characteristic symptoms is measurement of serum cardiac troponin I

(cTnI). The cTnI test is an in-vitro diagnostic test for the quantitative measurement of cardiac troponin I in whole blood or plasma samples. The cTnI enzyme-linked immunosorbent assay (ELISA) is based on the principle of a solid phase enzyme-linked immunosorbent assay. This assay uses different monoclonal antibodies, which target different epitopes on the cTnI. After a brief period of incubation, antibody-cTnI complex is formed and excess antibodies are washed away. The antibody-cTnI complex, which is fixed at the solid phase and labelled with fluorescent dyes, can then be quantified. Figure 4 further illustrates this process.

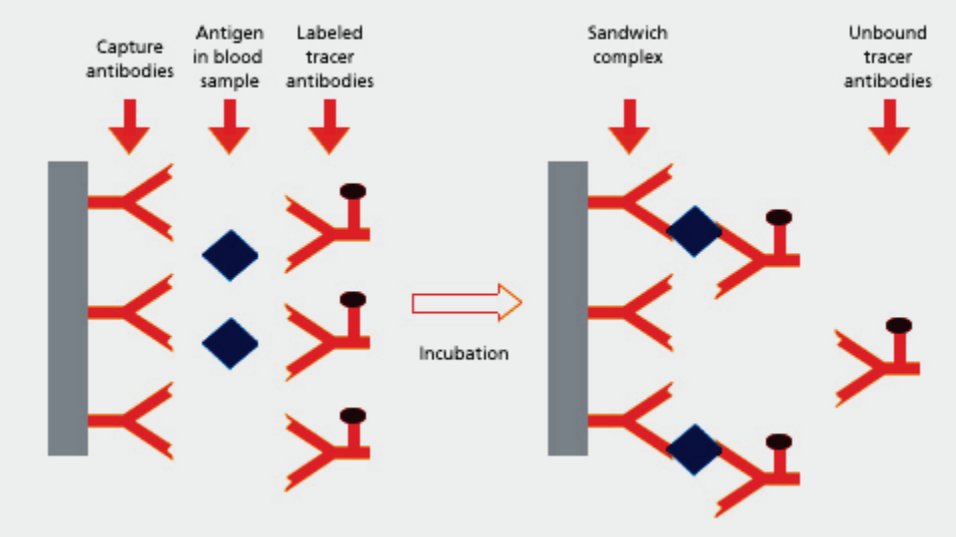

Figure 4: cTnI enzyme-linked immunosorbent assay (ELISA) test [15]

1.2.4. Limitations

While there are different available antibodies and various detection methods, most cTnI detection apparatus are ELISA based. Assays for cTnI demonstrate considerable variation in the assigned "cut-off" concentrations in order to define

abnormal values. Lack of standardization in cTnI assays imposes a great disadvantage. Firstly the results of troponin I assays from different manufacturers are not comparable because there is no standardization or consensus for troponin I results. The lack of comparability has been a source of confusion and frustration with clinicians. Studies have shown that troponin I results may vary by a factor of 100 fold from one assay and manufacturer to another. Aside from the lack of standardization and comparability, there is also wide debate on when should the test be performed. [16]

Shia et al demonstrate that because of cTnI degradation by proteolysis, significant variation in serum cardiac troponin I concentrations may be observed for a given patient sample with different analytical methods. [17] Different antibodies will target different regions of cTnI in various immunoassay and if the epitope region on cTnI for that specific antibody is degraded, immunoassay would not be able to detect the protein leading to false negative results. [17]

1.2.5. Cardiac Troponin T (cTnT) Measurement

Cardiac Troponin T (cTnT) is another biomarker, routinely measured for the diagnosis of MI. Since cTnT tests were commercially available prior to cTnI, there are relatively more peer-reviewed publications on their clinical utility. Measurement of cTnT is ELISA based and essentially founded on the same principles as measurement of cTnI; however, because of intellectual property protection, the manufacturing of the apparatus remains reserved to a single company. Therefore lack of standardization and

comparability of values is not an issue with cTnT measure, unlike cTnI measurement. Despite this advantage, more scientific research suggests lower specificity of cTnT measurements as compared to the cTnI test. Recent studies have questioned the diagnostic specificity of cTnT assays in patients with myocardial injury and chronic renal failure, muscular dystrophies and skeletal muscle damage. cTnI is the only Troponin expressed in myocardial cells during postnatal development, which is the main advantage of cTnI over cTnT. At least one recent paper concluded that using the recommended cut points for cTnT and cTnI where safe discharge was only achieved with patients tested using cTnI. [11] Another article showed that patients with inclusion body myositis and in the absence of any indication of myocardial damage had elevated cTnT with no elevation in cTnI. [11] While there remains a wide debate on specificity and sensitivity of both tests, we have focused our project on cTnI.

1.3. Biophotonic Measurement of cTnI

As discussed, current standard of care methods for serum detection of cardiac biomarkers lack adequate sensitivity to detect cardiac hypoxia prior to irreversible damage leading to false positive and negatives; further issues with a lack of standardization leads to inefficient and suboptimal efficacy in the clinical setting. Post release modifications of cardiac troponin, such as phosphorylation and proteolytic degradation, can result in failure of their detection by immunoassays.

Due to these reasons, we have focused our project on detection of circulating plasma concentrations of cTnI via biophotonics. This approach would overcome limitations of ELISA such as standardization and comparability. Furthermore, a real-time measurement would enable us to detect abnormal concentrations of cTnI much earlier and ideally prior to any irreversible damages to heart muscles. Accordingly, early medical intervention can be sought with arguably better overall prognosis.

1.4. Florescence Spectroscopy

1.4.1. Background

Florescence spectroscopy is an important analytic tool in many areas of sciences. Due to the extremely high sensitivity and specificity of this technique, even a single molecule can be detected. Thus, particularly in the areas of biochemistry and molecular genetics, florescence spectroscopy has become a dominating technique. Combined with other imaging techniques, florescence spectroscopy allows a real-time observation of biological systems with good resolution.

Florescence occurs when a molecule absorbs photons from the UV-Visible-NIR light spectrum (200-900 nm), causing transition of an electron to a high-energy electronic state (excited state) and subsequently emits photons as it returns to the ground state; this excited state decays exponentially with time. Through this process, which lasts under one nanosecond, some energy is lost secondary to heat or vibration.

Thus, the emitted energy is less than the exciting energy and therefore the emission wavelength is always longer than the excitation wavelength. The difference between the excitation and emission wavelengths is called Stokes shift, which is relative to the absorption band. Figure 5 illustrates the principle of Florescence.

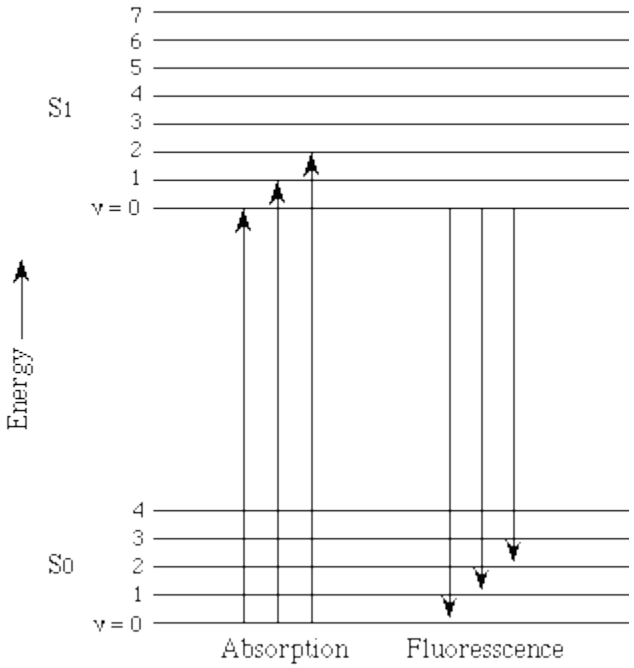

Figure 5: Principles of florescence [18]

Identification and quantification of fluorescent compounds can be analyzed based on their excitation and emission properties. Our first biophotonic approach was to use Florescence Spectroscopy for detection of circulating cTnI in blood plasma.

As Figure 6 depicts, due to the presence of aromatic amino acids, Tryptophan (W) (Figure 7) at residue 191, cTnI has florescence properties.

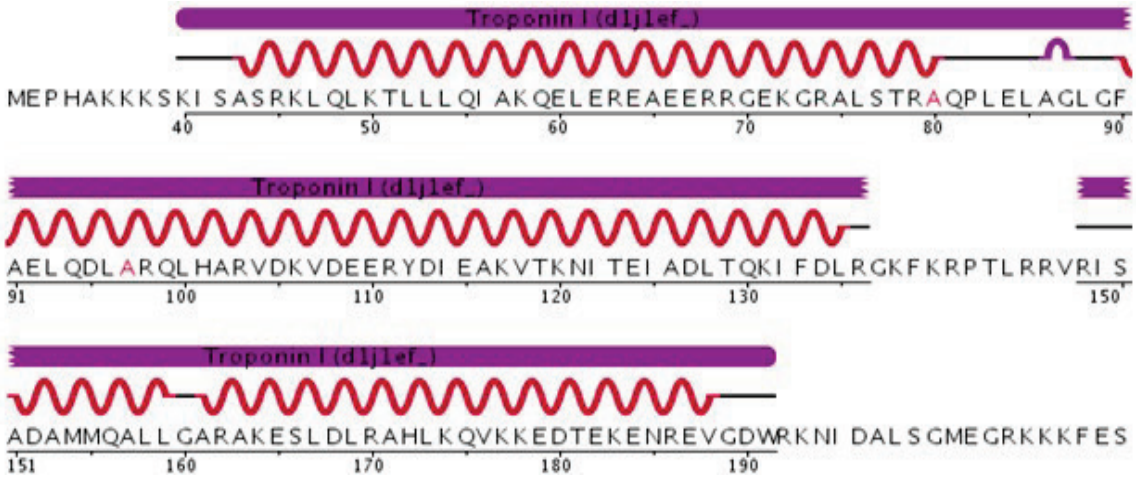

*Figure 6: Amino Acid sequence of cTnI (*www.pdb.org*)* [11].

Conjugated systems of fewer than eight conjugated double bonds absorb only in the UV region and therefore colorless to the human eye. With every double bond added, the system absorbs photons of lower energy [11].

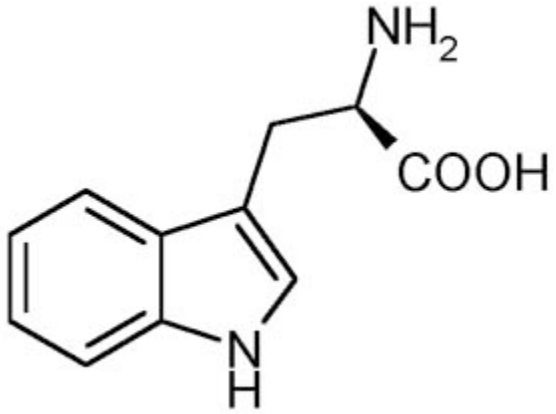

Figure 7: Tryptophan chemical structure, showing aromatic rings [19]

Table 2 presents the fluorescent excitation and emission wavelength of aromatic amino acids.

Table 2: Florescent profile of aromatic amino acids [11]

Amino Acid	*Excitation Wavelength*	*Emission Wavelength*
Tryptophan	280 nm	348nm
Tyrosine	274 nm	303 nm
Phenylalanine	257 nm	282 nm

1.4.2. Motivation

The purpose of this part of the project was to design a device, which could potentially detect concentration changes of circulating cTnI in the blood using florescence spectroscopy.

1.4.3. The Experiment

Since there was no information on florescence properties of cTnI in the existing literature, the initial approach was to characterize the excitation and florescence wavelength of the cTnI. This information would enable us to design and make a florescence spectrometer specific to cTnI.

To find the excitation and emission wavelength of cTnI, *PTI Quantamaster* UV-Vis Spectrofluorometer was used. To detect florescence, *SPM-002E Photon Controller* Spectrometer with the spectral range of 200-1090 nm was used. Also a *Newport PowerMeter* was used to measure the absorption characteristics of cTnI. This set up is

shown in the appendix section of this report. Table 3 lists components that were used to build an optical system for this project.

Table 3 : Components used to build an optical system

10 mm UV Quartz Florescence Cell
1800 grooves/mm Newport Plane Ruled Reflection Grating
11 mm uncoated lens
PTI Quantamaster UV-Vis Spectrofluorometer
First Surface Spherical Mirror
HBO 200 W Mercury Arc Lamp
SPM-002E Photon Controller Spectrometer
Newport PowerMeter

An experimental set up of this project is shown in the appendix section of this report.

1.4.4. Florescence Spectroscopy Experiment Results

Figure 8 shows the expected emission spectrum from mercury arc lamp UV-Vis. The actual spectrum shows a peak at 280 nm, which is our desired wavelength as demonstrated in Figure 9. By using the diffraction grating and higher integration time, the peak was selected.

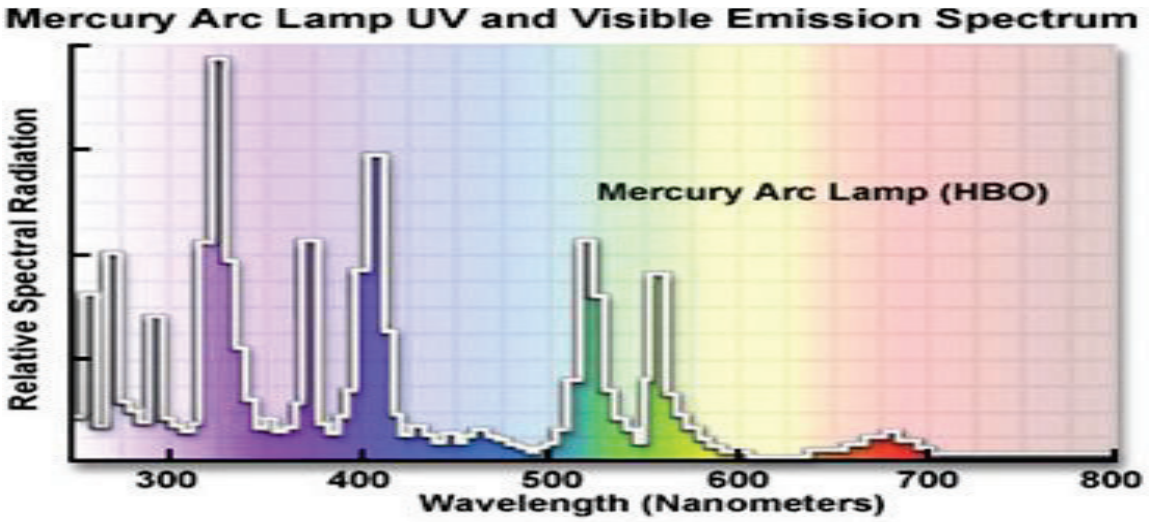

Figure 8: Mercury arc lamp expected spectrum [20]

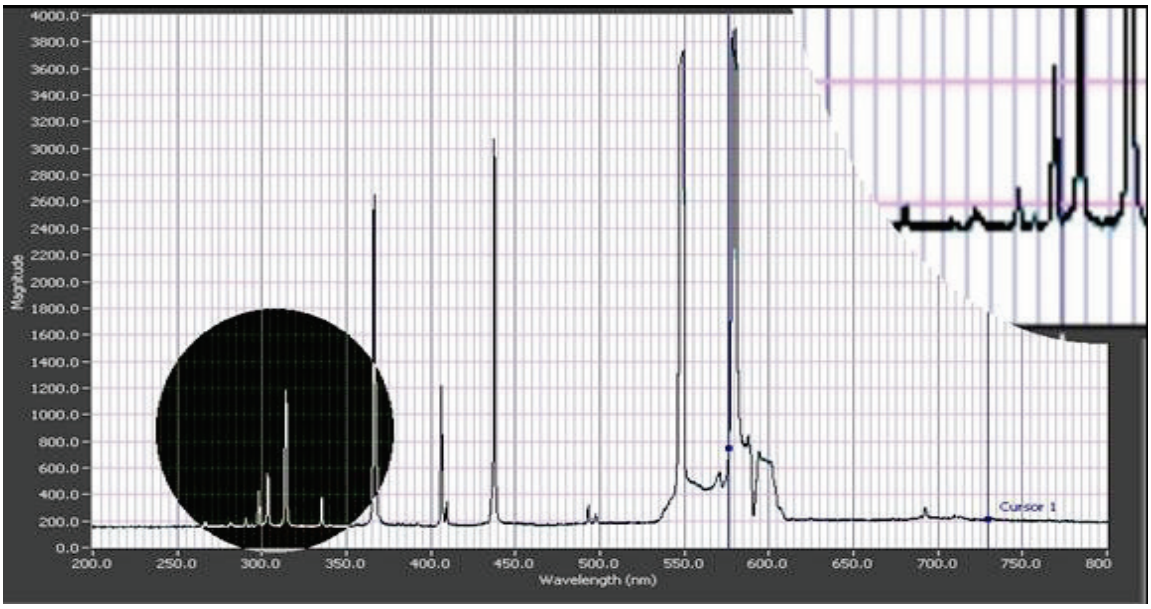

Figure 9: Mercury arc lamp spectrum from the spectrometer

To get the expected emission wavelength at approximately 348 nm, the alignments and components were adjusted repeatedly. The result shows a fluorescent signal at 347nm (Figure 10).

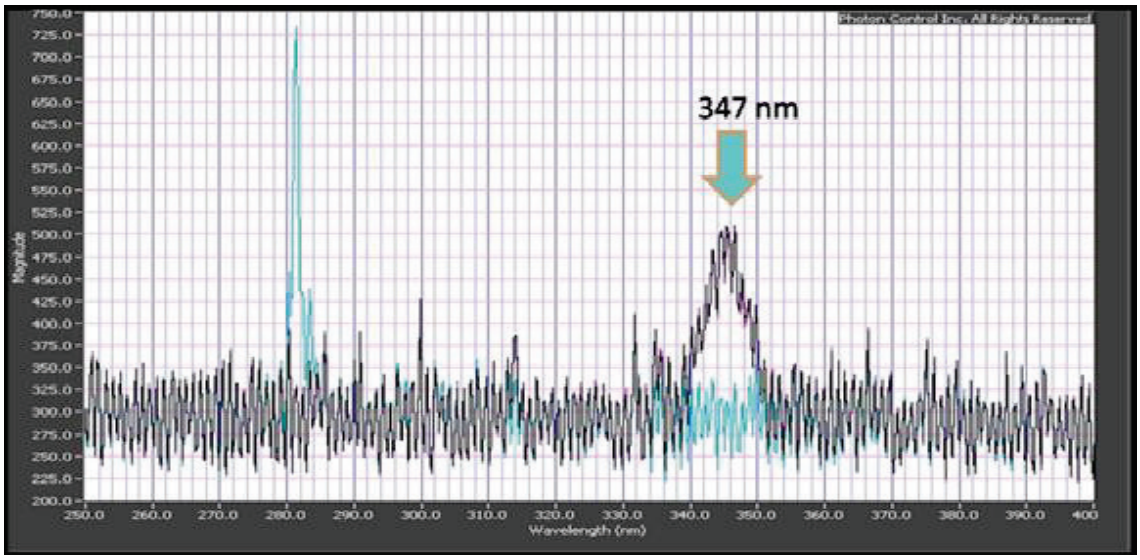

Figure 10: Florescence peak

1.5. Conclusion

Due to the presence of Tryptophan in cTnI, an expected excitation at 347 nm was seen as illustrated in Figure 10.

As our first biophotonic approach to detect the concentration of circulating cTnI in the blood, its Florescence characteristics were examined in this chapter. Since the data demonstrate a logarithmic fit, it was concluded that cTnI absorption characteristic follows the Beer-Lambert Law.

Due to our equipment limitation and to lack of UV specific components such as diffraction grating and more efficient lenses at UV, the concentration of cTnI in the sample were significantly higher than circulating cTnI in the human blood. Since the device and the set-up were not optimized for detecting very low florescent signals, most of the lights were absorbed by the optical components.

In order to extract a unique characteristic of the protein from its emission/excitation profile and to be able to distinguish cTnI protein from other proteins containing amino acids with conjugated properties, quantum effects should be considered. The high amount of noise and component limitations in emitted signal decreases the specificity of cTnI emission characteristics. Also detection of backscattered signal instead of the transmitted signal has higher amplitude and can be more reliable.

With florescence spectroscopy, any tryptophan containing amino acid will tend to dominate the spectrum and therefore leading to frequent overwhelming of signals from other amino acids. In addition, it is very challenging to quantitatively relate changes in florescence yields to structural changes in proteins.

Therefore, the only anticipation that allows for further examination of this project is through the study of quantum changes in the cTnI protein, which leads to investigation of the Raman signature of the protein.

2. Cardiac Biomarkers and Biophotonic Measurements

2.1. Cardiac Biomarkers

According to World Health Organization (WHO) [53], two of the following three criteria have to be present for a diagnosis of myocardial infarction (MI):

- Symptoms consistent with cardiac ischemia
- ECG changes.
- Elevated serum marker concentrations.

Myoglobin, CK-MB and Troponins are among the most widely used cardiac biomarkers for diagnosis of myocardial infarction. Myoglobin is a very non-specific cardiac biomarker with suboptimal concentration elevation and peak dynamics, due to an inability to remain sufficiently elevated as compared to Troponin; this characteristic renders Myoglobin ineffective as a sole agent to confirm an infarction.

CK-MB on the other hand is a more accurate indicator and can be validated as a marker for MI. However CK-MB can increase after muscle injury or muscular diseases and can also be found in the tongue, intestine, diaphragm, uterus, and prostate. Consequently, any damage to any of these tissues may lead to an elevated serum levels.

Therefore this lacks of specificity can result in a high number of false positives, rendering it impractical in clinical settings.

Table 4 illustrates diagnostic sensitivity and specificity of Troponin I and CK-MB and Total CK, suggesting measurement of cTnI concentration levels as a gold standard for diagnosis of MI.

Table 4: Diagnostic sensitivity and specificity of Troponin I, CK-MB and Total CK [21]

Marker	Sensitivity	Specificity
Cardiac troponin I	100%	96.3%
CK-MB	88.2%	93.2%
Total CK	73.5%	84.6%

Figure 11 further illustrates different cardiac biomarkers and their levels in the circulation as graphed versus time after an MI. It can be deduced that cTnI and cTnT have superior sensitivity and specificity compared to other cardiac biomarkers.

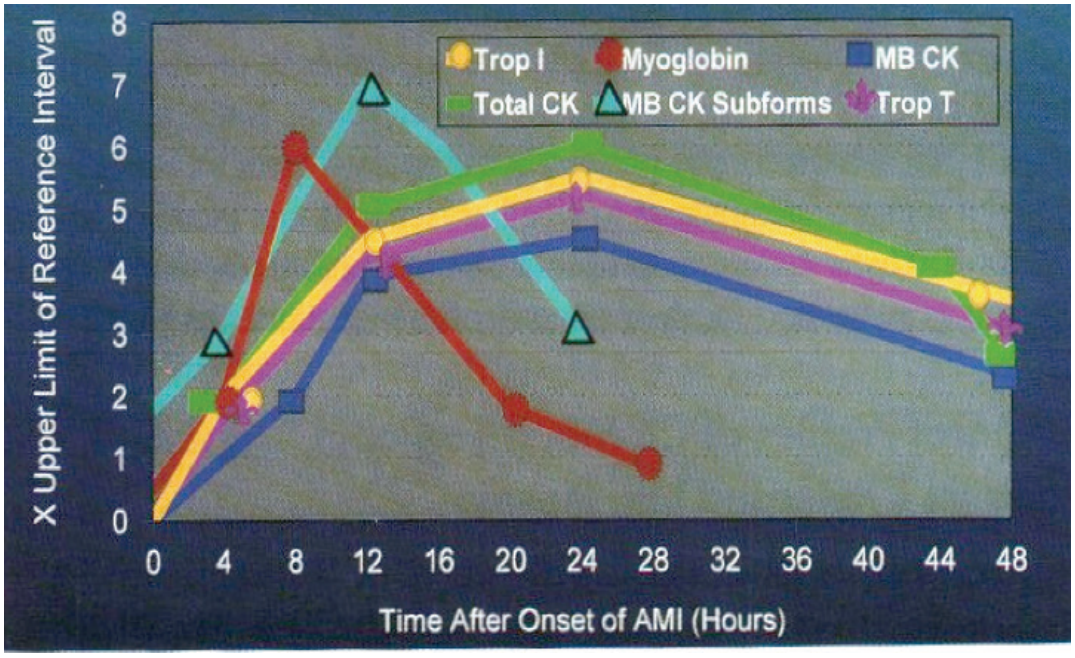

Figure 11: Plasma Temporal Profile of Cardiac Diagnostic Markers [22]

2.1.1. Cardiac Troponin

Troponin, a complex of three contractile regulatory proteins (troponin C, T and I), controls the calcium-mediated interactions between actin and myosin in cardiac and skeletal muscles. Troponin-I and T are specific to cardiac muscles, unlike troponin C which is associated with both cardiac and skeletal muscles. Hence, troponin-C is not used in the diagnosis of myocardial damage. Figure 12 depicts the functional structure of cardiac troponin.

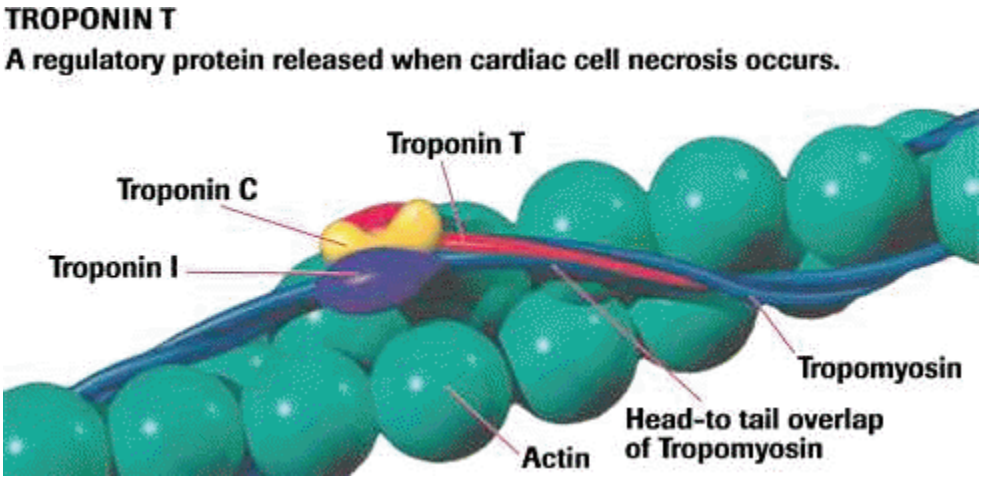

Figure 12: Functional Structure of cardiac troponin [23]

Cardiac troponins are released into the circulation in response to myocardial necrosis. As such, cardiac troponins, especially cardiac troponin I (cTnI), are the preferred biomarkers for the detection of cardiac injury, and have long assisted physicians in improving diagnostic strategies for the effective management of patients with chest pain.

The presence of cardiac troponin I and T are detected by immunoassays using specific antibodies. Due to patent protection, only one assay for cTnT is available from a single manufacturer (*Roche Diagnostics*); cTnT demonstrates a high degree of precision at the low end of measurement range and a relatively uniform cut-off concentration. By contrast, at least 20 different commercial assays for cTnI are available on automated and point of care instruments.

Assays for cTnI demonstrate considerable variation in the threshold concentration for the definition of an abnormal cTnI level. Lack of standardization in

cTnI assays imposes a great disadvantage. Firstly, the results of troponin I assays from different manufacturers are not comparable because there is no standardization or consensus for troponin I results as discussed above.

2.2. Post Release Modification

Enzymes inherent to human blood impose post release modifications to troponin, effectively altering its molecular structures and degrading epitopes identifiable by antibodies used for their detection. As briefly discussed, such post release modifications must be addressed and introduce particular challenges to this project. Structural changes consequent to these medications and degradations may potentially change Raman signals. An enhanced understanding of the nature of these modifications provides a more predictive platform for signal characterization and apparatus sensitivity.

2.3. Literature Review and Discussion

A series of literature reviews are presented herein to further discuss molecular characteristics prior to and after their release. Chandra et al investigated the effects of phosphorylation of cTnI by protein kinase A which takes place at the Ser 23 and Ser 24 location in an amino-terminal extension unique to cTnI. cTnI and cTnC fragments and mutations were used to investigate the effects of phosphorylation on cTnI - cTnC complex. Study results indicated that the transduction of PKA-induced phosphorylation

signal from cTnI to the regulatory site of cTnC involves a global change in the cTnI structure. [24] Similarly, Ward et al studied the structural consequences of cardiac troponin I phosphorylation. They produced a series of mutations and investigated the effects of various mutations on phosphorylation of cTnI. These authors suggest that deletion or mutation in residues 1-15 does not necessarily affect the phosphorylation process. On the other hand, removing or mutating further residues will mimic phosphorylation. Furthermore, they proposed that cTnI residues 16 –29 bind to cTnC stabilizing the "open" Ca^{2+} bound state. Phosphorylation prevents this binding, accelerating Ca^{2+} release. This result is consistent with the findings of Chandra et al. [24]

A study by Katrukh et al describes proteolytic degradation of cTnI in serum and necrotic tissue after onset of myocardial infarction (MI) by two immunological methods: sandwich immunoassay and Western blots. They demonstrate that cTnI in both necrotic tissues and serum undergoes proteolytic degradation resulting in different fragments with various stabilities. Furthermore, it is suggested that the region most resistant to proteolysis is the region located between amino acid residues 30 and 110. While other regions of cTnI are very susceptible to proteolysis, this region stayed intact even after an extended incubation time. Since the inhibitory domain of this protein is located within this region and interacts with cTnC, it was recommended that higher stability can be due to protection of this region from proteolysis by cTnC. [25]

Results from the discussed molecular studies are of direct importance for our project. Aiming to obtain a Raman signature from residues 30 to 110 would potentially

help us to detect cTnI fragments after degradation, which happens almost immediately after their release. An ablity to detect the fragments of cTnI would give our biophotonic approach a significant advantage over immunoassay methods currently being used. Many of implemented assays utilize antibodies incapable of identifying altered or degraded epitopes on modified troponin molecules. A study by Shia et al similarly suggests the inability of immunoassays to detect cTnI fragments. [17] Shia et al demonstrate that because of cTnI degradation by proteolysis, up to a 20-fold variation in serum cardiac troponin I (cTnI) concentration may be observed for a given patient sample with different analytical methods. [17] Therefore, using these parameters may result in a false negative assay, with potentially devastating outcomes in the clinical setting.

Labugger et al compared different forms of cTnI and cTnT obtained from the blood of patients after an acute MI and compared these biomarkers to recombinant cTnI from healthy individuals. This study concluded that the cTnI observed in acute MI patients undergoes specific proteolytic modifications, not present in cTnI obtained from healthy individuals. Furthermore, since the recombinant cTnT incubated in normal serum failed to demonstrate proteolytic susceptibility and acute MI patients possessed only a small amount of intact cTnT, it was suggested that these forms of cTnI and cTnT, only found in AMI patients, are generated in the diseased myocardium itself and are then subsequently released into serum. [26]

The findings in this article could be very beneficial to our non-invasive biophotonics approach. One of the main challenges our approach faces is the signal to noise ratio. The Raman back scattering, received by our detector, is influenced by many proteins and molecules. Much of these noise sources could be eliminated through signal processing and specializing our device to detect a very specific range of signals related to cardiac troponins. Despite such efforts, the free circulating cardiac and non cardiac troponin which are very similar in structure produce similar signals in Raman scattering. If the findings in Labugger et al are in fact accurate, unique cTnI and cTnT aree released which are structurally distinct from the normal cardiac troponin. This would help us instrument our device in a way to detect the presence of such unique biomarkers and reduce the probability of false positive result due to presence of free circulating cardiac troponins.

In a controversial article by A. van der Laarse, a hypothesis (figure 13) is presented which indicates that troponin degradation may potentially contribute to heart failure. This study claims that the cardiac troponin complex, which regulates the function of actin and myosin in heart muscles, may impair myocardial function when present in high concentrations in the cells and thus restrict contraction and relaxation of heart muscles. The author argues that troponin is targeted and degraded by activated Calpain, a calcium-dependent protease, when activated by elevated intracellular Ca^{2+} concentrations such as during ischemia. Consequently, the interaction between actin and myosin is impaired impinging contractile forces and leading to heart failure. [27]

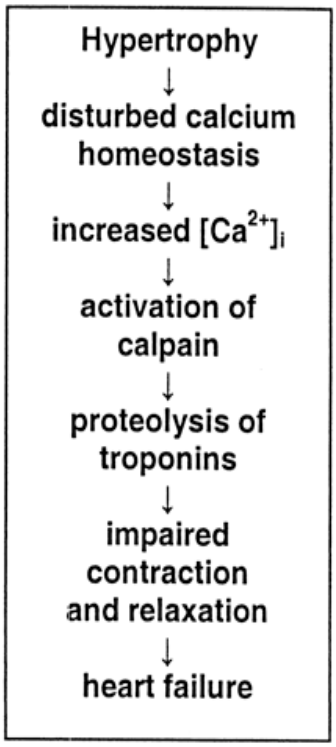

Figure 13: Sequence of events leading to MI based on A. van der Laarse Hypothesis [27]

Currently, most authors suggest that an elevation in the circulatory concentrations of cTnI will only take place if damage has been inflicted on cardiac tissue. However, the theory proposed by A. van der Laarse would suggest that elevated cTnI concentrations are theoretically detectable, prior to irreversible cardiac tissue damage. This theory has not been generally accepted, but its validity could mean that medical intervention can be initiated prior to even a small amount of cardiac tissue damage, in the setting of myocardial infarction. [27]

3. Raman Spectroscopy

3.1. Introduction and Background

Raman spectroscopy is a technology, principled on the quantitative measurement of the wavelength and intensity of inelastically scattered light from molecules. The Raman scattered light occurs at wavelengths that are shifted from the incident light by the energies of molecular vibrations. This vibration can be observed in either the Infrared (IR) or Raman Spectra. While IR spectroscopy measures the absorption of infrared light by the sample, Raman spectroscopy measures the scattered light.

In Raman Spectroscopy, the laser beam is used to irradiate the sample at UV-Visible-NIR spectrum (200-900 nm). The scattered beams are also at UV-Visible-NIR region and consist of two parts: Rayleigh scattering is strong and has the same frequency as the incident beam, and Raman scattering is very weak and has a frequency of higher or lower of the incident beam. These discrepancies in frequency of incident beam and Raman scattering is unique to each molecule, allowing an ability to confidently identify molecules through their characteristic properties. A *Stoke* is defined as a Raman scatter frequency that is lower than the incident beam frequency; similarly an *Anti-Stoke* is a Raman scatter frequency, higher than the initial incident beam.

As shown in equation 1, the Raman incident beam (V_0) is shifted due to molecular vibration and Stroke (V_0-V_m) or Anti-Stroke (V_0+V_m) results.

Force constant **(K)**, and mass effect **(μ)**, are both contributing factors that determine vibration frequencies.

$$v = \frac{1}{2\pi c}\sqrt{\frac{K}{\mu}} \qquad \text{(EQ 1)}$$

As previously mentioned, Raman spectroscopies are done in the UV region; subsequently, IR and Raman are considered complementary in that certain vibrations will be solely Raman active (e.g. totally symmetric vibrations), while others being exclusively IR active. Covalent bonds are generally very strong in Raman while ionic bonds are strong in IR. This feature of Raman makes it especially advantageous for our studies of proteins as it can adequately detect the vibration of the covalent bonds between the amino acids. Moreover, since the laser beam is about 1-2 mm, only a very small sample is needed for detection, further serving as an advantage over IR for our research purposes. Another advantage of Raman over IR spectroscopy is that proteins in the body are in an aqueous solution and IR is inconveniently, a strong absorber of water. On the contrast, water is a weak Raman scatterer. Once again, this inherent quality deems Raman a superior choice for bioscientific application. Lastly, with regards to instrumentation, Raman shift ranges from 4000 to 50 cm^{-1} and can be observed using a

single recording while gratings, beam splitters, filters and detectors must all be changed to cover the same range while operating IR spectroscopy.

3.2. Literature Review

The incident wavelength was chosen to be at 785 nm, as typically used in experimentation with organic compounds.[28] As shown in equation 2, the power of Raman scatter is directly proportional to the intensity of the incident light, while inversely proportional to the fourth power to the expectation wavelength. Thus, there is a mathematical compromise that needs to be considered.

$$E_{Sc} = \frac{\propto^2}{\lambda^4} (1 + \cos^2 \theta) E_\circ \qquad \text{(EQ 2)}$$

Because the Raman scatter is inversely proportional to the fourth power of the excitation wavelength, more Raman scatter will be observed as the energy of excitation wavelength increases. Therefore, as we lower the excitation wavelength, we see more Raman back scattering. However, since the florescence region spans from 275 nm to 975 nm, we would promote florescence with sometime very strong signals that completely overwhelm the Raman signals. Therefore, as we increase the excitation wavelength, we see less florescence effect and at the same time we observe attenuation in the power of Raman scattering. [28]

3.3. cTnI versus cTnT

As mentioned in the previous chapter, both cTnI and cTnT are specific cardiac biomarkers that are released as part of the cTnI complex into the blood stream following myocardial damages. For the purpose of this research we initially conducted all of our experiments for both cTnI and cTnT. The Appendix includes a representative portion of the results from cTnT Raman spectroscopy. However, during our literature review process we discovered that cTnT forms different configurations after it is released into the blood stream, which makes the concentration of a single isoform of the protein even lower. An increase in the number of isoforms decreases the concentration of each isoform. Since Raman is sensitive to each isoform, a progressive decrease in the concentration of each form, secondary to this alteration in configuration, resulted in a similarly progressive attenuation in Raman signal intensity. This suboptimal characteristic of cTnT prevented us from further investigation of this biomarker. The costume buffer containing the cTnI, used in this part of the project was prepared based on a study by I.M. Vlasova. [29]

3.4. Remarks

3.4.1. Savitzky-Golay Filter

Savitzky-Golay smoothing filters (also called digital smoothing polynomial filters or least squares smoothing filters) are typically used to "smooth out" a noisy signal

whose frequency span (without noise) is large. In this type of application, Savitzky-Golay smoothing filters perform much better than standard averaging FIR (finite impulse response) filters, which tend to filter out a significant portion of the signal's high frequency content along with the noise. Savitzky-Golay filters are optimal in that they minimize the least-squares error in fitting a polynomial to each frame of noisy data. [54]

3.4.2. Wavelet Transform

The Fast Wavelet Transform is a mathematical algorithm that facilitates changing a waveform or signal that is originally in time domain into a series of coefficients. This transformation is based on an orthogonal basis of small finite wavelets. Wavelet transform can be simply applied to multidimensional signals, such as images, where the time domain is replaced with the space domain. In this research Wavelet Transform is used to analyze the Raman peaks of cTnI and BSA.

3.5. Spectral Result of Raman Spectroscopy Measurement of cTnI

In order to investigate the possibility of cTnI detection using Raman spectroscopy, we designed and performed a number of experiments using various Raman spectroscopes with different experimental set ups. In our first experiment, we used a commercialized SpectraCode RP-1 Portable Raman Spectrometer, located at the SFU Physics Department. Five different instruments where used during this research in

order to verify and confirm reproducibility of our results. The rest of the instruments used in this research were generously provided by: The department of Chemistry (SFU), National Research Council Canada (UBC), and the department of Chemistry, under Professor Edward Grant Group (UBC).

This section outlines various results from the second set of experiments, which was conducted using the two industrial and research Raman Spectrometers at UBC Grant Groups Lab. A summary of many iterations, further measurements, as well as verification results are presented in the next chapter. The apparatus setting for the result of this section is as follows: laser excitation wavelength of 785 nm and the full laser power of 140 mW. In each experiment an average of 30 trials are attempted, and the background noise is subtracted from the collective signals. In this section, mouse cTnI is diluted in a buffer solution of 200mL of 0.1M- KH_2PO_4 and 0.1M-NaOH. The raw signal is presented in Figure 14.

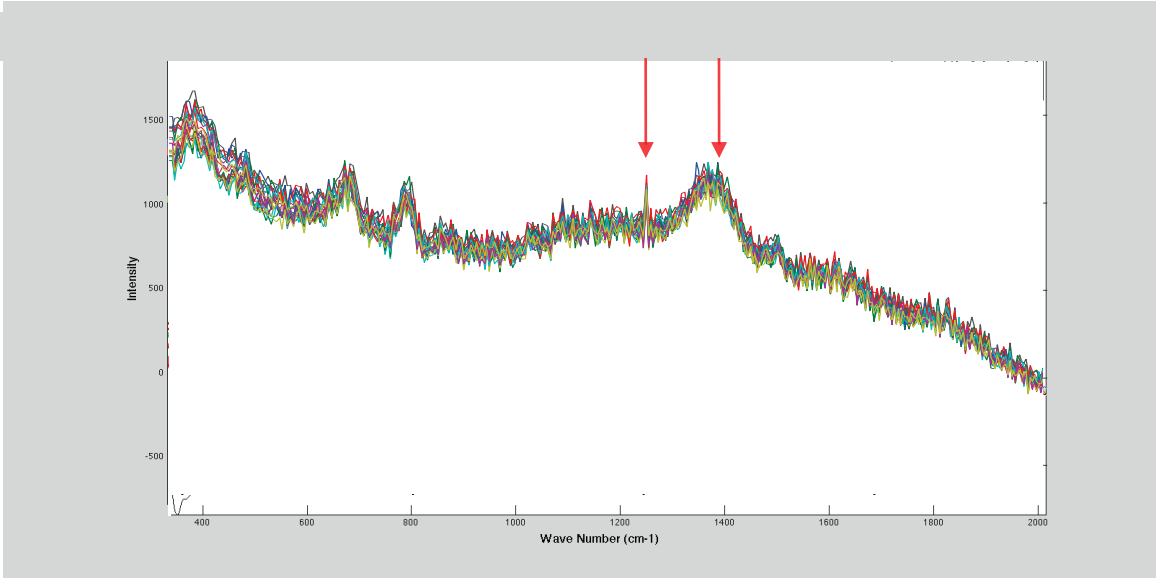

Figure 14: Raw cTnI [0.5 mg/mL] in Buffer Sample Raman Spectroscopy

3.5.1. Signal Processing

In the next set of experiments, water is substituted from the solution to decrease the noise level. In processing the signal, first Polyfit of the spectrum was subtracted from the raw signal using the Matlab™ polyfit function. After application of the polyfit with both the raw signal as well as signal with the water subtracted, we discovered that the graph from the latter was more difficult to analyze as compared to the former. One reason for this observation can be the presence of florescent contaminants in the signal. Moreover, after reviewing articles that have presented the same type of analysis and confirming with other graduate students working with similar proteins on the same spectrometer, we have found the polyfit analysis of the raw data to be the conventional way to analyse the Raman data of a very low intensity signal characteristic level.

In Figure 15, the pink graph (polyfit data) is subtracted from the blue graph (raw data), yielding the red line as the resulting graph. Final results are illustrated in Figure 16.

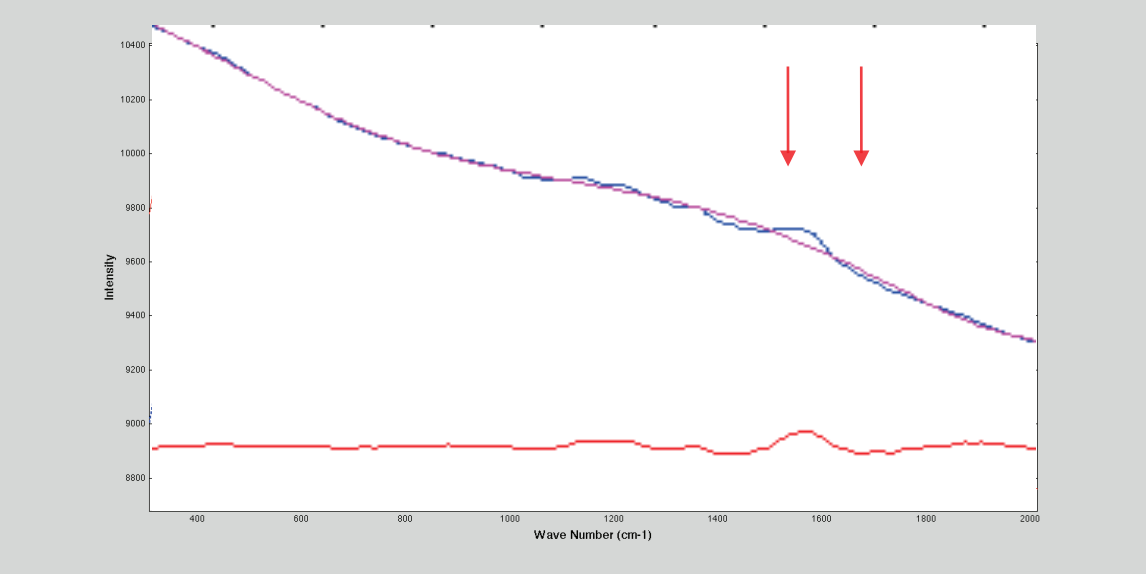

Figure 15: Polyfit subtraction steps for new cTnI.

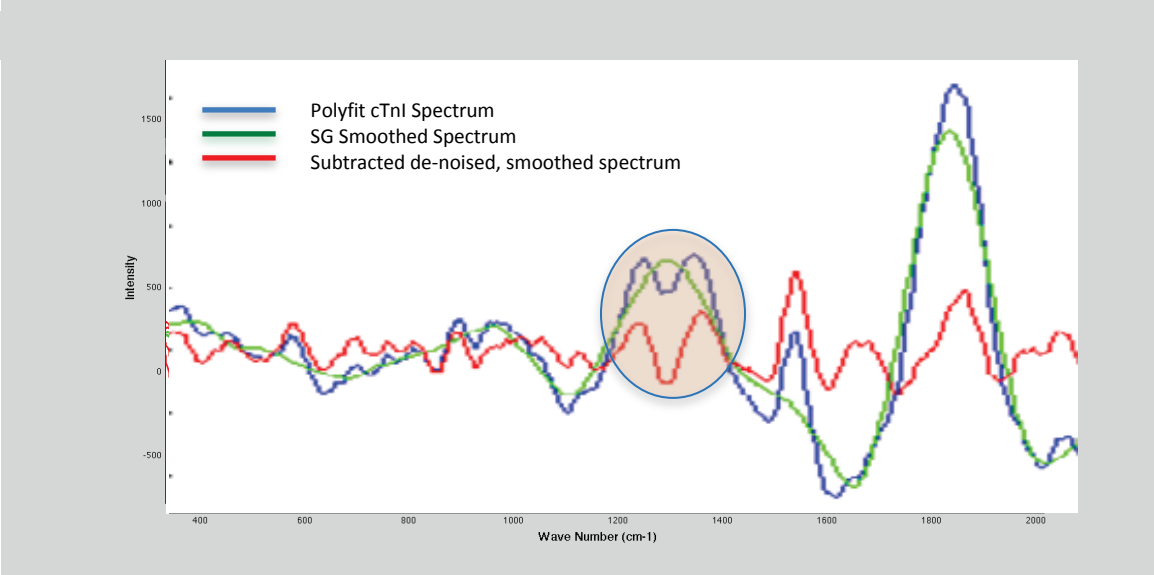

Figure 16: SG Smoothing process for the cTnI

Next Savitzky–Golay (SG), smoothing tools were applied to de-noise the data. Then this graph was subtracted from the previous polyfit graph to remove the baseline.

3.5.2. cTnI Raman Signiture for the First Time

After conducting several iterations of cTnI signal processing and experiments, we were able to characterize Raman signature of cTnI. To our knowledge, this is the first time this has been reported in the scientific literature. Figure 17 outlines our findings.

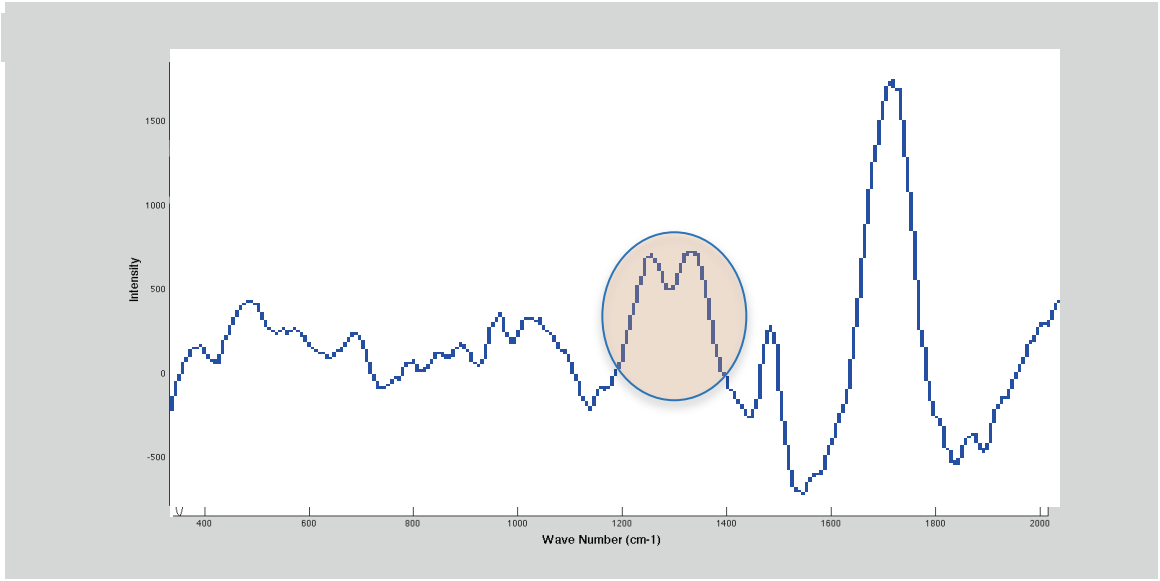

Figure 17: First cTnI signature

We have compared the result of all 30 iterations of our experiment and have consistently observed that the peak of 1700cm^{-1}, is Raman's peak for water and the peaks between 1200 cm^{-1} -1400cm^{-1} are related to cTnI Raman signature as shown in Figure 17.

3.5.3. Results and Discussions

Limited by the sensitivity and signal-to-noise ratio (SNR) of our first Raman instrument, one of the main challenges in this research was the low intensity of the different signals when the buffer Raman signature is subtracted from the cTnI raw sample. These results carry a relatively large noise ratio compared to the signals that were determinants of cTnI signature. Although difference amplitude in some regions of the signal was observed, it was difficult to draw a conclusion to find the essential difference.

As it will be presented in the following descriptive chapters, further investigation and signal processing measures were carried through a combination of the latest Raman instrument and chemometrics methods, which greatly improved the SNR of Raman signal and made the differences more revealing. These new strategies, presented herein, made the relationship between Raman spectral difference and cTnI intensity more objectively evident.

Also from the Figure 17, we can conclude that despite the low intensity of the signal, by characterizing the spectra, the change in concentration of cTnI can be measured in the plasma or blood. These results were behind the motivation to continue this research and further compare plasma from a normal mouse as well as a mouse, which suffered from an MI. As it will be outlined, further experiments were conducted to identify the differences in the Raman signal peak. Figure 18 is an overlay of two types

of cTnI spectra (prepared two years apart) for various concentrations. The red signal is from the more recent cTnI and the green signal is from the old cTnI samples.

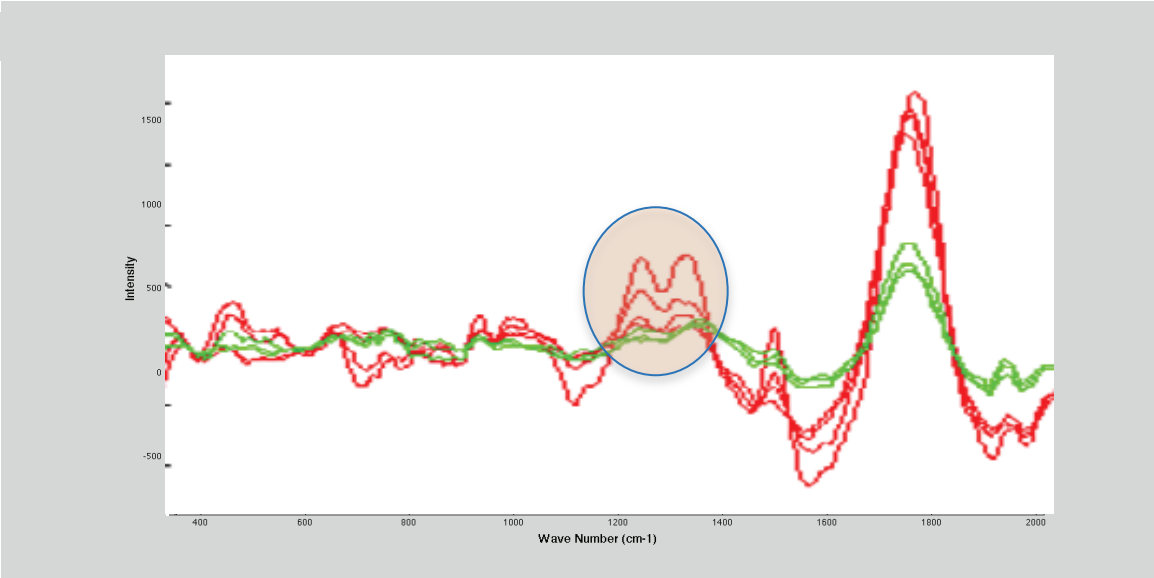

Figure 18: New and Old cTnI spectra different concentration

The less recent samples are more than two years old and have been stored in frozen powder form. Several factors such as multiple thawing and cooling of the samples may have caused a portion of the proteins in this sample to be denatured over time. Moreover, from the acquired signals, we can conclude that there are more impurities which may potentially cause florescence signal and to decrease the intensity of the Raman signal. The effect of the fluorescent signal is not visible in these samples. These explanations can collectively explain the variability observed in Figure 18 between the two samples.

Raman spectroscopy is a quantitative and qualitative technique, able to delineate a unique 'finger print' of a given molecule or substance. For quantitative

molecular measurements of Raman spectroscopy, enhancing chemometric methods can be supplemented for low sample concentrations. As previously discussed, florescence can often contaminate Raman spectra. The use of a Near-IR 785 nm laser helps with reduction of the possibility of fluorescent contamination; regardless, our sample still contains a relatively large portion of fluorescent in the signal, which can cause photo bleaching and saturation, resulting in the Raman signal to be quenched. Therefore, even though we can conclude that cTnI Raman is quantitative, the relationship between the change in concentration of cTnI and its Raman signal is not linear; the inconsistency between the increase in sample concentration and sensitivity of detection suggests the ultimate need for a yet more sensitivity apparatus. In general, despite the low magnitude of signal characteristics, we are confident that the signature peaks are identifiable after signal processing as well as utilizing more precise instruments.

4. Verification of cTnI Signature

4.1. Experiment procedure

In order to replicate and verify the unique Raman signature of cTnI discussed in our previous chapter, an experiment was conducted on mouse cTnI to find its Raman spectra. The specifications of the Raman Spectrometer instrument used for this experiment are as follows: wavelength is 785 nm and the full laser power is 140 mW. For the particular measurement presented in this report, the integration time is 5 seconds and 2 seconds. In previous experiments, the background noise of the spectrum was removed, wavelet transform was performed and the portion of the wavelength related to cTnI was extracted. However, when whole mouse serum was analyzed, the resulting signal contained excessive noise caused by various components in the blood as outlined previously. Therefore, it was concluded that without completely characterizing the protein, conducting an experiment in the blood is not possible with the available technology. Therefore, the first step towards implementation of this project is to verify the cTnI spectra in water.

The research in this report is conducted in a completely different experimental environment, consisting of new samples and instruments, as compared to previous

experiments. More specifically, the results presented in the following section have been generated from a 20mg/mL mouse cTnI sample in double distilled water.

4.2. Verification Result and Discussion

Figure 19 represents data acquired from double distilled water and a 20 mg/mL cTnI for the purpose of verification of previous finding in the same research.

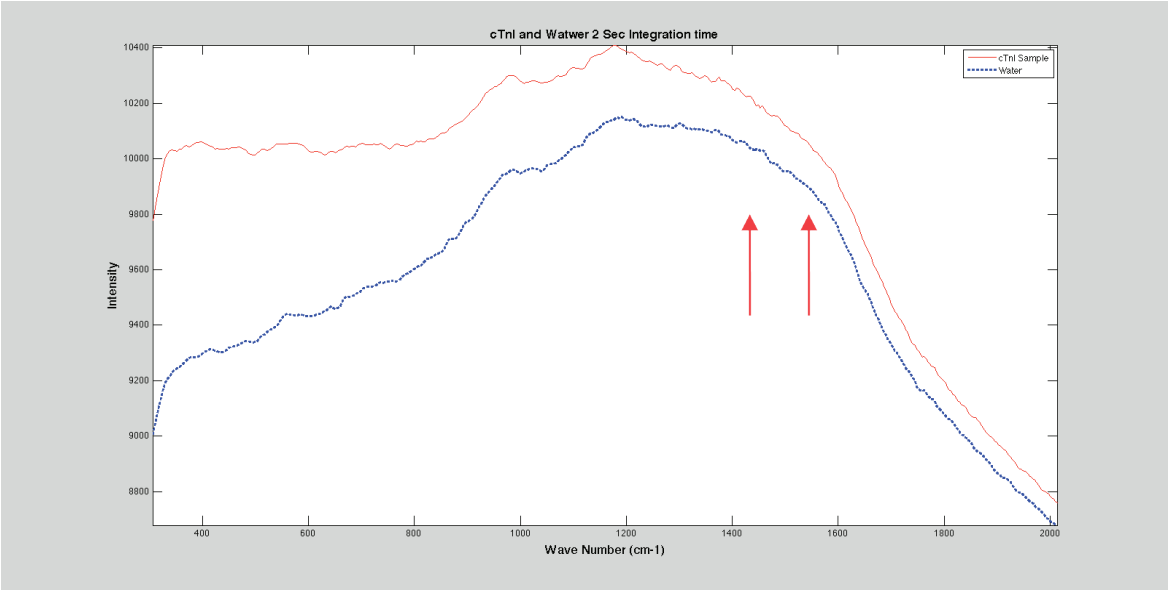

Figure 19: Water and cTnI sample after noise reduction.

Figure 20 provides a comparison between various noise reduction levels of adjusted cTnI spectra.

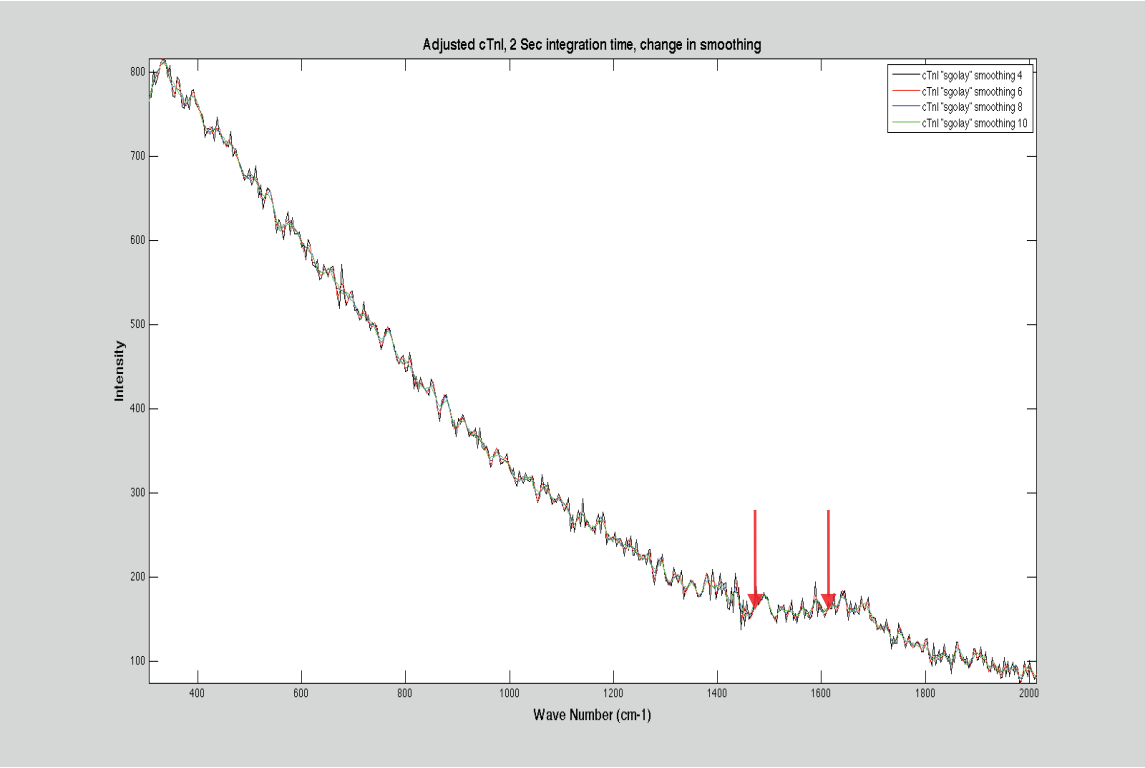

Figure 20: Different levels of Smoothing of water and sample.

Figure 21 illustrates a snapshot of the part of cTnI signal with more characteristic peaks at various noise reduction and smoothing levels.

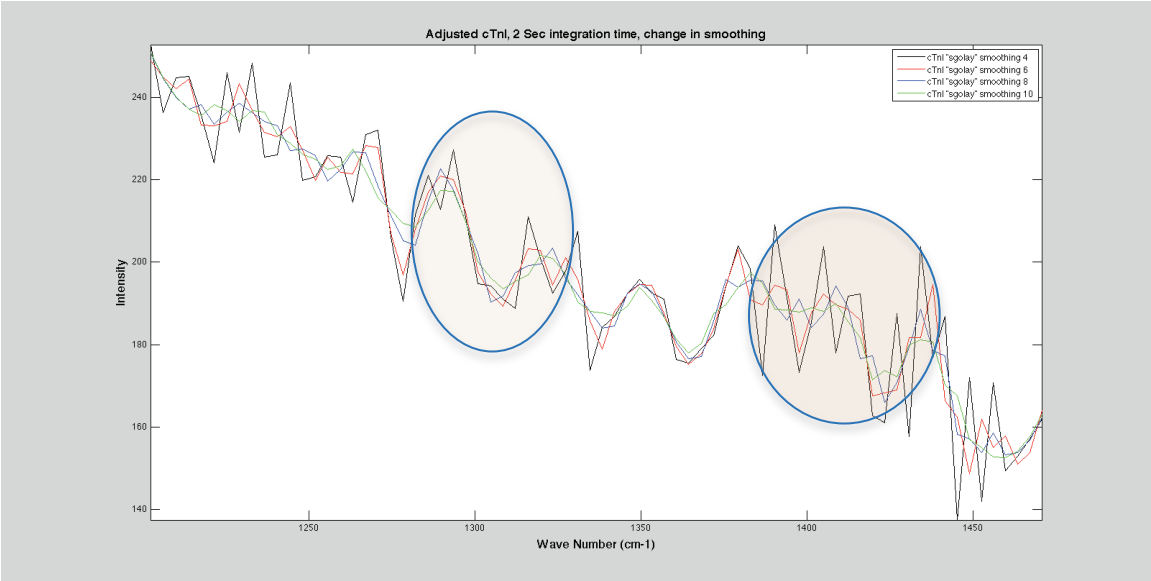

Figure 21: Snapshot of cTnI sample subtracted from water signal.

From the above graph we can conclude that polynomial fit of smoothing level using sgloay() function in *Matlab* presents the optimal noise reduction at level 6. Therefore, this level of noise reduction was used throughout this project.

4.2.1. Effect of change in concentration

Figure 22 illustrates the effects of concentration change on the adjusted cTnI sample using 5 seconds integration time. It can be confirmed from this graph that the intensity of the Raman spectra elevates as the concentration of cTnI the increases.

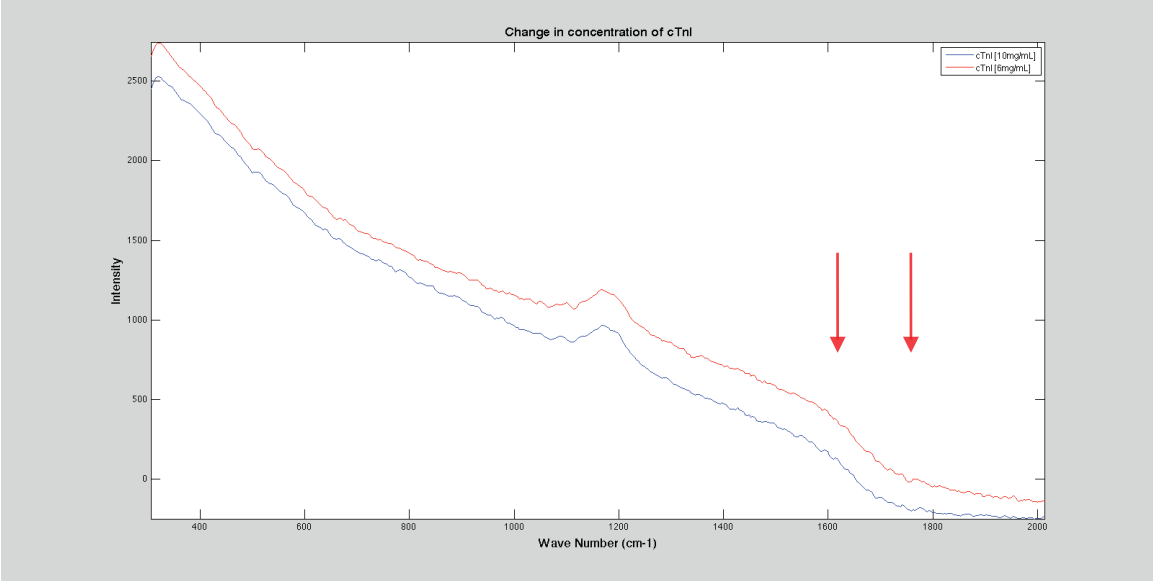

Figure 22: Effect of change in concentration, adjusted cTnI, 5 seconds integration time

4.2.2. Comparison with Previous Results

A close up of cTnI sample spectra is shown in Figure 23, which demonstrates the same signature presented in previous findings (shown Figure 24). We believe the region defined within the circle on the graph is the signature associated with cTnI in aqueous solution. This characteristic was seen with various concentrations of the samples.

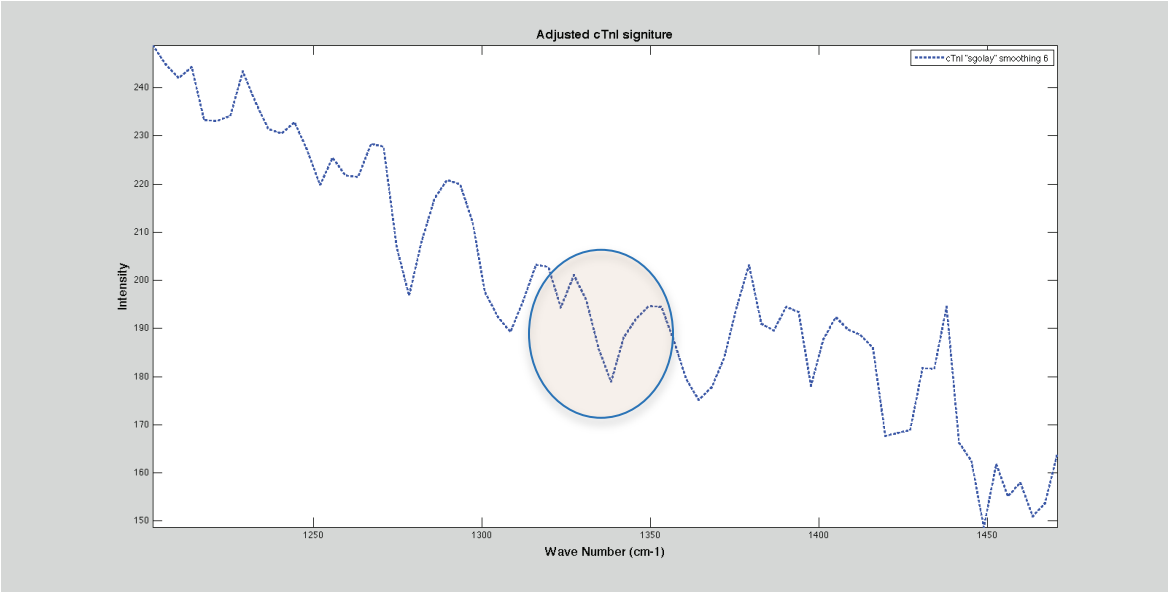

Figure 23: cTnI signature.

Figure 23 verifies previous findings regarding the location of cTnI signature, and serves as further indication that the protein can be characterized using Raman spectroscopy.

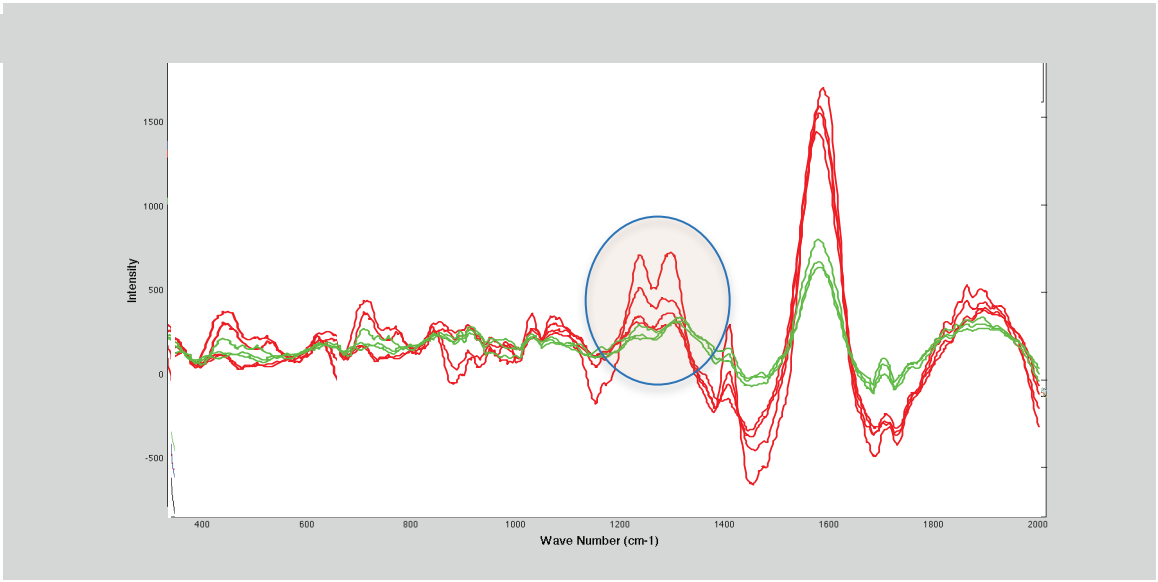

Figure 24: Previous results for cTnI signature.

5. The latest Spectral Result of cTnI in BSA

The novelty of this research is the fact that for the first time Raman spectroscopy of cTnI is observed and documented through designing and performing a series of experiments. After re-evaluating and reproducing the cTnI Raman signature in the previous chapter, in this section our final experimental result is presented. Herein, we identify the exact position of the mouse wild type non-phosphorylated cTnI peaks when measured in Bovine Serum Albumin (BSA). Moreover, results in this chapter define a boundary for concentration, as well as integration time conditions for future instrumentation purposes of this research.

5.1. Results and Discussions

In order to further verify the possibility of cTnI measurement using Raman spectroscopy, we designed and performed a number of experiments in various experimental environments and conditions. As stated in the previous section, we continued the assessment after we verified the cTnI signature. This section presents various results from the latest set of experiments. Further measurements on several iterations of different concentrations of cTnI and BSA in water are shown in the following figures. The experiments presented in this section are measured with a new Raman spectroscopy device and the apparatus setting is as follows: laser wavelength of

785 nm and the full laser power of 140 mW. Moreover two types of cTnI samples in various concentrations were used for all of the following experiments (marked as cTnI[1] and cTnI[2]) in order to verify that the observed peaks are validly related to the cTnI protein. cTnI[2] is a more recently synthesized protein and the date of preparation is September 14, 2011 as compared to cTnI[1] which was prepared on March 24, 2009, and stored in powder form since then.

Figure 25 illustrates the raw cTnI, BSA and water spectra. These spectra can be used to initially distinguish between the three samples and pinpoint the visible differences in the signals.

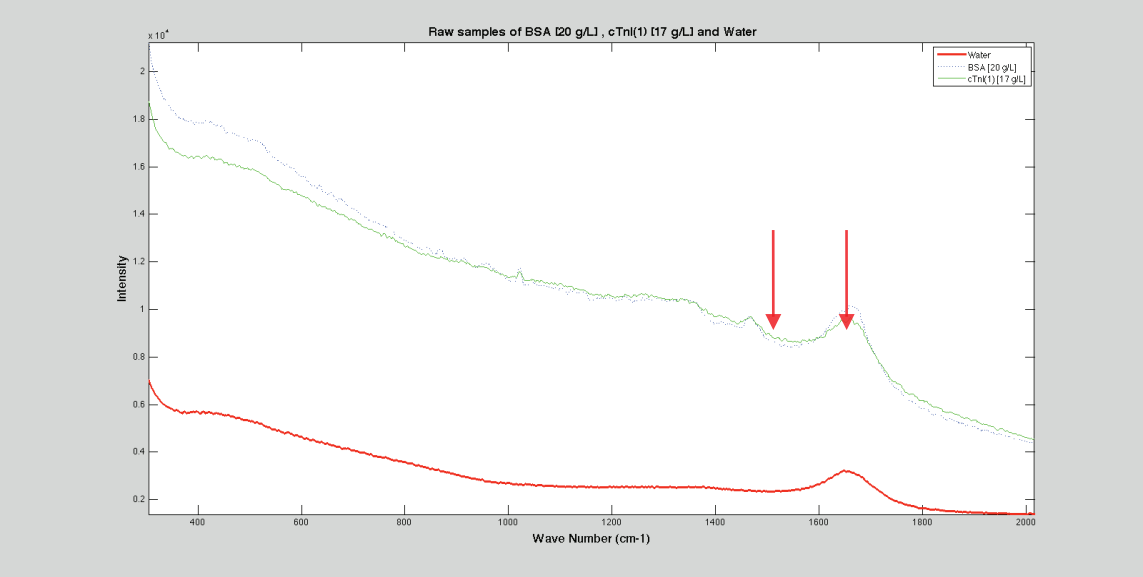

Figure 25: Raw samples of BSA [20 g/L] , cTnI(1) [17 g/L] and Water

Based on differences in the raw spectra of cTnI and BSA in the above figure, we have concluded that by performing signal processing of the spectra, a unique

characteristic of the signal can be extracted and used as detection strategy to distinguish cTnI from the noise.

5.1.1. Effects of Change in integration time

Figure 26 and Figure 27 present the change in concentration of the cTnI sample spectra with respect to change in integration time.

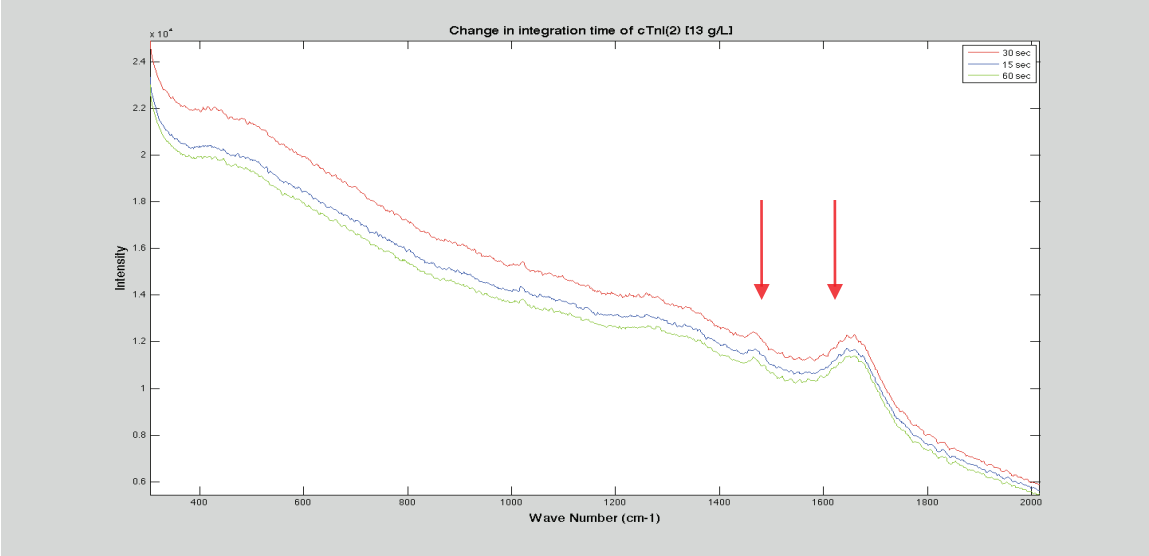

Figure 26: Change in integration time of cTnI(2) [13 g/L]

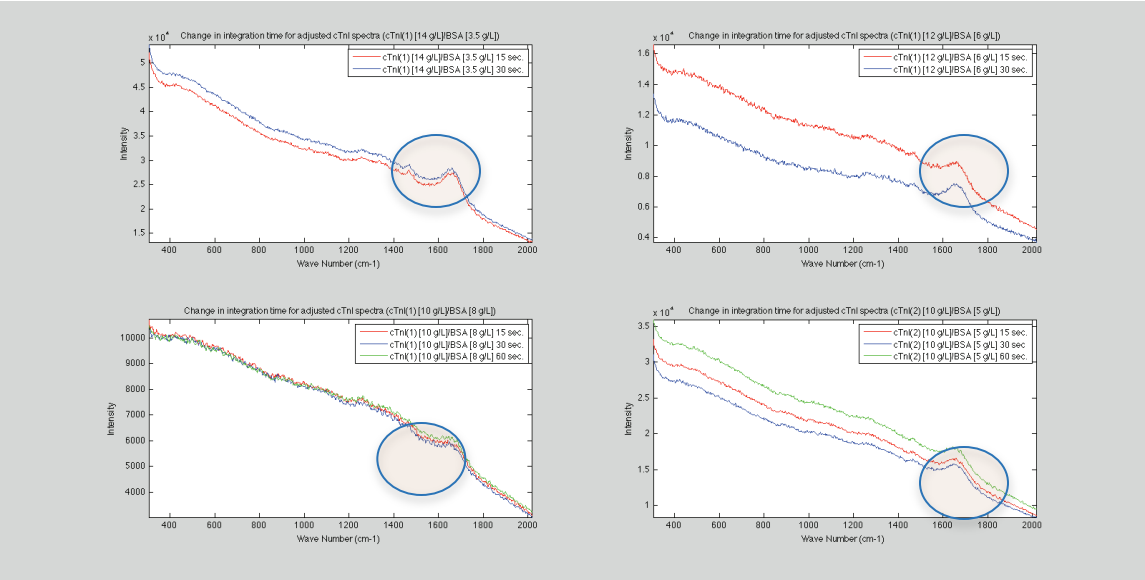

Figure 27: Change in integration time for adjusted cTnI spectra (cTnI(1) [14 g/L]/BSA [3.5 g/L]), (cTnI(1) [12 g/L]/BSA [6 g/L]), (cTnI(1) [10 g/L]/BSA [8 g/L]), (cTnI(2) [10 g/L]/BSA [5 g/L])

From Figure 26 and Figure 27, it can be appreciated that as the integration time decreases, the signal-to-noise ratio is also decreased. Other than the effect of signal to noise ratio, we have observed that when the laser is on the sample for 60 seconds or longer, the signal intensity decreases. This can be explained by the degeneration of the cTnI sample, secondary to heating from the laser. This degeneration does not compensate for the increased SNR and we can conclude that increasing the integration time is a compromise. Therefore, for the purpose of this research 30 seconds of integration time reproduces the most optimal results.

5.1.2. Effect of Change in concentration

Figure 28 represents processed data for increasing concentration of new cTnI samples. It can be noted from the graph that the signal intensity increases as the concentration of cTnI is increased. However, this relationship is non-linear and when the concentration of the protein is increased by 10 fold, the signal intensity does not increase by the same amount.

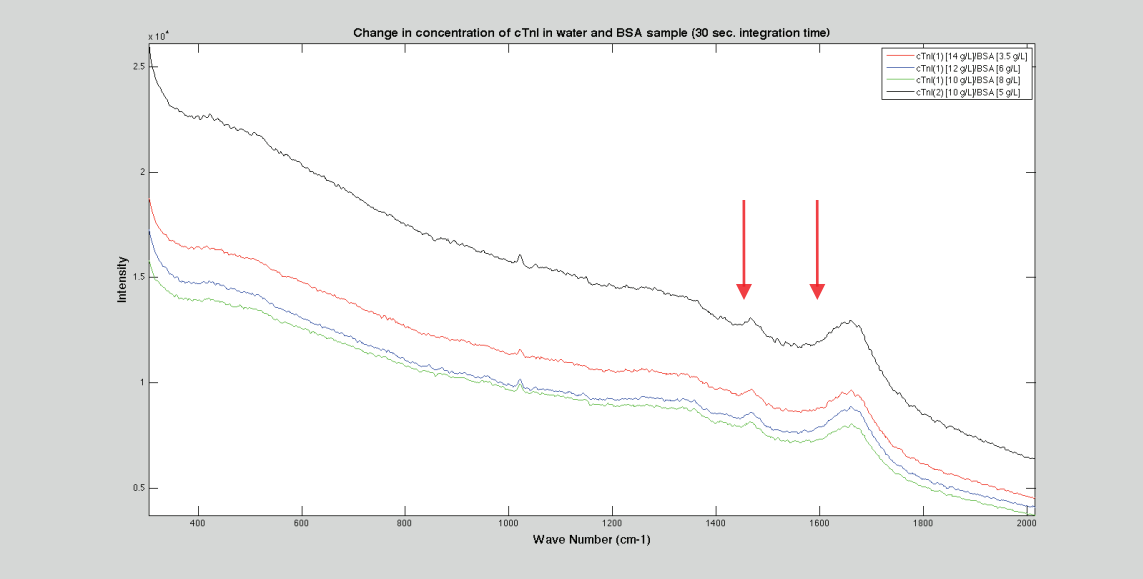

Figure 28: Change in concentration of cTnI in water and BSA sample (30 sec. integration time)

Therefore, even though we can conclude that cTnI Raman is quantitative, the relationship between the change in concentration of cTnI and its Raman signal is not linear and the intensity increase with the change in concentration is not very evident which again calls for a more sensitive signal processing method. Moreover, the black line in Figure 28 which represents the cTnI[2] Sample (the newly prepared cTnI) has a

relatively higher intensity compared to cTnI[1]. In fact, the more recently prepared sample has undergone less degeneration, providing a stronger detected signal. This further reiterates the fact that higher concentrations of the protein are directly correlated with higher intensity of the raw spectra.

5.1.3. Adjusted cTnI Spectra

In this section, signals are presented after deduction of noise caused by BSA in the sample. Further, the spectra are presented in Figure 29 after smoothing and filtration.

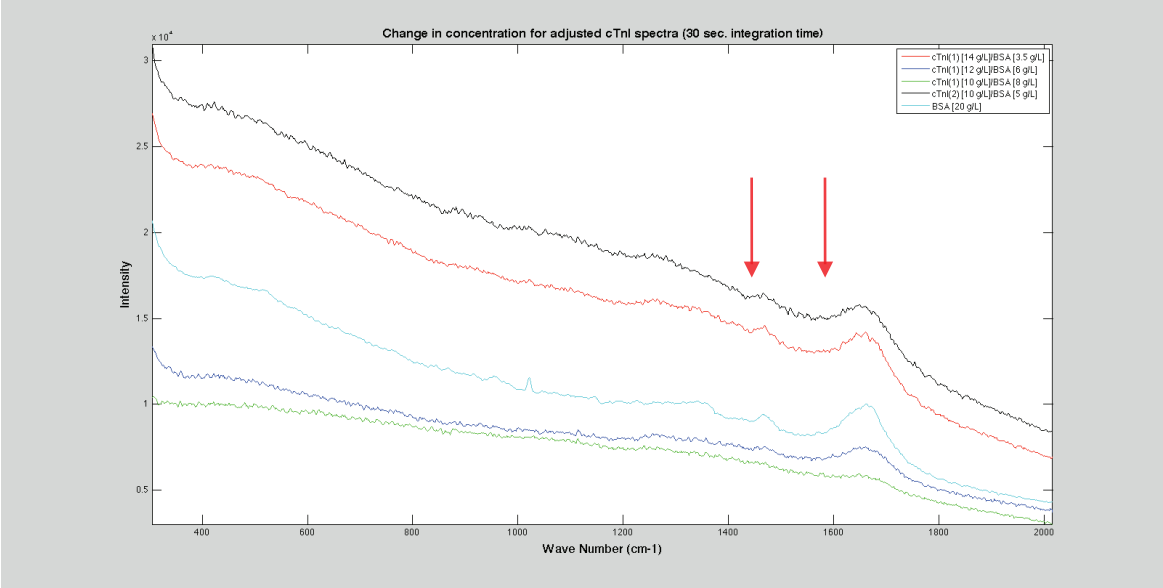

Figure 29: Change in concentration for adjusted cTnI spectra (30 sec. integration time)

From the above graph it can be noted that the peaks related to cTnI are not visible without performing signal processing. Limited by the sensitivity and SNR of the current Raman instrument, the difference signal carries a large noise ratio. Although,

slight amplitude differences in some regions of the signal are observed, it is difficult to conclude an essential difference. Further investigation and signal processing can greatly improve the SNR of Raman signal and make the difference more revealing. The new strategy will make the relationship between Raman spectral difference and cTnI absorption more clear and convincing.

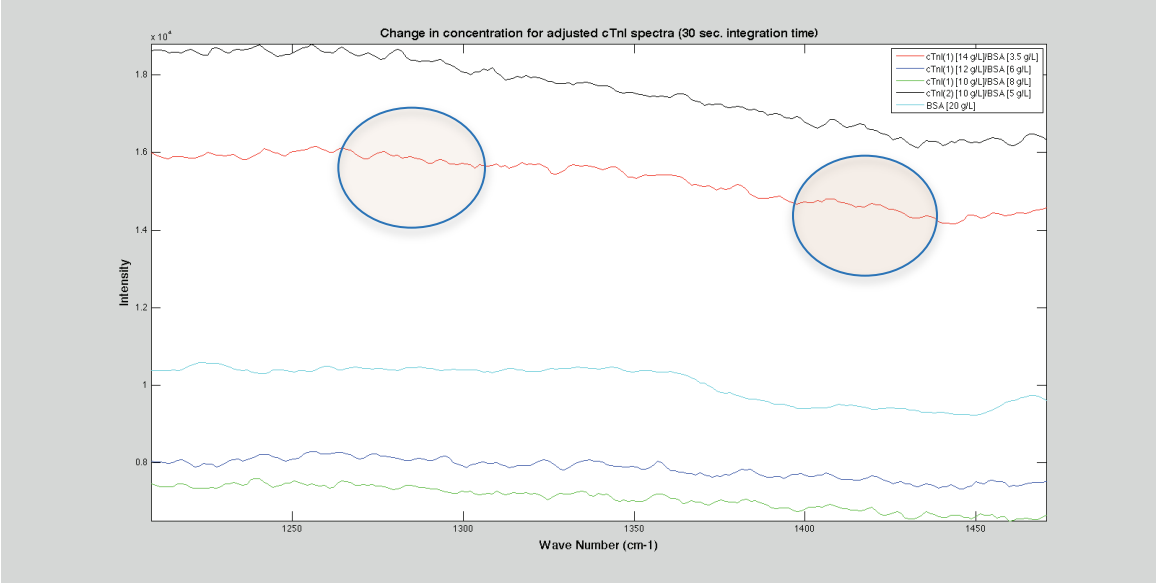

Figure 30: cTnI signiture zone, Change in integration time for adjusted cTnI spectra (cTnI(1) [10 g/L]/BSA [8 g/L])

As it will be shown in the wavelet transform result in the next section, the two unique windows related to cTnI's unique signature are between 1237 cm^{-1} to 1303 cm^{-1}, and 1375 cm^{-1} to 1450 cm^{-1}.

5.2. Wavelet Transform

The following experiments are performed using an industrial Raman spectrometer, located at the UBC Grant Group Laboratory, using a 785 nm laser with full laser power at 140mW. The analyzed data in the following graphs represent the subtracted, averaged, and de-noised version of the raw cTnI spectra. Moreover, wavelet transform analysis has been performed on the results for easier distinction between the peaks of interest.

Figure 31 illustrates the Fast Wavelet Transform result for water, BSA and cTnI. It can be seen that this method creates a frame of reference to compare the spectra.

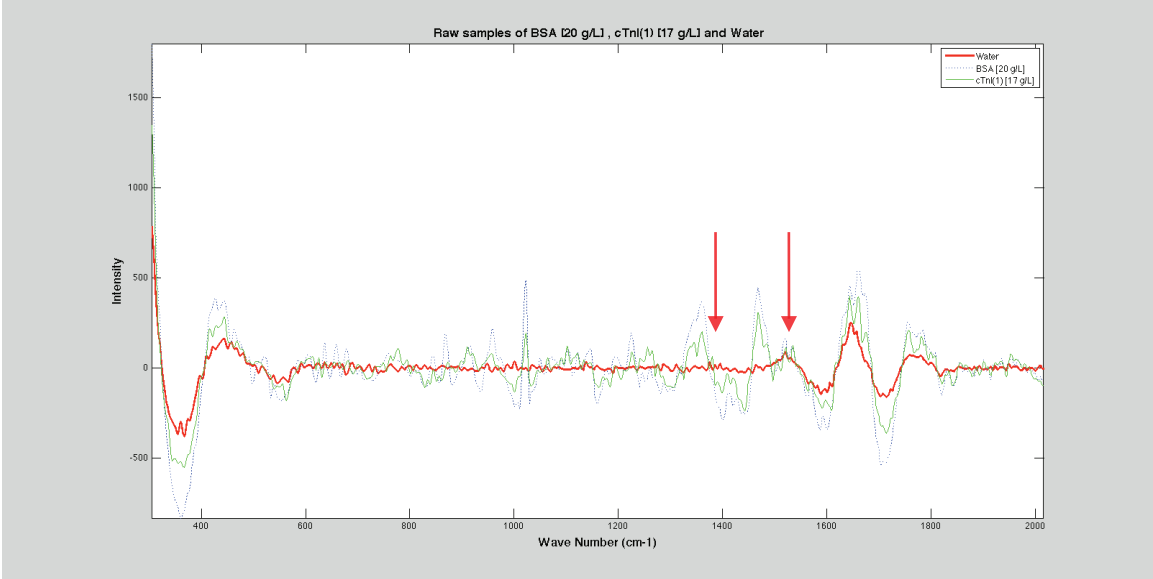

Figure 31: FWT Raw samples of BSA [20 g/L] , cTnI(1) [17 g/L] and Water

5.2.1. Effect of Change in integration time

After a series of literature review on the Raman signal processing of biological compounds, we have found the polyfit analysis of the raw data to be the conventional way to analyse the Raman data of a very low intensity signal level.

After finding the polyfit spectra, this signal was subtracted from the raw spectra of cTnI in order to reduce all signals to the baseline for easier comparison. In addition, Savitzky–Golay (SG) smoothing tools were used to de-noise the data using sgolay() function in Matlab.

Figure 32 and Figure 33 illustrate the effect of change in the integration time on the fast wavelet transform processed cTnI spectra.

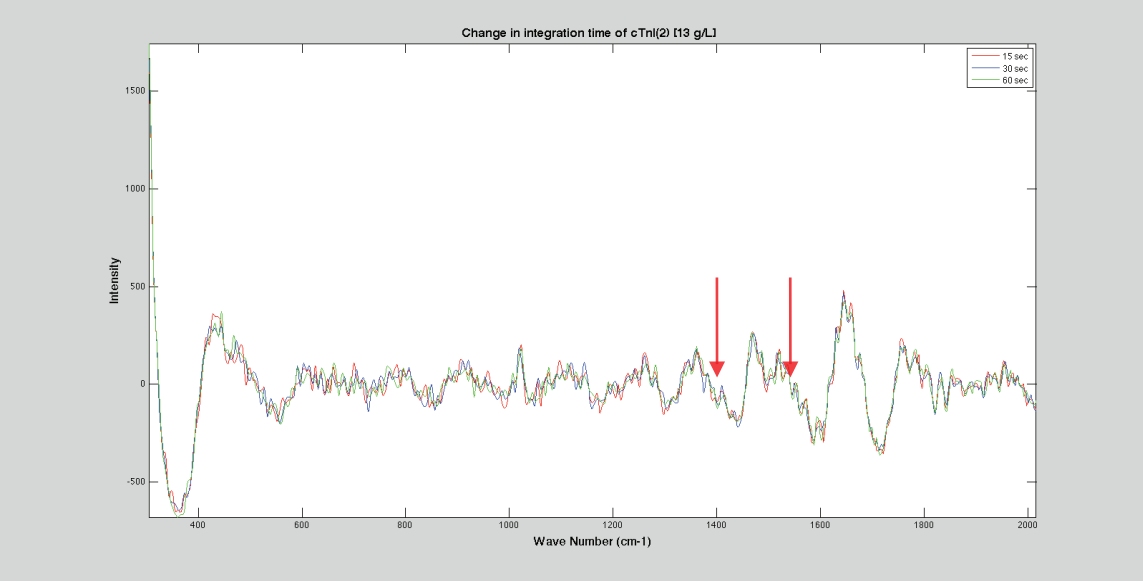

Figure 32: FWT Change in integration time of cTnI(2) [13 g/L]

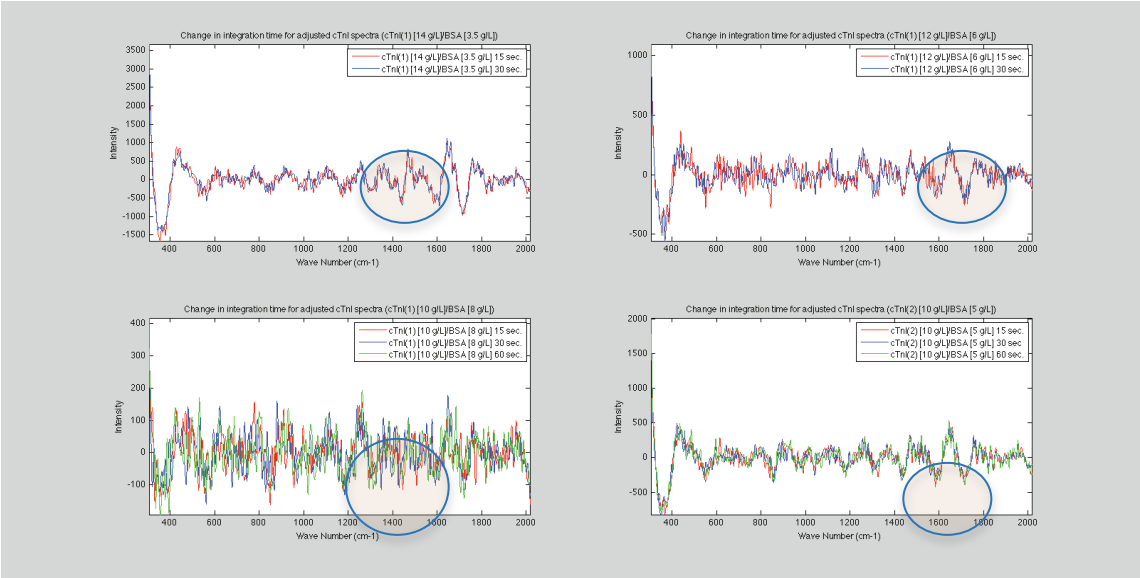

Figure 33: FWT Change in integration time for adjusted cTnI spectra (cTnI(1) [14 g/L]/BSA [3.5 g/L]), (cTnI(1) [12 g/L]/BSA [6 g/L]), (cTnI(1) [10 g/L]/BSA [8 g/L]), (cTnI(2) [10 g/L]/BSA [5 g/L])

These graphs indicate that after performing the wavelet transform on the same signals with different integration time, only the SNR changes with no appreciable changes to the peak. Therefore, collectively from the new experiments as well as the previous experiments on changing the laser power for the same measurements, we can conclude that the experimental conditions such as laser power and integration time do not affect the positioning of the peaks of interest.

5.2.2. Effect of Change in concentration

Figure 34 is an overlay of both old and new cTnI spectra for various concentrations. The black signal is from the new cTnI and other signals are from different concentrations of cTnI samples. The graph shows that Raman intensity of the

cTnI[1] sample at various concentrations does not demonstrate a large change in the intensity after the wavelet transform is performed.

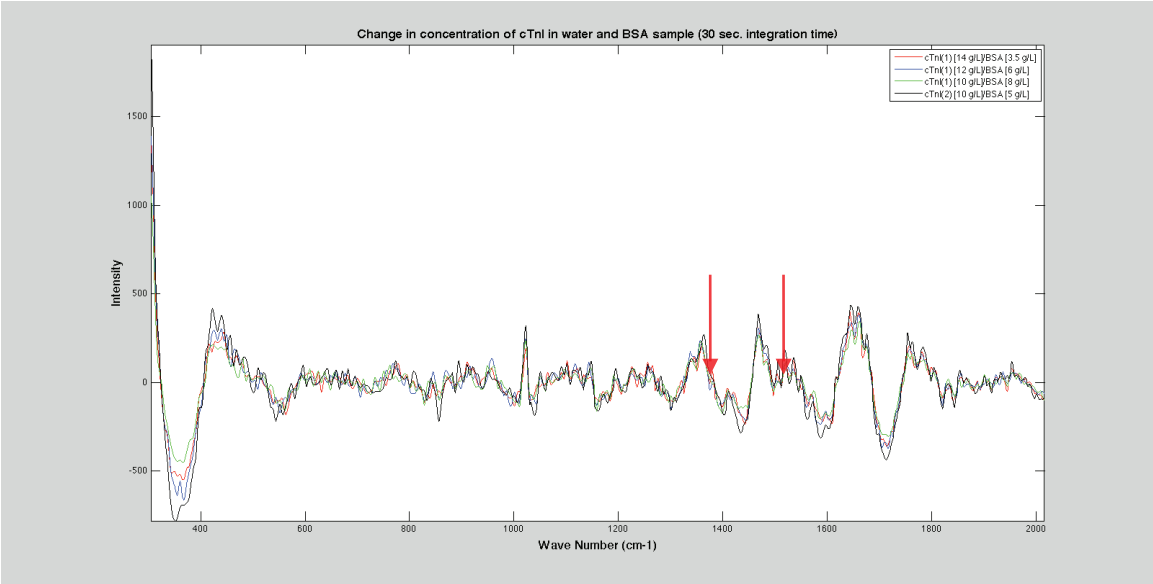

Figure 34: FWT Change in concentration of cTnI in water and BSA sample (30 sec. integration time)

Considering the graph above, it can be noted that even though the concentration of the old cTnI samples were higher than the newer samples, the intensity is lower. A possible explanation for this is that the amount of impurities was larger with more denaturation of the proteins in the old cTnI samples. However, this result is only valid to a point where the concentration and SNR allows for detection of cTnI. The peaks change as the noise level increases and cTnI peaks are not visible. In all of the experiments conducted for this research, we can measure the cTnI protein in concentrations 100 times higher than physiological concentrations.

5.2.3. Adjusted cTnI Spectra

As previously mentioned, the purpose of this research is to find the unique Raman signature of cTnI to be later used as a mean for early prediction of myocardial infarction. Figure 35 present the fast wavelet transform of various concentrations of cTnI sample (cTnI -BSA samples after subtraction of BSA) and the BSA spectrum shown in blue. Segments of cTnI spectra, determinant of the protein's signature and its intensity, are above that of BSA and can be seen in Figure 35 for all cTnI concentrations.

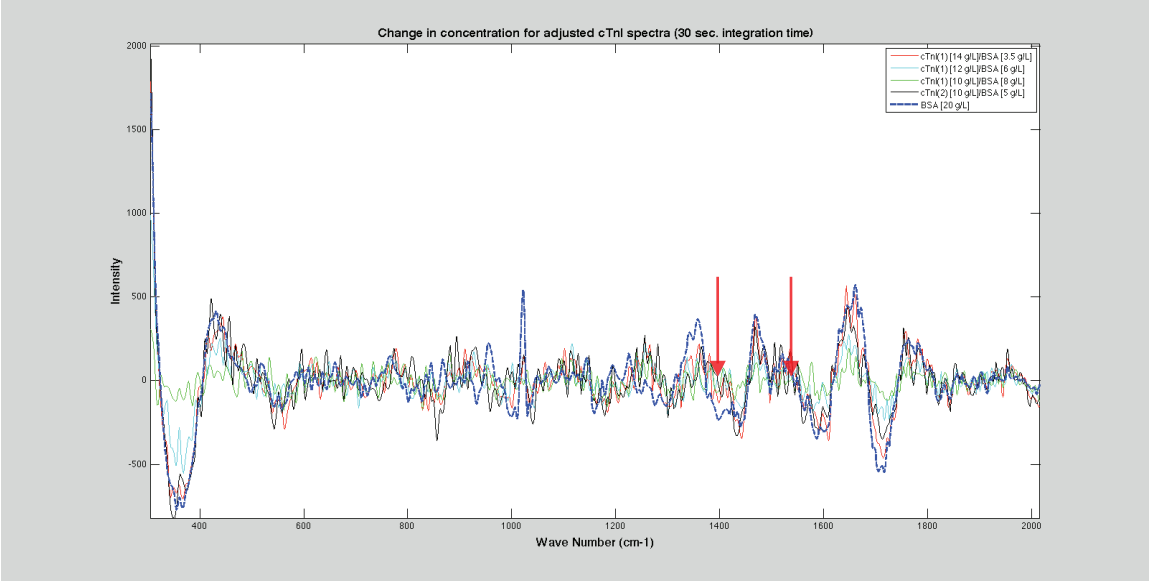

Figure 35: FWT Change in concentration for adjusted cTnI spectra (30 sec. integration time)

Figure 36, shows the overlay graph of various concentrations of cTnI and BSA spectra in the 1200 cm^{-1} to 1470 cm^{-1} window where most of the cTnI characteristic resides. From the results in this section, it can be deduced that both the wavelet

transformed data and raw signals are required to be able to first locate the exact peaks, and detect the concentration increase.

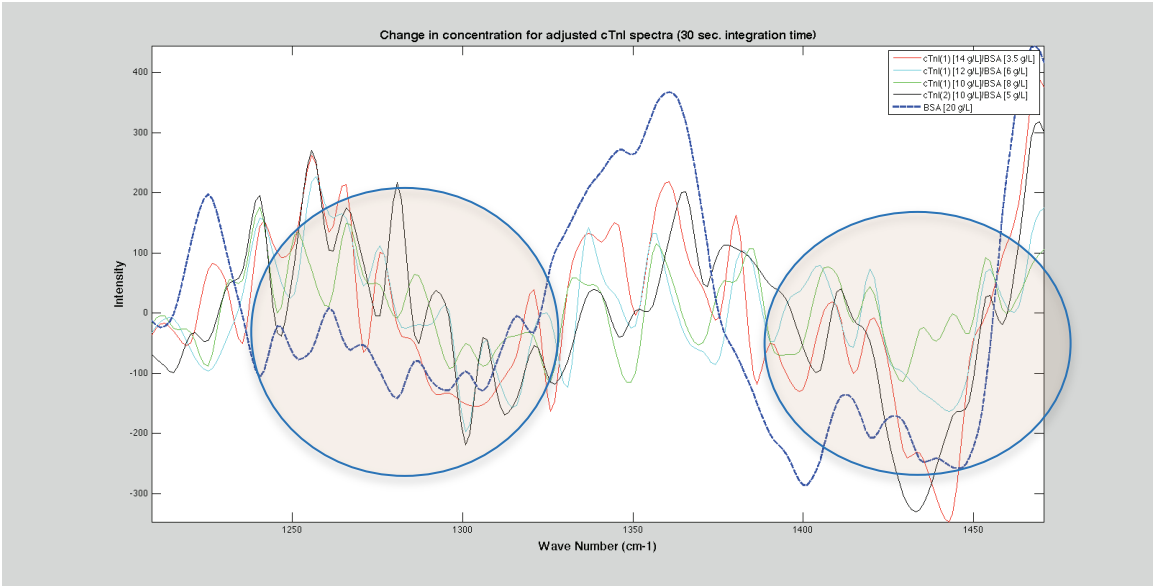

Figure 36: FWT Change in integration time for adjusted cTnI spectra (cTnI(1) [10 g/L]/BSA [8 g/L])

As demonstrated in Figure 36, the two smallest windows related to cTnI's unique signature is between 1237 cm^{-1} to 1303 cm^{-1} and 1375 cm^{-1} to 1450 cm^{-1}. These results verify the possibility of extracting cTnI spectra from BSA, which is one of the larger proteins that can be used as an arbitrary noise. Arguably, BSA was a logical next step after experimentation in water, before this apparatus can be optimized for detection of cTnI in intact human blood.

5.3. Discussion and Conclusion

Figure 38 illustrate discrepancies between peaks present on the BSA and water Raman scattering of cTnI. These peaks were analyzed using existing literature, amino acid sequence and protein foldings. The region outlined in the figure (approximately 600 cm-1) demonstrates three peaks in BSA Raman signals, which are absent in water and cTnI. One possible explanation for this inconsistency is the presence of disulfide bonds in BSA, which are nonexistent in the water and cTnI. In fact, BSA contains 17 disulfide bridges from residues 77 to 590.

Further, the arrow indicating the region at approximately 850 cm^{-1} may be secondary to the presence of Tyrosine (Try). BSA contains 21 tyrosines (3.5% of the amino acids) while cTnI contains 4 Try (1.9% of amino acids). While the orientation, different substitution symmetry and neighbouring amino acids might shift signals and alter the intensities; a sharp peak observed at the region is characteristics of Tyrosine. [30]

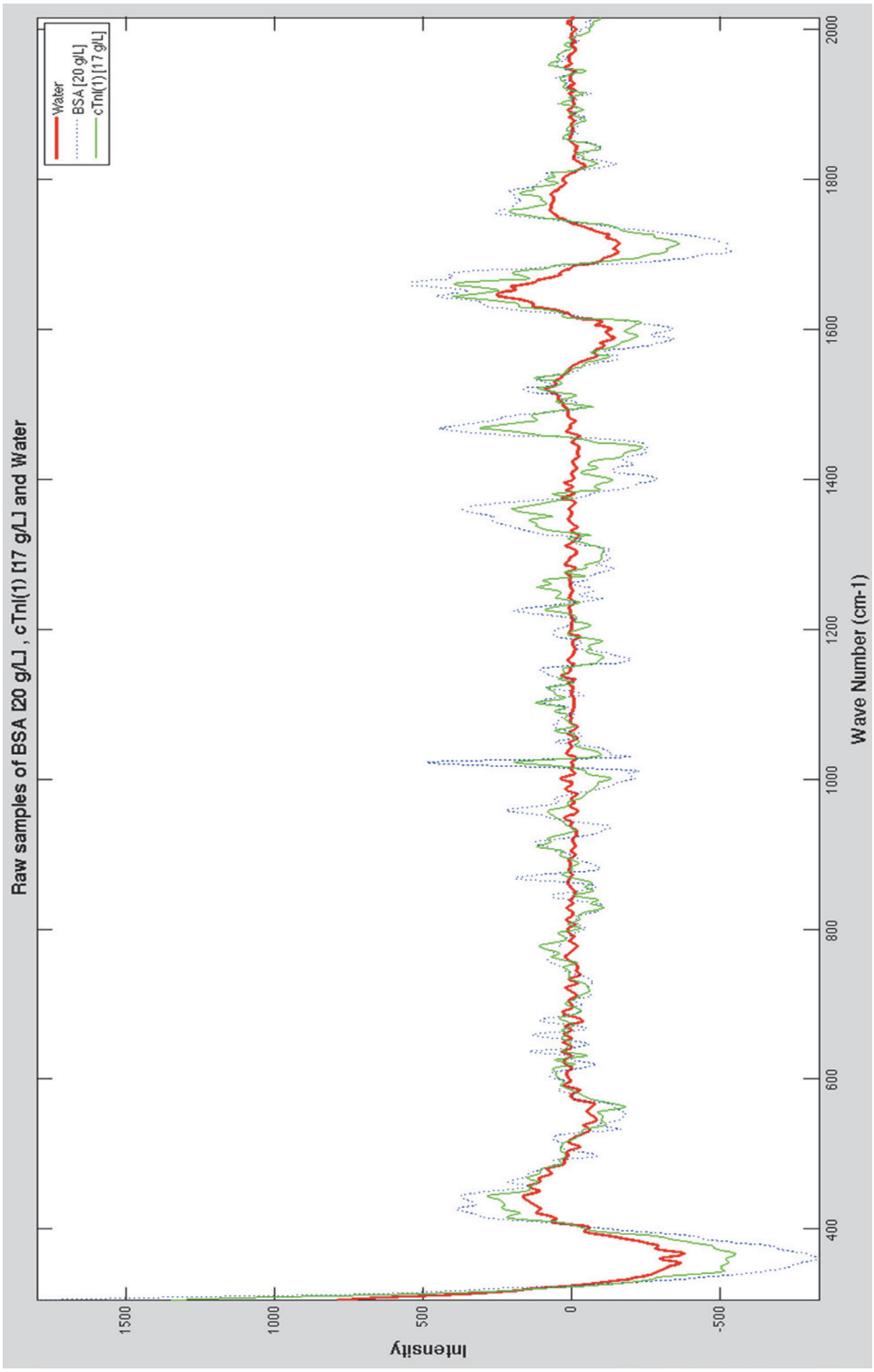

Figure 37: cTnI and BSA Raman Peak Analysis

The region shown by rectangular, at about 1000 cm^{-1} suggests the characteristics of Phenylalanine (Phe). BSA has 30 Phenylalanine (5% of the amino acids) while cTnI has three (1.4% of the amino acids). This can explain the higher intensity of BSA peak in comparison to cTnI. The peak shown by an arrow at approximately 1350 cm^{-1}, may explain the presence of Tryptophan (Trp), which is also shown in Figure 38.

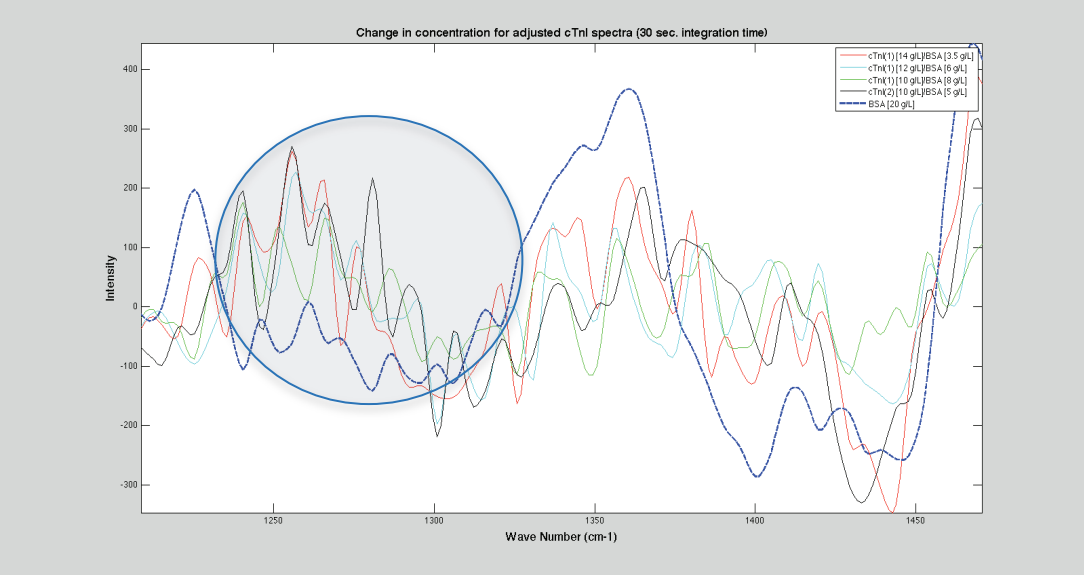

Figure 38: cTnI Raman Signature Region

As illustrated in the graph, these peaks are absent in the BSA Raman signals, despite the fact that BSA has three Tryptophan at residues, 3, 158 and 237, while cTnI has only one Tryptophan at the 191 residue. The BSA Tryptophan at residue 3 belongs to this protein's signal peptide and consequently is highly exposed to the environment. As shown in yellow in Figure 39, BSA Tryptophan at residues 158 and 237 are also largely exposed to the surroundings. Since Tryptophan has significant fluoresces properties, the florescence emission from this amino acid overwhelm the Raman back scattering

which results in absents of these peaks as number of Tryptophan residues increase in a protein.

The interpretations of these peaks are based on the current literature. [30] Considering the limited number of scientific studies published on the topic, further reports are necessary to confirm these findings. Moreover, due to the particular sensitivity of Raman spectroscopy to orientation and protein folding, the associated wave numbers are only approximate and must be further researched using more intricate equipment.

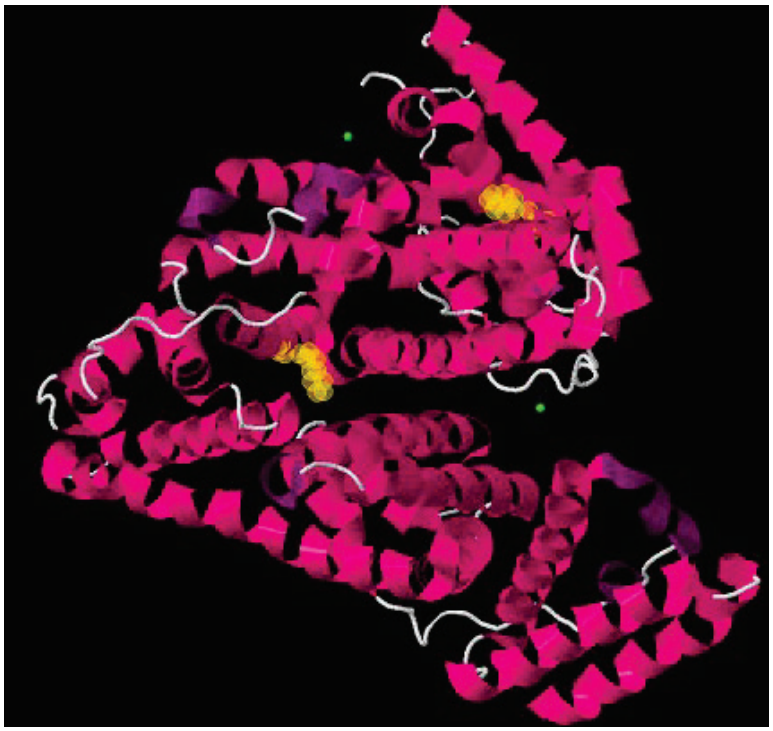

Figure 39: The Tertiary structural model of BSA

6. Conceptual Design of Raman Detection of cTnI System

6.1. Literature Review

To our knowledge the most similar technological design to our concept is one patented by Anthony J. Durkin in 2004. This patent utilizes Raman spectroscopy through the human eye and is designed as a glucose monitoring device, intended for management of Diabetes Mellitus. This device provides further encouragement for our eventual goal of concept implementation in the setting of MI. Figure 40 is a representative diagram, outlining the principles behind this patent. Through this device, Raman spectroscopy is used "to non-invasively detect the molecular characteristics [as well as] constituents of the aqueous humor, vitreous humor, lens or retina". [34] Through a step wise apparatus, light is introduced into the patient's eye using laser, Raman spectra are collected onto the detector and analyzed, and the detected spectra are used for identification of molecular changes. [34]

Our intended future approach is similar to the mentioned system; differences included our intended collection site, which is the area in the back of the human eye, on the surface of the retina and close to the optical nerve, which serves as the only area of the body where blood vessels can be directly visualized. In fact, this strategic area is routinely visualized by ophthalmologists in patients with high blood sugar levels in order

to assess the extent of direct damage to the vessels from states of chronic hyperglycemia. For experimental purposes, we can integrate principles from confocal microscopy in order to focus the laser as a specified blood vessel on the retina and obtain signals from this selected region of interest. [34]

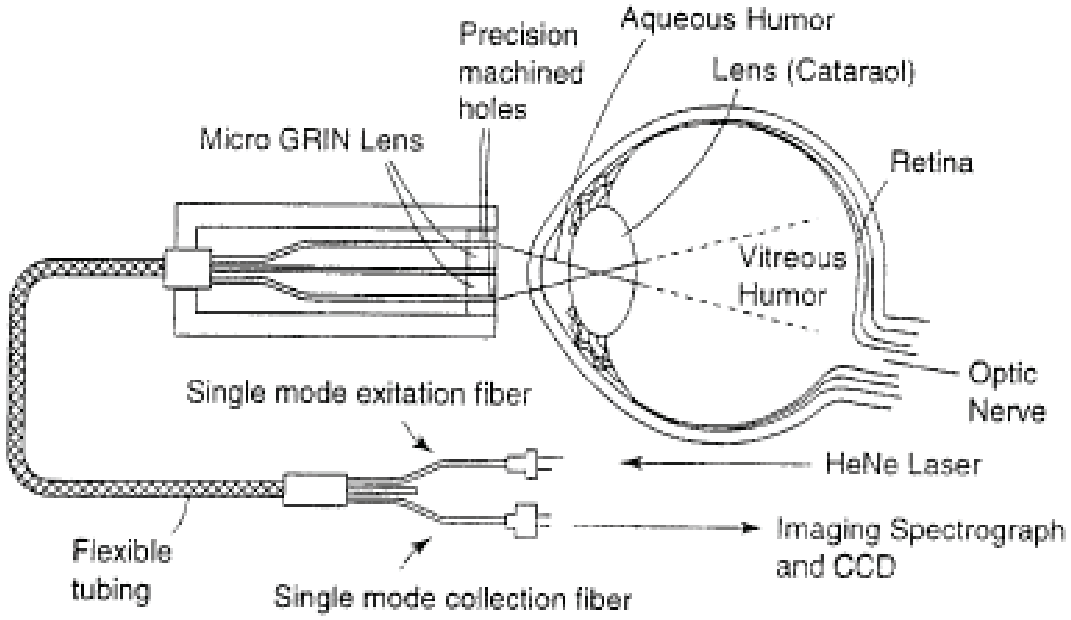

Figure 40: Patent diagram of Raman Spectrometer for Glucose Measurement form Human Eye [34]

6.2. Conceptual Design of Raman Detection of cTnI System

The focus of this research so far has been on finding the Raman spectrum of cTnI. The last part of the proceeding research is based on designing a conceptual proof of concept for a device to be used as Raman spectroscope for measuring cTnI from the eye. Figure 41 diagrams anatomical landmarks in the human eye, illustrating the minimal barriers between the external environment and visualization of internal blood

vessels. This unique anatomical feature of the eye is used commonly in clinical diagnosis and also allows optimal implementation for our project as the retinal vasculature can serve as a good platform for spectroscopic reading. In addition to the vascularity, the transparent nature of the aqueous humour further aids device implementation.

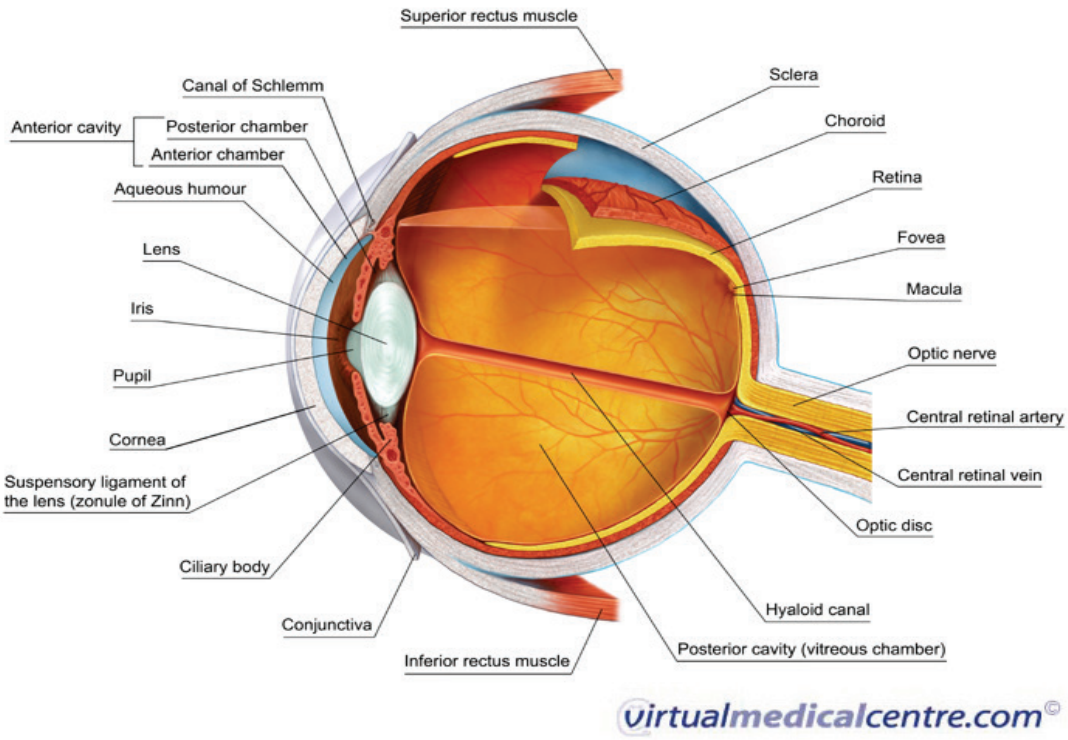

Figure 41: Anatomy of the eye [35]

Figure 42 further demonstrate the abundance of blood vessels in the region juxtaposed and overlying the entrance of the optic nerve into the eye. Due to inherent anatomical characteristics of the retina and image processing of the eye, this region of the retina does not contain any photoreceptors and is often called the “blind spot”; this characteristic is beneficial in our device will likely be more safe for use if the laser

applied for detection does not come in contact with the natural photoreceptors of the eye and utilizes vessels from the blind spot.

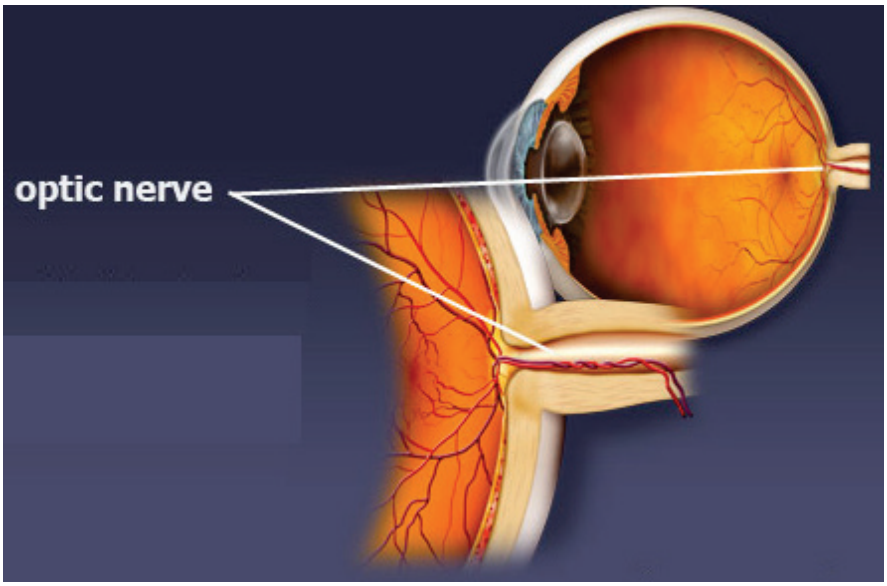

Figure 42: Optic Nerve, Sampling point of interest [36]

Figure 43 presents a potential Raman spectroscopy configuration in the human eye. A major difference between our illustrations as compared to that depicted in Figure 40 is that the former is focused at a specific point on a chosen vessel whereas the latter is full field focused.

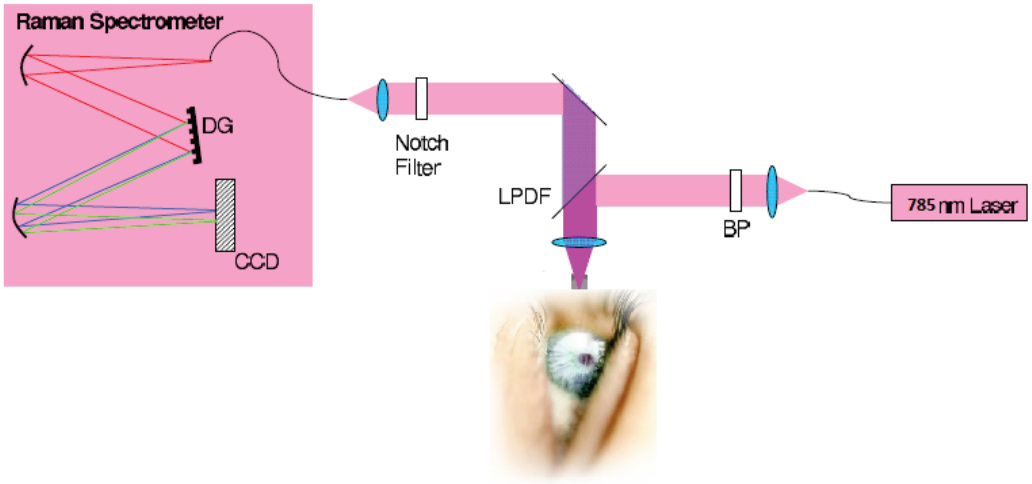

Figure 43: Possible Raman Spectroscopy configuration for conceptual system. In this configuration, DG stands for Diffraction Grating, LPDF for Long Pass Dichroic Filter, and BP for Band pass Filter.

Figure 44 presents a combination of subsystems, which can be used as our conceptual design and only uses Raman spectroscopy. The sample arm is used to find the point of interest to focus on, which in this case will be the optimal blood vessels near the optic nerve.

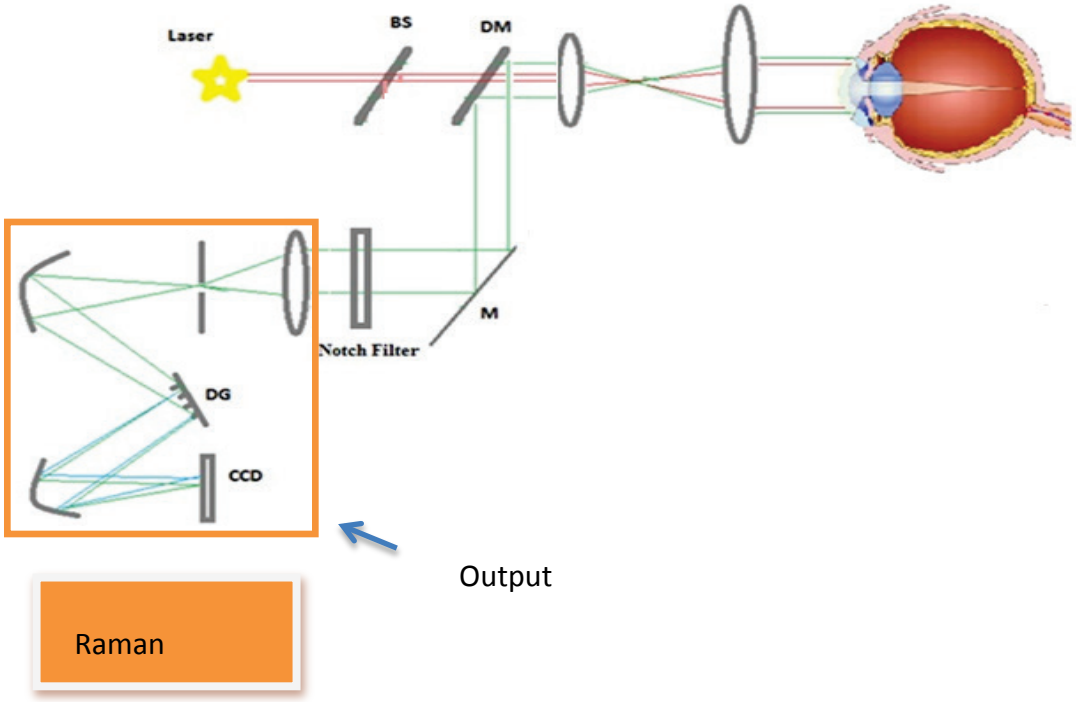

Figure 44: Overall Conceptual Optical Configuration

Finally, Figure 45 presents part of an overall conceptual design of the system. The excitation beam will be transmitted (in a short pulse form) from a small laser diode through the pupil and on to the retina. Consequently, the emission light is reflected back through the pupil and to a small prism, which in turn will reflect the light to a miniaturized CCD camera for measurement.

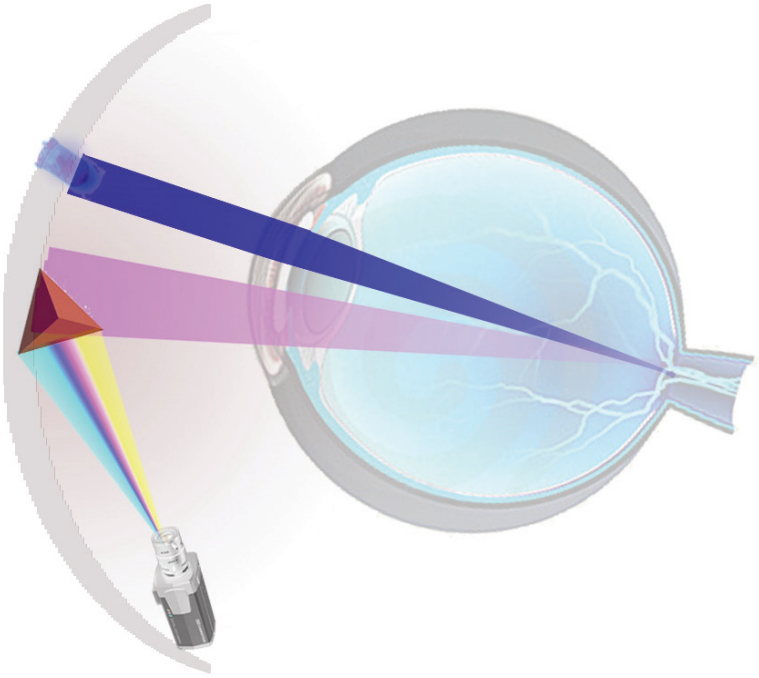

Figure 45: Conceptual Design of the system

7. Conclusion

The ultimate goal of this project was to decrease morbidity, mortality and the significant burden of disease associated with MI, using novel technology. Our very first design envisioned a device capable of wirelessly and continuously monitoring, recording and analyzing ECG readings from high-risk patients. The concept included ability for the device to automatically contact emergency crew with an abnormal reading. This concept was soon abandoned, realizing the relative lack of sensitivity and specificity associated with ECG readings in the setting of an MI. We consequently re-designed our concept, implementing florescence spectroscopy. Cardiac biomarkers are clinically and diagnostically superior to ECG readings, and were the most logical indicators of MI for the apparatus to detect; therefore, an attempt was made to detect cTnI concentrations using florescence spectroscopy. The Tryptophan amino acid in the protein sequence of cTnI was hypothesized to provide unique molecular florescence characteristics. However, limitations in currently available technology prevented us from successfully obtained a unique spectrum. Finally, in the current project, Biophotonics measurements of cTnI were successfully utilized as extensively discussed. Through this project, and to our knowledge for the first time in literature, we consistently characterized the unique Raman spectrum of mouse cTnI protein. This spectrum was verified several times and in different experimental and analytical settings, initially in water and subsequently in BSA.

Our choice of BSA as the experimental milieu represented its structural similarity to intact blood and served as a progressive step prior to apparatus optimization in human blood. The two narrowest and most consistently verified windows, relating to the unique spectrum of cTnI in BSA are between 1237 cm^{-1} to 1303 cm^{-1} and 1375 cm^{-1} – 1450 cm^{-1}.

However, we still face sensitivity limitations with our apparatus and the lowest concentrations of cTnI at which we were able to accurately characterize Raman peaks were one hundred times the physiological concentrations. Our approach to minimize this limitation was to enhance the signal to noise ratio (SNR) of the spectrum, through a wavelet transform analysis as discussed. We further optimized the apparatus by discovering that an attenuation of the integration time to as low as 2 seconds do not effectively alter our results and this finding will be beneficial in the latter instrument optimization and standardization stages of the project. Our results indicate that both wavelet transformation data as well as raw Raman signaling data are necessary in order to detect associated peaks as protein concentrations increase. We further learnt that under in *vitro* settings, changes in integration time with respect to Raman signal intensity is not linear, likely secondary to the degenerative effects of heating from the exposure to the laser, on the cTnI protein. Similarly, changes in concentration with respect to Raman signal intensity is not linear, secondary to the fact that our instruments are unable to linearly decrease block florescence signals, with linear decrease of cTnI concentrations. Perhaps, more advanced signal processing and CCD

cameras can further improve the SNR as well as the sensitivity of the apparatus to more physiological concentrations. In addition to this, further goals of this project include device miniaturization and calibration. The finalized device can eventually be supplemented by telemedicine ECG measurements as briefly discussed above, in order to serve as a comprehensive and non-invasive diagnostic apparatus for MI.

8. References

1. D. Lloyd-Jones et al. “Lifetime risk of developing coronary heart disease.” *The Lancet*, Vol. 353, Issue 9147, pp. 89 - 92, Jan. 1999.

2. D. Cullen et al. “Therapeutic Hypothermia Initiated in the Pre-Hospital Setting: A Meta-Analysis.” *Advanced Emergency Nursing Journal*, Vol. 33, pp. 314–321, Dec. 2011.

3. C. Baigent. “10 year survival among patients with suspected acute myocardial infarction in randomised comparison of intravenous streptokinase, oral aspirin, both, or neither”. *BMJ*, pp. 316:1337, May 1998.

4. E. Braunwald. “Biomarkers in Heart Failure”. *N Engl J Med*. Vol. 358, pp. 2148-2159, May 2008.

5. H. B. A. Wu. “Gender-Specific Decision Limits for Cardiac Troponin for Risk Stratification?”*International Anesthesia Research Society*, 2009.

6. A. Hans-Richard Arntz et al. “Initial management of acute coronary syndromes.” *European Resuscitation Council Guidelines for Resuscitation.* pp. 1353 – 1363, Oct. 2010,

7. T. Reichlin, et al. “Early Diagnosis of Myocardial Infarction with Sensitive Cardiac Troponin Assays”. *N Engl J Med*, vol 361, pp. 858-867, Aug. 2009.

8. A. Rasekh, M. Razavi and A. Massumi, “Sudden Cardiac Death”. *Cardiovascular Medicine*, Sec. IX, pp. 2039-2083, 2007.

9. H.M. Piper, Y. Abdallah and C. Schäfer, “The first minutes of reperfusion: a window of opportunity for cardioprotection”. *European Society of Cardiology*, 2003.

10. P. Anversa, and E. Sonnenblick, “Ischemic cardiomyopathy: pathophysiologic mechanisms.” *Prog Cardiovasc Dis*., vol. 33, pp. 49-70, 1990.

11. S. Moghaddamjoo, “Prediction Of Myocardial Infarctions, Using Non Invasive Biophotonics Measurement Of Cardiac Troponin I”, Thesis Submitted to Simon Fraser University Library, Dec. 2010.

12. L.M. Buja, “Myocardial ischemia and reperfusion injury”. *Cardiovascular Pathology*, vol. 14, issue 4, pp 170–175, Aug. 2005.

13. G. Ermak, and K. Davies, “Calcium and oxidative stress: from cell signalling to cell death”. *Molecular Immunology*, vol. 38, issue 10, pp713–721, Feb. 2002.

14. D.M. Bers, S. Despa and J. Bossuyt, “Regulation of Ca2+ and Na+ in Normal and Failing Cardiac Myocytes”. *Annals of the New York Academy of Sciences,* vol. 1080, pp. 165–177, Oct. 2006.

15. A. G. Katrukha et al. “Degradation of cardiac troponin I: implication for reliable immunodetection.” *Clin Chem* vol. 44 pp. 2433–440, 1998.

16. G. Lum, D. Solarz and L. Farney. “False Positive Cardiac Troponin Results in Patients Without Acute Myocardial Infarction”. *American Society for Clinical Pathology*, Mar. 2006.

17. Q. Shia et al. “Degradation of Cardiac Troponin I in Serum Complicates Comparisons of Cardiac Troponin I Assays”. *Clinical Chemistry*, vol. 45, no. 7 pp. 1018-1025, Jul. 1999.

18. D. I. Ellis and R. Goodacre, “Metabolic fingerprinting in disease diagnosis: biomedical applications of infrared and Raman spectroscopy,” *Analyst,* 2006.

19. The Encyclopaedia of Science, “Tryptophan”. Internet: http://www.daviddarling.info/encyclopedia/T/tryptophan.html [Mar. 23, 2012]

20. Microscopy Resource Center. “*Olympus Microscopy Resource Center”*. Internet: http://www.olympusmicro.com/primer/anatomy/sources.html [Apr. 15, 2009]

21. J. S. Alpert et al. “Myocardial infarction redefined: A consensus document of The Joint European Society of Cardiology/American College of Cardiology Committee for the redefinition of myocardial infarction”. *Journal of American College of Cardiology, vol* 36, pp. 959-69, 2000.

22. K. Hideo and K. Hirose. “Diagnostic accuracy of cardiac markers for myocardial damage after radiofrequency catheter ablation”. *Journal of Interventional Cardiac Electrophysiology*, pp. 169-174, 2009.

23. D. C. Collinson. “Multiple molecular forms of circulating cardiac troponin: analytical and clinical significance”. *Association for Clinical Biochemistry.* , pp. 349–355. 2008.

24. D. Ward, M. Cornes, I. Trayer. “Structural Consequences of Cardiac Troponin I Phosphorylation.” *The American Society for Biochemistry and Molecular Biology,* Aug. 2002.

25. A. G. Katrukha et al. “Degradation of cardiac troponin I: implication for reliable immunodetection”. *Clin Chem. vol.* 44, pp. 2433–440, 1998.

26. R. Labugger et al. “Extensive troponin I and T modification detected in serum from patients with AMI.” *Circulation*, vol. 102, pp. 1221–1226, 2000.

27. A. Van der Laarse. “Hypothesis: troponin degradation is one of the factors responsible for deterioration of left ventricular function in heart failure.” *Cardiovascular Res.* vol. 56, pp. 8–14, 2002.

28. Laser Focus World, “The American Society for Biochemistry and Molecular Biology”, Feb. 2012.

29. I.M. Vlasova and A.M. Saletsk. "*Raman spectroscopy in investigations of mechanism of binding of human serum albumin to molecular probe fluorescein".* Moscow: Lomonoaoy Moscow State University. *vol 5, Issue 5, 2008.*

30. A. Jenkins, R. Larsen and T. Williams, "Characterization of amino acids using Raman spectroscopy". *Spectrochimica Acta.* vol. 61, pp. 1585–1594, 2005.

32. A. Durkin, E. Marwood and C. Vivian, "Method for non-invasive identification of individuals at risk for diabetes." United States. *Patent No. US 6,721,583 B1,* 2004.

33. Virtual Medical Centre. "Anatomy of the eye and visions." Internet: http://www.virtualmedicalcentre.com/anatomy/the-eye-and-vision/28, 2012 [March 23, 2012]

34. National Eye Institute, Internet: http://www.nei.nih.gov/health/eyediagram/index.asp , 2008 [March 23, 2012]

35. J. Evans et al. "Optical coherence tomography and Raman spectroscopy of the ex-vivo retina." *Multimodal Biomedical Imaging IV, vol. 7171, pp. 13768-13784,* 2009.

36. A. Hans-Richard et al. "Initial management of acute coronary syndromes." *European Resuscitation Council Guidelines for Resuscitation*, pp. 1353 – 1363, Oct. 2010.

37. R. Labugger et al. “Extensive troponin I and T modification detected in serum from patients with AMI.” *Circulation*. vol. 102, pp. 1221–1226, 2000.

38. W. Neagoe et al. “Titin isoform switch in ischemic human heart disease.” *Circulation, vol.* 106, pp. 1333-1341, 2002.

39. T.J. Wang “Significance of circulating troponins in heart failure: if these walls could talk.” *Circulation*, vol. 116 pp. 1217-1220, 2007.

40. R. S. Vasan, “Inflammatory markers and risk of heart failure in elderly subjects without prior myocardial infarction: The Framingham Heart Study.” *Circulation* vol. 107, pp. 1486-1491, 2003.

41. R. Latini et al. “Prognostic value of very low plasma concentrations of troponin T in patients with stable chronic heart failure.” *Circulation*, pp. 116: 1242, 2007.

42. A. M. Annika et al. “Blood analysis by Raman spectroscopy”. *Optics letters*, vol. 27, issue 22, pp. 2004-2006, 2002.

43. F.S. Apple, “Cardiac Troponin Testing for Detection of Myocardial Infarction. Minneapolis” *Humana Press*, 2008.

44. D. M. Char, E. Israel, and J. Ladenson, “Early laboratory indicators of myocardial infarction,” *Emergency Medicine Clinics of North America*, 1998.

45. J. Clark. “Absorption Spectra-the beer-lambert law.” http://www.chemguide.co.uk/analysis/uvvisible/beerlambert.html, 2007, [April 26, 2009]

46. D. C. Collinson. “Multiple molecular forms of circulating cardiac troponin: analytical and clinical significance.” *Association for Clinical Biochemistry*, pp. 349–355, 2008

47. V. R. Eisenman. “Are all troponin assays equivalent in the emergency department?” *Singapore Medical Journal* , pp. 325-327, 2005.

48. G. D. Lewis et al. “Metabolite profiling of blood from individuals undergoing planned myocardial infarction reveals early markers of myocardial injury.” *Bioinformatics, vol 26, Issue 14*, pp. 3503–3512, 2008.

49. K. P. Soreng, “*Troponin I and troponin T in myocardial infarction diagnosis and risk assessment.” Tarrytown*, Bayer HealthCare LLC Diagnostics Division, 2008.

50. J. R. Lakowicz. *Principles of Florescence Spectroscopy. New York: Springer*. 2002.

51. S. Nie and S. R. Emory, “Probing Single Molecules and Single Nanoparticles by Surface-Enhanced Raman Scattering.” *Science*, vol. 275, issue 5303, pp. 1102-1106, 1997.

52. S. A. Takeda et al. “Structure of the core domain of human cardiac troponin in the Ca2+- saturated form,” *Nature*, 2003.

53. World Health Organization, “Deaths by cause, sex and mortality stratum in WHO regions,” *The world health report*, 2004.

54. Savitzky and M. J. E. Golay, "Smoothing and Differentiation of Data by Simplified Least Squares Procedures," Analytical Chemistry, vol. 36, pp. 1627-1639, 1964.

9. Appendix

9.1. cTnT

"*Figure 46* to

Figure 50 are the processed spectra of the samples. In these figures, the spectrum of 10 trials for each concentration is averaged and the background noise is subtracted from the signal. As mentioned in previous sections with respect to sensitivity and specificity cTnT possess similar characteristics to cTnI, therefore we acquired spectrum form this protein as well. The significance of analyzing cTnT in both the costume made buffer and BSA is to get insight on the differences between cTnI and cTnT and possibly investigate advantages of cTnT over cTnI for our purposes".[11]

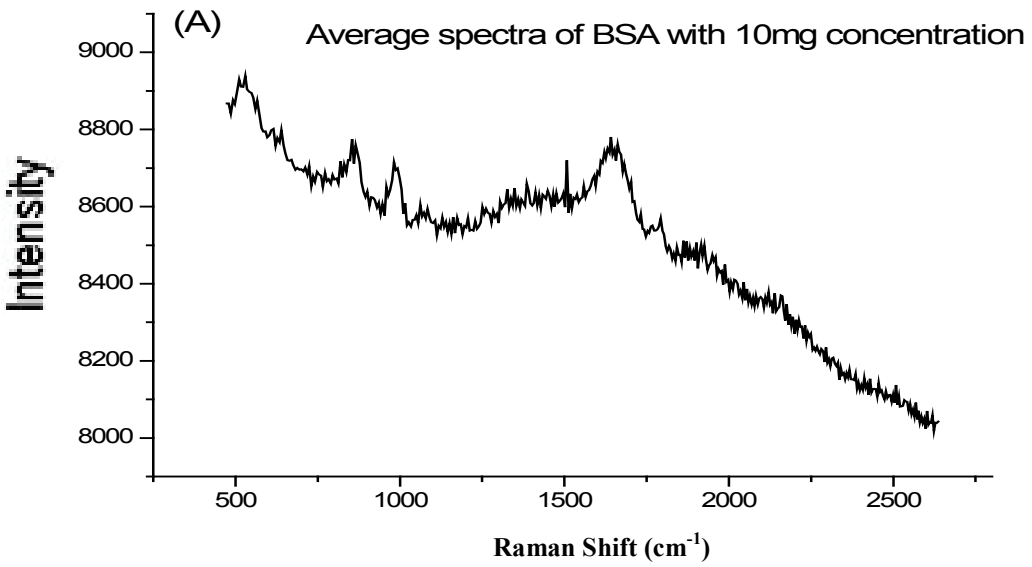

Figure 46: 10 mg/mL cTnI in Buffer Sample Raman Averaged

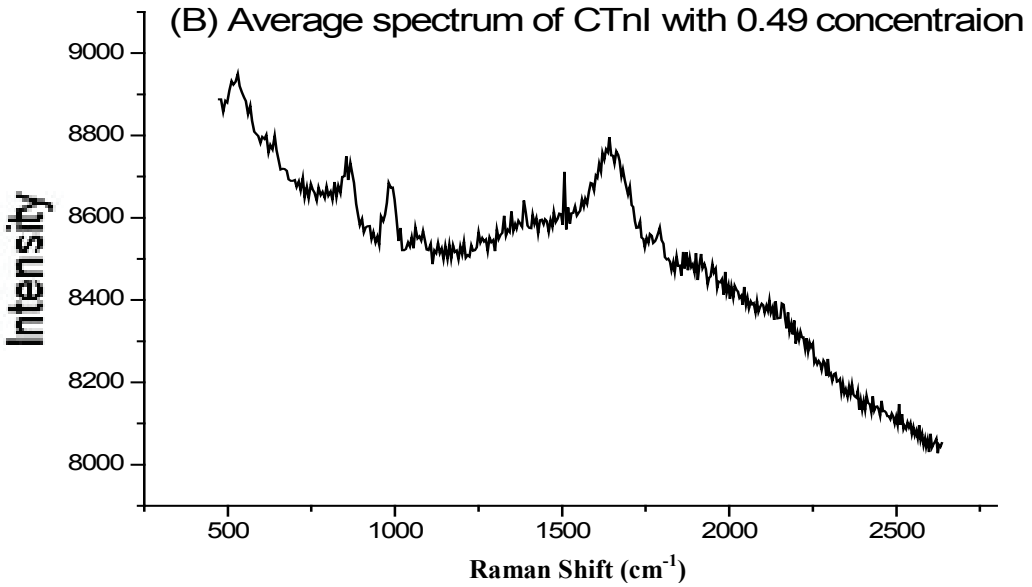

Figure 47: 0.49 mg/mL cTnI in Buffer Sample Raman Averaged

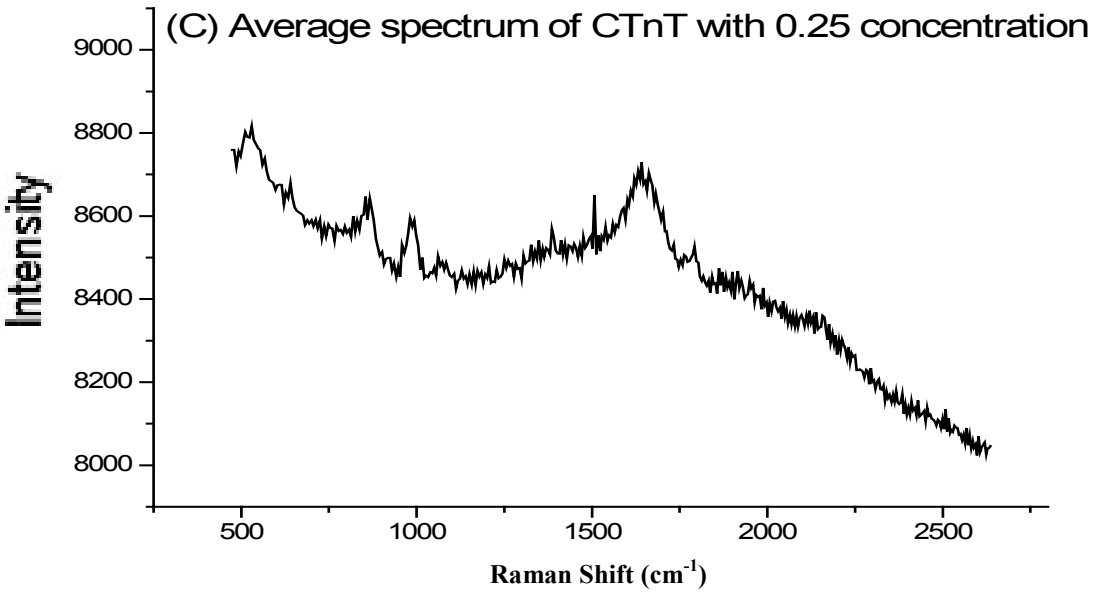

Figure 48: 0.25 mg/mL cTnT in Buffer Sample Raman Averaged

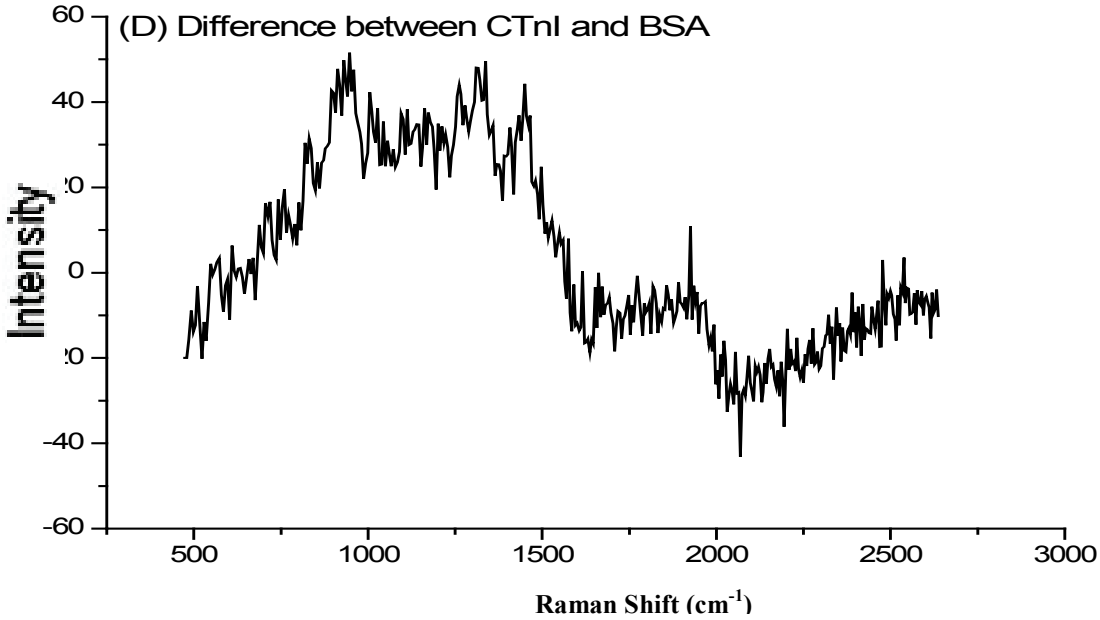

Figure 49: Difference between BSA and cTnI Raman signals

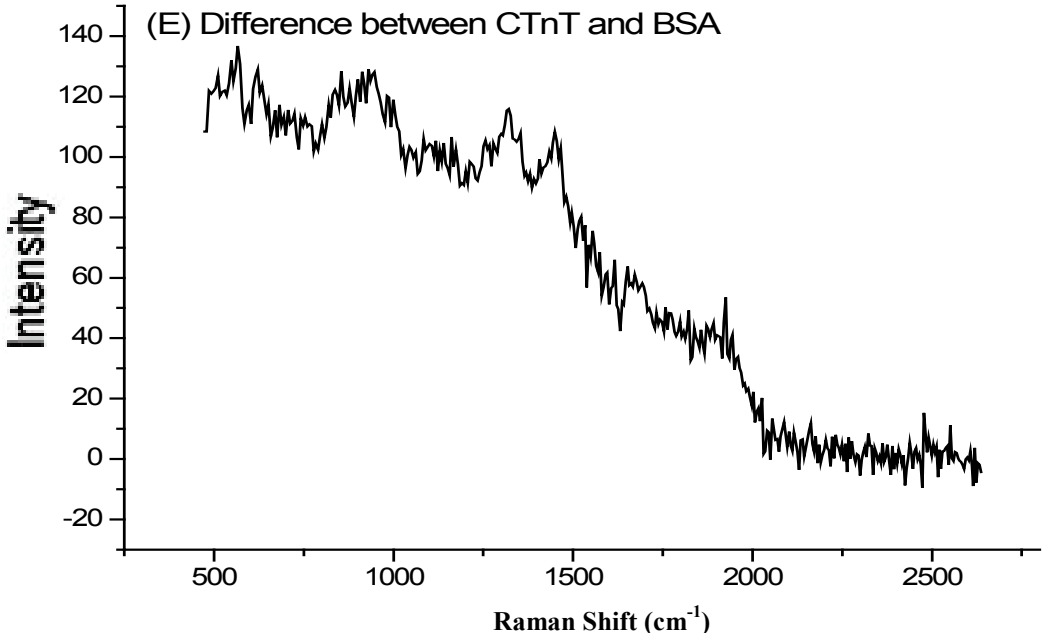

Figure 50: Difference Between cTnT and Buffer Raman Signal

9.2. Florescence Experiment Set Up

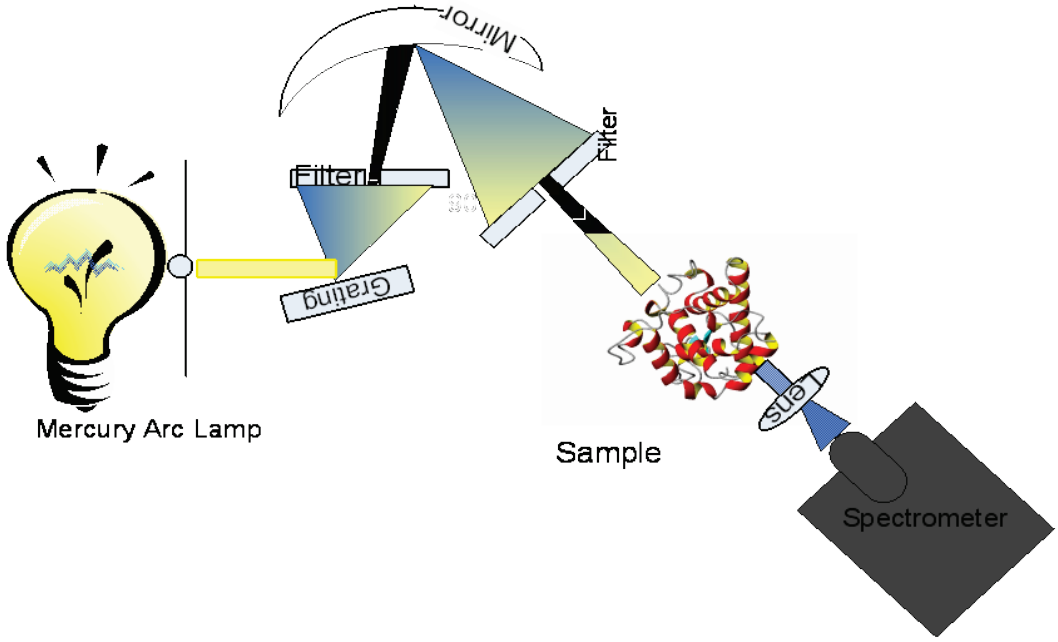

Figure 51: Optical Florescence Experimental Setup

Figure 52: Physical set up for florescence

Figure 53: Physical set up for absorption

9.3. Florescence Spectroscopy

"Using the result acquired from the PTI Quantamaster UV-Vis Spectrofluorometer of a complete scan through the cTnI sample, the excitation wavelength of the protein was acquired. As illustrated in Figure 54, the excitation wavelength of cTnI is 283 nm as expected from the existence of Tryptophan".[11]

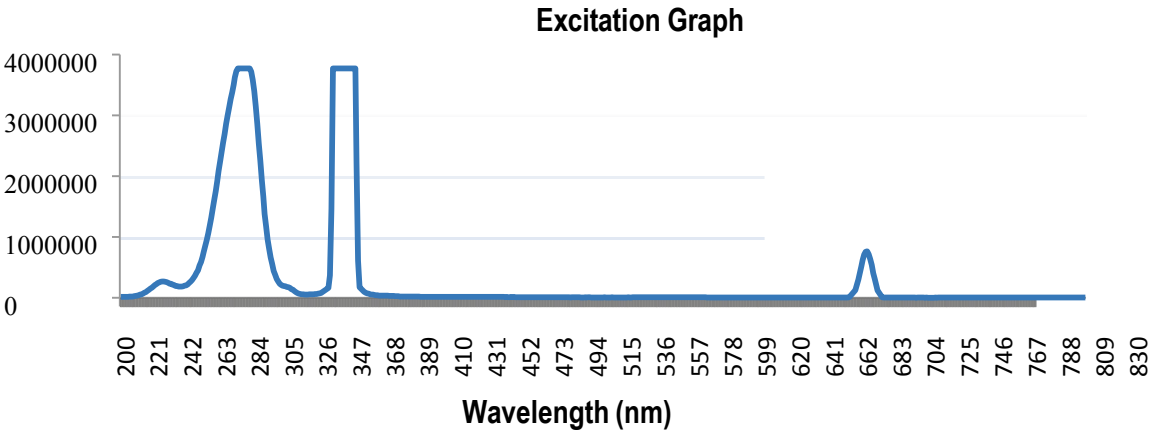

Figure 54: Scan through cTnI sample to find the excitation wavelength

"The data graph of the emission of cTnI sample when excited at 280nm is shown in Figure 55. The peaks at higher frequencies than expected are artifacts due to PTI Quantamaster Spectrofluorometer performance since they have also appeared when scanning the negative control (water). The emission wavelength for different concentrations of cTnI in water happens at 347 nm as expected. The device again causes the second peak, which appears at higher wavelength. Table 5 summarizes the peak values at various concentrations."[11]

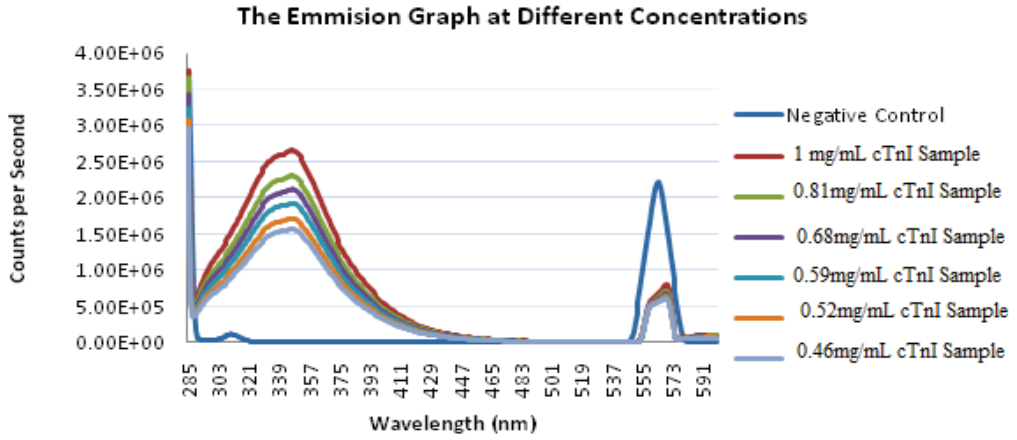

Figure 55: The emission wavelength at different concentrations when excited at 283nm

Table 5: The peak values at various concentrations of cTnI

Molarity (uM)	Peak Values
0	173657
18.96	2659630
21.44	2312060
24.73	2124130
28.03	1933120
33.39	1713940
41.22	1573370

The molecular weight of cTnI is 24,259 Da. Table 6 summarizes the molarity of cTnI calculated using the molecular weight versus the absolute peak amplitude of intensity (where peak value at zero concentration is subtracted from the rest of the intensities). These values are plotted in Figure 56.

Table 6: The delta peak values at various molarities of cTnI

Molarity(uM)	Delta Peak Amplitude(count/sec)
0	0
18.96	1399713
21.44	1540283
24.73	1759463
28.03	1950473
33.39	2138403
41.22	3485973

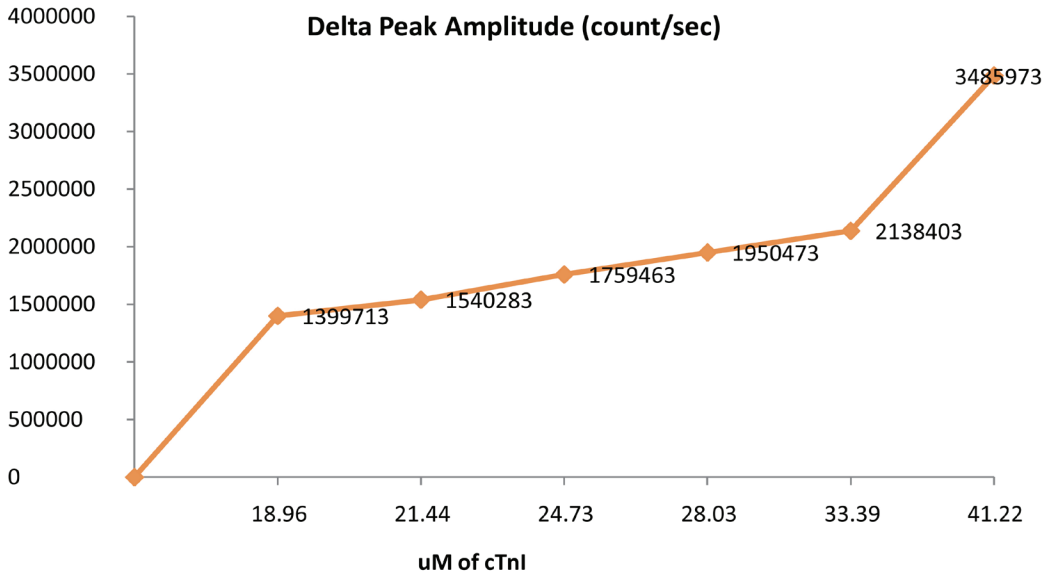

Figure 56: Absolute florescence intensity of various molarities of cTnI

In order to monitor the fluorescent behavior of the protein with an increase in concentration, a linear regression analysis was performed (Figure 57). From the regression analysis output, the slope of the line is 48252 counts/, the y-intercept is 529833.6 counts and the coefficient of determination (R^2) is 0.95. This gives an indication of the florescence characteristic of this protein with respect to increase in concentration within the experimental and human error.[11]

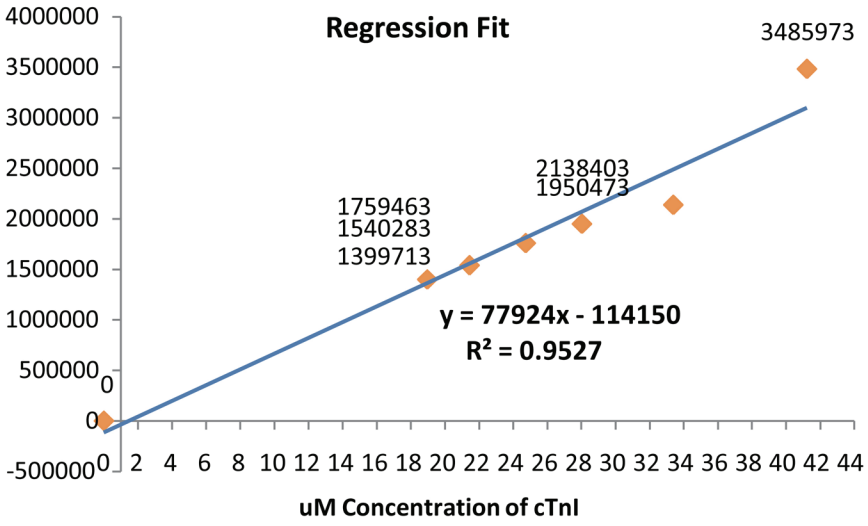

Figure 57: Linear Regression Graph

The data presented in Table 7 was obtained at various concentrations.

Table 7: Absorption data

Power (uW)	Concentration (uM)
1165	0.00
519	76.26
488	83.19
428	91.51
402	101.68
342	114.391
314	130.732
272	152.521
245	183.025
197	228.781

The absorption data is plotted in Figure 58. It can be seen that the power versus concentration graph has a logarithmic behavior. Therefore we can conclude

the absorption characteristic is in agreement with the Beer-Lambert law as expected, which is shown in the following equation.

$$A = -\log_{10}\left(\frac{I}{I_0}\right)$$

Where I_0 and I are the intensity (power) of the incident light and that after the material, respectively.

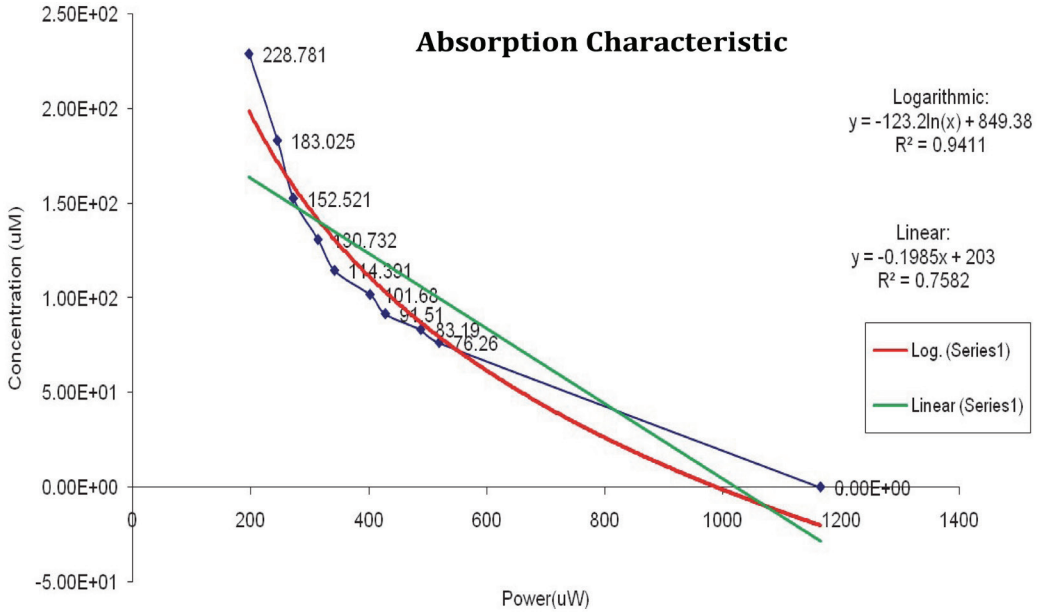

Figure 58: Absorption characteristic

9.4. cTnI Amino Acid Sequence

```
        10         20         30         40         50         60
MADESSDAAG EPQPAPAPVR RRSSANYRAY ATEPHAKKKS KISASRKLQL KTLMLQIAKQ

        70         80         90        100        110        120
EMEREAEERR GEKGRVLSTR CQPLVLDGLG FEELQDLCRQ LHARVDKVDE ERYDVEAKVT

       130        140        150        160        170        180
KNITEIADLT QKIYDLRGKF KRPTLRRVRI SADAMMQALL GTRAKESLDL RAHLKQVKKE

       190        200        210
DIEKENREVG DWRKNIDALS GMEGRKKKFE G
```

9.5. BSA Amino Acid Sequence

```
        10         20         30         40         50         60
MKWVTFISLL LLFSSAYSRG VFRRDTHKSE IAHRFKDLGE EHFKGLVLIA FSQYLQQCPF

        70         80         90        100        110        120
DEHVKLVNEL TEFAKTCVAD ESHAGCEKSL HTLFGDELCK VASLRETYGD MADCCEKQEP

       130        140        150        160        170        180
ERNECFLSHK DDSPDLPKLK PDPNTLCDEF KADEKKFWGK YLYEIARRHP YFYAPELLYY

       190        200        210        220        230        240
ANKYNGVFQE CCQAEDKGAC LLPKIETMRE KVLASSARQR LRCASIQKFG ERALKAWSVA

       250        260        270        280        290        300
RLSQKFPKAE FVEVTKLVTD LTKVHKECCH GDLLECADDR ADLAKYICDN QDTISSKLKE

       310        320        330        340        350        360
CCDKPLLEKS HCIAEVEKDA IPENLPPLTA DFAEDKDVCK NYQEAKDAFL GSFLYEYSRR

       370        380        390        400        410        420
HPEYAVSVLL RLAKEYEATL EECCAKDDPH ACYSTVFDKL KHLVDEPQNL IKQNCDQFEK

       430        440        450        460        470        480
LGEYGFQNAL IVRYTRKVPQ VSTPTLVEVS RSLGKVGTRC CTKPESERMP CTEDYLSLIL

       490        500        510        520        530        540
NRLCVLHEKT PVSEKVTKCC TESLVNRRPC FSALTPDETY VPKAFDEKLF TFHADICTLP

       550        560        570        580        590        600
DTEKQIKKQT ALVELLKHKP KATEEQLKTV MENFVAFVDK CCAADDKEAC FAVEGPKLVV
```

9.6. BSA Sample Information

Molecular weight	68.000 Da (583 amino acids; see Ref. 3 for amino acid sequence)	
pH	7.0 ± 0.2	
Analysis	Albumin (electrophoresis)	> 99%
	Protein	> 98%
	H_2O	< 5%
	Fatty acids (total)	< 0.2 mg/g
	Triglycerides (enzym.)	not detectable
	Immunoglobulins (Ouchterlony)	not detectable
	Sodium (flame photometry)	< 0.5%
	Potassium (flame photometry)	< 0.01%
	Calcium (AAS)	< 0.02%
	Magnesium (AAS)	< 0.01%
	Iron (AAS)	< 0.001%
	Copper (AAS)	< 0.002%
	P (inorganic)	< 0.001%
	Heavy metals (as Pb)	< 0.001%
	Albumin, fraction V, free from fatty acids, is manufactured using a modification of the methods of Saint-Blancard (4) and Chen (5).	
Stability	At 2-8° C the lyophilisate is stable until the expiry date specified on the label. In solution, albumin is stable for about 3 months at −15 to −25° C.	
Solubility	Solutions with a concentration of 50–100 mg/ml can be produced without problems. It is recommended to add a non-ionic detergent to avoid the formation of foam when preparing solutions (gentle stirring).	

9.7. Sample Codes

```
clear all

Spectrum1 = xlsread('CtNI5 3water BSA 15.xls');
Spectrum2 = xlsread('CtNI5 3water BSA 30.xls');

Spectrum3 = xlsread('CtNI5 3water 2BSA 15.xls');
Spectrum4 = xlsread('CtNI5 3water 2BSA 30.xls');

Spectrum5 = xlsread('CtNI5 3water3BSA 15.xls');
Spectrum6 = xlsread('CtNI5 3water3BSA 30.xls');
Spectrum7 = xlsread('CtNI5 3water3BSA 60.xls');

Spectrum8 = xlsread('ctni2 3x125 h2o then 1bsa 15.xls');
Spectrum9 = xlsread('ctni2 3x125 h2o then 1bsa 30.xls');
Spectrum10 = xlsread('ctni2 3x125 h2o then 1bsa 60.xls');

Spectrum11 = xlsread('ctni2 3x125 h2o 15.xls');
Spectrum12 = xlsread('ctni2 3x125 h2o 30.xls');
Spectrum13 = xlsread('ctni2 3x125 h2o 60.xls');

Spectrum14 = xlsread('BSA 15.xls');
Spectrum15 = xlsread('BSA 30.xls');
Spectrum16 = xlsread('BSA 60.xls');

Spectrum17 = xlsread('water.xls');

sample15=Spectrum5-Spectrum14;
sample30=Spectrum6-Spectrum15;
sample60=Spectrum7-Spectrum16;

x=xlsread('WN.xls');
xx=(x(:,1));

figure

%water, BSA, cTnI

plot(xx,smooth(Spectrum17,
8,'sgolay'),'r','LineWidth',1.25);
hold on
plot(xx,smooth(Spectrum15, 8,'sgolay'),'b:');
```

```
hold on
plot(xx,smooth(Spectrum2, 8,'sgolay'),'g');
xlabel('Wave Number (cm-1)','fontsize',14);
ylabel('Intensity','fontsize',14);
legend('Water','BSA [20 g/L]','cTnI(1) [17
g/L]','fontsize',14);
title('Raw samples of BSA [20 g/L] , cTnI(1) [17 g/L] and
Water','fontsize',14,'fontweight','b')
axis tight;
hold off

%Change in integration time of cTnI in water

figure

plot(xx,smooth(Spectrum11, 8,'sgolay'),'r');
hold on
plot(xx,smooth(Spectrum12, 8,'sgolay'),'b');
hold on
plot(xx,smooth(Spectrum13, 8,'sgolay'),'g');
xlabel('Wave Number (cm-1)','fontsize',14);
ylabel('Intensity','fontsize',14);
legend('15 sec','30 sec','60 sec');
title('Change in integration time of cTnI(2) [13 g/L]
','fontsize',14,'fontweight','b')
axis tight;
hold off

%Change in concentration time of cTnI in water and BSA

figure

plot(xx,smooth(Spectrum2, 8,'sgolay'),'r');
hold on
plot(xx,smooth(Spectrum4, 8,'sgolay'),'b');
hold on
plot(xx,smooth(Spectrum6, 8,'sgolay'),'g');
hold on
plot(xx,smooth(Spectrum9, 8,'sgolay'),'k');

xlabel('Wave Number (cm-1)','fontsize',14);
ylabel('Intensity','fontsize',14);
legend('cTnI(1) [14 g/L]/BSA [3.5 g/L]','cTnI(1) [12
```

```
g/L]/BSA [6 g/L]','cTnI(1) [10 g/L]/BSA [8 g/L]','cTnI(2)
[10 g/L]/BSA [5 g/L]');
title('Change in concentration of cTnI in water and BSA
sample (30 sec. integration
time)','fontsize',14,'fontweight','b')

axis tight;
hold off

%Subtracted water and BSA from cTnI spectra (CtNI5 3water
BSA)

figure

subplot(2,2,1)

plot(xx,smooth(4.*Spectrum1-Spectrum14, 8,'sgolay'),'r');
hold on
plot(xx,smooth(4.*Spectrum2-Spectrum15, 8,'sgolay'),'b');
hold on

xlabel('Wave Number (cm-1)');
ylabel('Intensity');
legend('cTnI(1) [14 g/L]/BSA [3.5 g/L] 15 sec.','cTnI(1)
[14 g/L]/BSA [3.5 g/L] 30 sec.');
title('Change in integration time for adjusted cTnI spectra
(cTnI(1) [14 g/L]/BSA [3.5 g/L])')

axis tight;
hold off

%Subtracted water and BSA from cTnI spectra (CtNI5 3water
2BSA)

subplot(2,2,2)

plot(xx,smooth(2.*Spectrum3-Spectrum14, 8,'sgolay'),'r');
hold on
plot(xx,smooth(2.*Spectrum4-Spectrum15, 8,'sgolay'),'b');
hold on


xlabel('Wave Number (cm-1)');
```

```
ylabel('Intensity');
legend('cTnI(1) [12 g/L]/BSA [6 g/L] 15 sec.','cTnI(1) [12
g/L]/BSA [6 g/L] 30 sec.');
title('Change in integration time for adjusted cTnI spectra
(cTnI(1) [12 g/L]/BSA [6 g/L])')

axis tight;
hold off

%Subtracted water and BSA from cTnI spectra (CtNI5 3water
3BSA)

subplot(2,2,3)

plot(xx,smooth(2.*Spectrum5-Spectrum14, 12,'sgolay'),'r');
hold on
plot(xx,smooth(2.*Spectrum6-Spectrum15, 12,'sgolay'),'b');
hold on
plot(xx,smooth(2.*Spectrum7-Spectrum16, 12,'sgolay'),'g');

xlabel('Wave Number (cm-1)');
ylabel('Intensity');
legend('cTnI(1) [10 g/L]/BSA [8 g/L] 15 sec.','cTnI(1) [10
g/L]/BSA [8 g/L] 30 sec.','cTnI(1) [10 g/L]/BSA [8 g/L] 60
sec.');
title('Change in integration time for adjusted cTnI spectra
(cTnI(1) [10 g/L]/BSA [8 g/L])')

axis tight;
hold off

%Subtracted water and BSA from cTnI spectra (ctni2 3x125
h2o then 1bsa)

subplot(2,2,4)

plot(xx,smooth(2.*Spectrum8-Spectrum14, 8,'sgolay'),'r');
hold on
plot(xx,smooth(2.*Spectrum9-Spectrum15, 8,'sgolay'),'b');
hold on
plot(xx,smooth(2.*Spectrum10-Spectrum16, 8,'sgolay'),'g');

xlabel('Wave Number (cm-1)');
```

```
ylabel('Intensity');
legend('cTnI(2) [10 g/L]/BSA [5 g/L] 15 sec.','cTnI(2) [10
g/L]/BSA [5 g/L] 30 sec','cTnI(2) [10 g/L]/BSA [5 g/L] 60
sec.');
title('Change in integration time for adjusted cTnI spectra
(cTnI(2) [10 g/L]/BSA [5 g/L])')

axis tight;
hold off

%all
figure
plot(xx,smooth(2.*Spectrum2-0.5.*Spectrum15,
8,'sgolay'),'r');
hold on
plot(xx,smooth(2.*Spectrum4-Spectrum15, 8,'sgolay'),'b');
hold on
plot(xx,smooth(2.*Spectrum6-Spectrum15, 8,'sgolay'),'g');
hold on
plot(xx,smooth(2.*Spectrum9-Spectrum15, 8,'sgolay'),'k');

hold on
plot(xx,smooth(Spectrum14, 8,'sgolay'),'c');


xlabel('Wave Number (cm-1)','fontsize',14);
ylabel('Intensity','fontsize',14);
legend('cTnI(1) [14 g/L]/BSA [3.5 g/L]','cTnI(1) [12
g/L]/BSA [6 g/L]','cTnI(1) [10 g/L]/BSA [8 g/L]','cTnI(2)
[10 g/L]/BSA [5 g/L]','BSA [20 g/L]');
title('Change in concentration for adjusted cTnI spectra
(30 sec. integration time)','fontsize',14,'fontweight','b')
axis tight;
hold off


%all
figure
plot(xx(649:860,1),smooth(2.*Spectrum2(649:860,1)-
0.5.*Spectrum15(649:860,1), 8,'sgolay'),'r');
hold on
plot(xx(649:860,1),smooth(2.*Spectrum4(649:860,1)-
Spectrum15(649:860,1), 8,'sgolay'),'b');
```

```
hold on
plot(xx(649:860,1),smooth(2.*Spectrum6(649:860,1)-
Spectrum15(649:860,1), 8,'sgolay'),'g');
hold on
plot(xx(649:860,1),smooth(2.*Spectrum9(649:860,1)-
Spectrum15(649:860,1), 8,'sgolay'),'k');

hold on
plot(xx(649:860,1),smooth(Spectrum15(649:860,1),
8,'sgolay'),'c');

xlabel('Wave Number (cm-1)','fontsize',14);
ylabel('Intensity','fontsize',14);
legend('cTnI(1) [14 g/L]/BSA [3.5 g/L]','cTnI(1) [12
g/L]/BSA [6 g/L]','cTnI(1) [10 g/L]/BSA [8 g/L]','cTnI(2)
[10 g/L]/BSA [5 g/L]','BSA [20 g/L]');
title('Change in concentration for adjusted cTnI spectra
(30 sec. integration time)','fontsize',14,'fontweight','b')
axis tight;
hold off

%
% figure
%
% subplot(3,1,1);
% plot(xx,smooth(sample15))
% legend('smoothed cTnI in BSA 15 sec integration time')
%
% subplot(3, 1, 2);
% plot(xx,smooth(sample30))
% legend('smoothed cTnI in BSA 30 sec integration time')
% subplot(3, 1, 3);
% plot(xx,smooth(sample60))
% legend('smoothed cTnI in BSA 60 sec integration time')
%
% hold off

%x=xlsread('x.xls');

% N=4;
% F=21;
% %xx=1;
% output=zeros(size(sample15));
```

```
%
%
% [b,g]=sgolay(N,F);
% [calrow,calcol]=size(sample15);
% %[xrow,xcol]=size(x);
% kk=1;
% % if nargin==3
% %     kinds=0;
% % end
%
% %output = nan(calrow,calcol);
%
% for n = (F+1)/2:calcol-(F+1)/2,
% % Zero-th order derivative (equivalent to sgolayfilt
except
% % that it doesn't compute transients)
%  %if kinds==0
%
%     output(:,kk)=(g(:,1)'*sample15(:,n - (F+1)/2 + 1: n +
(F+1)/2 - 1)')';
%  %end
%   kk=kk+1;
% end
% Sample= (Spectrum1(:,2) + Spectrum2(:,2) + Spectrum3(:,2)
+ Spectrum4(:,2))./4;
% Container= (Spectrum6(:,2) + Spectrum7(:,2) +
Spectrum8(:,2) )./3;
% Water= (Spectrum9(:,2) + Spectrum10(:,2) +
Spectrum11(:,2) + Spectrum12(:,2))./4;
% CtnI=Sample-Water;

%output=sgdiff(sample15,2,21,0);

% figure
 %plot ([sample15(1:length(output))', output']);
% plot (smooth(sample15));
% hold off
%
% plot (sample30);
% hold off
%
% plot (sample60);
```

```
%
% [scs,p] = csaps(x,sample15);
% fnplt(scs,3)
% hold on
% fnplt(csaps(x,sample15,p/2),1,'r--')
% set(gca,'Fontsize',12)
% fnplt(csaps(x,sample15,(1+p)/2),2,'b:')
% %plot(Spectrum1(:,1),CtnI,'y')
% legend('smoothing spline','more smoothed','less
smoothed',...
% 'noisy data')
% hold off

% figure
% [scs,p] = csaps(x,sample30);
% fnplt(scs,3)
% hold on
% fnplt(csaps(x,sample30,p/2),1,'r--')
% fnplt(csaps(Spectrum1(:,1),Water,p/2),1,'g--')
%
% set(gca,'Fontsize',12)
% %fnplt(csaps(Spectrum1(:,1),CtnI,(1+p)/2),2,'r:')
% %plot(Spectrum1(:,1),CtnI,'o')
% legend('smoothing spline Sample','more smoothed
Sample','more smoothed Water',...
% 'noisy data')
% hold off
% subplot(3,1,1);
% plot(smooth(sample15))
% legend('smoothed cTnI in BSA 15 sec integration time')
%
% subplot(3, 1, 2);
% plot(smooth(sample30))
% legend('smoothed cTnI in BSA 30 sec integration time')
% subplot(3, 1, 3);
% plot(smooth(sample60))
% legend('smoothed cTnI in BSA 60 sec integration time')
clear all

Spectrum1 = xlsread('ctni5 3water BSA 15.xls');
Spectrum2 = xlsread('ctni5 3water BSA 30.xls');

Spectrum3 = xlsread('ctni5 3water 2BSA 15.xls');
```

```
Spectrum4 = xlsread('ctni5 3water 2BSA 30.xls');

Spectrum5 = xlsread('ctni5 3water3BSA 15.xls');
Spectrum6 = xlsread('ctni5 3water3BSA 30.xls');
Spectrum7 = xlsread('ctni5 3water3BSA 60.xls');

Spectrum8 = xlsread('ctni2 3x125 h2o then1bsa 15.xls');
Spectrum9 = xlsread('ctni2 3x125 h2o then1bsa 30.xls');
Spectrum10 = xlsread('ctni2 3x125 h2o then1bsa 60.xls');

Spectrum11 = xlsread('ctni2 3x125 h2o 15.xls');
Spectrum12 = xlsread('ctni2 3x125 h2o 30.xls');
Spectrum13 = xlsread('ctni2 3x125 h2o 60.xls');

Spectrum14 = xlsread('BSA 15.xls');
Spectrum15 = xlsread('BSA 30.xls');
Spectrum16 = xlsread('BSA 60.xls');

Spectrum17 = xlsread('water.xls');

% ctni5 3water3BSA
sample15=Spectrum5-Spectrum14;
sample30=Spectrum6-Spectrum15;
sample60=Spectrum7-Spectrum16;

% ctni2 3x125 h2o then1bsa

sample_2_15=Spectrum8-Spectrum14;
sample_2_30=Spectrum9-Spectrum15;
sample_2_60=Spectrum10-Spectrum16;

%ctni5 3water BSA

sample_4_15=Spectrum1-Spectrum17;
sample_4_30=Spectrum2-Spectrum17;

%ctni2 3x125 h2o

sample_3_15=Spectrum11-Spectrum17;
sample_3_30=Spectrum12-Spectrum17;
sample_3_60=Spectrum13-Spectrum17;
```

```
x=xlsread('WN.xls');
xx=(x(:,1));

%water, BSA, cTnI

plot(xx,smooth(Spectrum17,
8,'sgolay'),'r','LineWidth',1.25);
hold on
plot(xx,smooth(Spectrum15, 8,'sgolay'),'b:');
hold on
plot(xx,smooth(Spectrum2, 8,'sgolay'),'g');
xlabel('Wave Number (cm-1)','fontsize',14);
ylabel('Intensity','fontsize',14);
legend('Water','BSA [20 g/L]','cTnI(1) [17
g/L]','fontsize',14);
title('Raw samples of BSA [20 g/L] , cTnI(1) [17 g/L] and
Water','fontsize',14,'fontweight','b')
axis tight;
hold off

%Change in integration time of cTnI in water

figure

plot(xx,smooth(Spectrum11, 8,'sgolay'),'r');
hold on
plot(xx,smooth(Spectrum12, 8,'sgolay'),'b');
hold on
plot(xx,smooth(Spectrum13, 8,'sgolay'),'g');
xlabel('Wave Number (cm-1)','fontsize',14);
ylabel('Intensity','fontsize',14);
legend('15 sec','30 sec','60 sec');
title('Change in integration time of cTnI(2) [13 g/L]
','fontsize',14,'fontweight','b')
axis tight;
hold off

%Change in concentration time of cTnI in water and BSA

figure

plot(xx,smooth(Spectrum2, 8,'sgolay'),'r');
hold on
```

```
plot(xx,smooth(Spectrum4, 8,'sgolay'),'b');
hold on
plot(xx,smooth(Spectrum6, 8,'sgolay'),'g');
hold on
plot(xx,smooth(Spectrum9, 8,'sgolay'),'k');

xlabel('Wave Number (cm-1)','fontsize',14);
ylabel('Intensity','fontsize',14);
legend('cTnI(1) [14 g/L]/BSA [3.5 g/L]','cTnI(1) [12
g/L]/BSA [6 g/L]','cTnI(1) [10 g/L]/BSA [8 g/L]','cTnI(2)
[10 g/L]/BSA [5 g/L]');
title('Change in concentration of cTnI in water and BSA
sample (30 sec. integration
time)','fontsize',14,'fontweight','b')

axis tight;
hold off

%Subtracted water and BSA from cTnI spectra (CtNI5 3water
BSA)

figure

subplot(2,2,1)

plot(xx,smooth(4.*Spectrum1-Spectrum14, 8,'sgolay'),'r');
hold on
plot(xx,smooth(4.*Spectrum2-Spectrum15, 8,'sgolay'),'b');
hold on

xlabel('Wave Number (cm-1)');
ylabel('Intensity');
legend('cTnI(1) [14 g/L]/BSA [3.5 g/L] 15 sec.','cTnI(1)
[14 g/L]/BSA [3.5 g/L] 30 sec.');
title('Change in integration time for adjusted cTnI spectra
(cTnI(1) [14 g/L]/BSA [3.5 g/L])')

axis tight;
hold off

%Subtracted water and BSA from cTnI spectra (CtNI5 3water
2BSA)
```

```
subplot(2,2,2)

plot(xx,smooth(2.*Spectrum3-Spectrum14, 8,'sgolay'),'r');
hold on
plot(xx,smooth(2.*Spectrum4-Spectrum15, 8,'sgolay'),'b');
hold on


xlabel('Wave Number (cm-1)');
ylabel('Intensity');
legend('cTnI(1) [12 g/L]/BSA [6 g/L] 15 sec.','cTnI(1) [12
g/L]/BSA [6 g/L] 30 sec.');
title('Change in integration time for adjusted cTnI spectra
(cTnI(1) [12 g/L]/BSA [6 g/L])')

axis tight;
hold off

%Subtracted water and BSA from cTnI spectra (CtNI5 3water
3BSA)

subplot(2,2,3)

plot(xx,smooth(2.*Spectrum5-Spectrum14, 12,'sgolay'),'r');
hold on
plot(xx,smooth(2.*Spectrum6-Spectrum15, 12,'sgolay'),'b');
hold on
plot(xx,smooth(2.*Spectrum7-Spectrum16, 12,'sgolay'),'g');

xlabel('Wave Number (cm-1)');
ylabel('Intensity');
legend('cTnI(1) [10 g/L]/BSA [8 g/L] 15 sec.','cTnI(1) [10
g/L]/BSA [8 g/L] 30 sec.','cTnI(1) [10 g/L]/BSA [8 g/L] 60
sec.');
title('Change in integration time for adjusted cTnI spectra
(cTnI(1) [10 g/L]/BSA [8 g/L])')

axis tight;
hold off

%Subtracted water and BSA from cTnI spectra (ctni2 3x125
h2o then 1bsa)
```

```
subplot(2,2,4)

plot(xx,smooth(2.*Spectrum8-Spectrum14, 8,'sgolay'),'r');
hold on
plot(xx,smooth(2.*Spectrum9-Spectrum15, 8,'sgolay'),'b');
hold on
plot(xx,smooth(2.*Spectrum10-Spectrum16, 8,'sgolay'),'g');

xlabel('Wave Number (cm-1)');
ylabel('Intensity');
legend('cTnI(2) [10 g/L]/BSA [5 g/L] 15 sec.','cTnI(2) [10
g/L]/BSA [5 g/L] 30 sec','cTnI(2) [10 g/L]/BSA [5 g/L] 60
sec.');
title('Change in integration time for adjusted cTnI spectra
(cTnI(2) [10 g/L]/BSA [5 g/L])')

axis tight;
hold off

%all
figure
plot(xx,smooth(2.*Spectrum2-0.5.*Spectrum15,
8,'sgolay'),'r');
hold on
plot(xx,smooth(2.*Spectrum4-Spectrum15, 8,'sgolay'),'c');
hold on
plot(xx,smooth(2.*Spectrum6-Spectrum15, 8,'sgolay'),'g');
hold on
plot(xx,smooth(2.*Spectrum9-Spectrum15, 8,'sgolay'),'k');

hold on
plot(xx,smooth(Spectrum14, 8,'sgolay'),'b--
','LineWidth',1.25);

xlabel('Wave Number (cm-1)','fontsize',14);
ylabel('Intensity','fontsize',14);
legend('cTnI(1) [14 g/L]/BSA [3.5 g/L]','cTnI(1) [12
g/L]/BSA [6 g/L]','cTnI(1) [10 g/L]/BSA [8 g/L]','cTnI(2)
[10 g/L]/BSA [5 g/L]','BSA [20 g/L]');
title('Change in concentration for adjusted cTnI spectra
(30 sec. integration time)','fontsize',14,'fontweight','b')
axis tight;
hold off
```

```
%all
figure
plot(xx(649:860,1),smooth(2.*Spectrum2(649:860,1)-
0.5.*Spectrum15(649:860,1), 8,'sgolay'),'r');
hold on
plot(xx(649:860,1),smooth(2.*Spectrum4(649:860,1)-
Spectrum15(649:860,1), 8,'sgolay'),'c');
hold on
plot(xx(649:860,1),smooth(2.*Spectrum6(649:860,1)-
Spectrum15(649:860,1), 8,'sgolay'),'g');
hold on
plot(xx(649:860,1),smooth(2.*Spectrum9(649:860,1)-
Spectrum15(649:860,1), 8,'sgolay'),'k');

hold on
plot(xx(649:860,1),smooth(Spectrum15(649:860,1),
8,'sgolay'),'b--','LineWidth',1.25);

xlabel('Wave Number (cm-1)','fontsize',14);
ylabel('Intensity','fontsize',14);
legend('cTnI(1) [14 g/L]/BSA [3.5 g/L]','cTnI(1) [12
g/L]/BSA [6 g/L]','cTnI(1) [10 g/L]/BSA [8 g/L]','cTnI(2)
[10 g/L]/BSA [5 g/L]','BSA [20 g/L]');
title('Change in concentration for adjusted cTnI spectra
(30 sec. integration time)','fontsize',14,'fontweight','b')
axis tight;
hold off

% figure
%
% subplot(3,1,1);
% plot(xx,smooth(sample15))
% legend('smoothed cTnI in BSA 15 sec integration time')
%
% subplot(3, 1, 2);
% plot(xx,smooth(sample30))
% legend('smoothed cTnI in BSA 30 sec integration time')
% subplot(3, 1, 3);
% plot(xx,smooth(sample60))
% legend('smoothed cTnI in BSA 60 sec integration time')
%
% hold off
```

```
% N=4;
% F=21;
% %xx=1;
% output=zeros(size(sample15));
%
%
% [b,g]=sgolay(N,F);
% [calrow,calcol]=size(sample15);
% %[xrow,xcol]=size(x);
% kk=1;
% % if nargin==3
% %     kinds=0;
% % end
%
% %output = nan(calrow,calcol);
%
% for n = (F+1)/2:calcol-(F+1)/2,
% % Zero-th order derivative (equivalent to sgolayfilt
except
% % that it doesn't compute transients)
%  %if kinds==0
%
%     output(:,kk)=(g(:,1)'*sample15(:,n - (F+1)/2 + 1: n +
(F+1)/2 - 1)')';
%  %end
%   kk=kk+1;
% end
% Sample= (Spectrum1(:,2) + Spectrum2(:,2) + Spectrum3(:,2)
+ Spectrum4(:,2))./4;
% Container= (Spectrum6(:,2) + Spectrum7(:,2) +
Spectrum8(:,2) )./3;
% Water= (Spectrum9(:,2) + Spectrum10(:,2) +
Spectrum11(:,2) + Spectrum12(:,2))./4;
% CtnI=Sample-Water;

%output=sgdiff(sample15,2,21,0);


 %plot ([sample15(1:length(output))', output']);
% plot (smooth(sample15));
% hold off
%
```

```
% plot (sample30);
% hold off
%
% plot (sample60);

%
% [scs,p] = csaps(x,sample15);
% fnplt(scs,3)
% hold on
% fnplt(csaps(x,sample15,p/2),1,'r--')
% set(gca,'Fontsize',12)
% fnplt(csaps(x,sample15,(1+p)/2),2,'b:')
% %plot(Spectrum1(:,1),CtnI,'y')
% legend('smoothing spline','more smoothed','less
smoothed',...
% 'noisy data')
% hold off

% figure
% [scs,p] = csaps(x,sample30);
% fnplt(scs,3)
% hold on
% fnplt(csaps(x,sample30,p/2),1,'r--')
% fnplt(csaps(Spectrum1(:,1),Water,p/2),1,'g--')
%
% set(gca,'Fontsize',12)
% %fnplt(csaps(Spectrum1(:,1),CtnI,(1+p)/2),2,'r:')
% %plot(Spectrum1(:,1),CtnI,'o')
% legend('smoothing spline Sample','more smoothed
Sample','more smoothed Water',...
% 'noisy data')
% hold off




clear all

Spectrum1 = xlsread('2thirdsample3.xls');
Spectrum2 = xlsread('2thirdsample4.xls');
Spectrum3 = xlsread('2thirdsample9.xls');
Spectrum4 = xlsread('2thirdsample10.xls');
```

```
Spectrum5 = xlsread('halfSample3.xls');
Spectrum6 = xlsread('halfSample4.xls');
Spectrum7 = xlsread('halfSample9.xls');
Spectrum8 = xlsread('halfSample10.xls');

Spectrum13 = xlsread('1thirdsample3.xls');
Spectrum14 = xlsread('1thirdsample4.xls');
Spectrum15 = xlsread('1thirdsample9.xls');
Spectrum16 = xlsread('1thirdsample10.xls');

Spectrum17 = xlsread('20mgpermL3.xls');
Spectrum18 = xlsread('20mgpermL4.xls');
Spectrum19 = xlsread('20mgpermL9.xls');
Spectrum20 = xlsread('20mgpermL10.xls');


Spectrum9 = xlsread('water3.xls');
Spectrum10 = xlsread('water4.xls');
Spectrum11 = xlsread('water9.xls');
Spectrum12 = xlsread('water10.xls');

Sample1= (Spectrum17(1:446,2) + Spectrum18(1:446,2) +
Spectrum19(1:446,2) + Spectrum20(1:446,2))./4;

Sample2= (Spectrum1(1:446,2) + Spectrum2(1:446,2) +
Spectrum3(1:446,2) + Spectrum4(1:446,2))./4;

Sample3= (Spectrum5(1:446,2) + Spectrum6(1:446,2) +
Spectrum7(1:446,2) + Spectrum8(1:446,2))./4;

Sample4= (Spectrum13(1:446,2) + Spectrum14(1:446,2) +
Spectrum15(1:446,2) + Spectrum16(1:446,2))./4;



Water= (Spectrum9(1:446,2) + Spectrum10(1:446,2) +
Spectrum11(1:446,2) + Spectrum12(1:446,2))./4;

CtnI1=Sample1-Water;
CtnI2=Sample2-Water;
CtnI3=Sample3-Water;
CtnI4=Sample4-Water;
```

```
x=xlsread('xx.xls');
xx=(x(:,1));

figure

% plot(xx,smooth(CtnI1, 8,'sgolay'),'r');
% hold on
plot(xx,smooth(CtnI2, 8,'sgolay'),'b');
hold on
plot(xx,smooth(CtnI3, 8,'sgolay'),'r');
% hold on
% plot(xx,smooth(CtnI4, 8,'sgolay'),'c');

xlabel('Wave Number (cm-1)','fontsize',14);
ylabel('Intensity','fontsize',14);
legend('cTnI [10mg/mL]','cTnI [6mg/mL]');
title('Change in concentration of
cTnI','fontsize',14,'fontweight','b')

axis tight;
hold off

figure

plot(xx(215:287,1), smooth(CtnI4(215:287,1),
6,'sgolay'),'r:','LineWidth',1.5);

xlabel('Wave Number (cm-1)','fontsize',14);
ylabel('Intensity','fontsize',14);
legend('cTnI "sgolay" smoothing 6','fontsize',14);
title('Adjusted cTnI
signiture','fontsize',14,'fontweight','b')
axis tight;
hold off

% figure
%
% plot(xx,smooth(Spectrum17(1:446,2), 8,'sgolay'),'r');
% hold on
% plot(xx,smooth(Spectrum1(1:446,2), 8,'sgolay'),'b');
% hold on
% plot(xx,smooth(Spectrum5(1:446,2), 8,'sgolay'),'k');
```

```
% hold on
% plot(xx,smooth(Spectrum13(1:446,2), 8,'sgolay'),'c');
%
% xlabel('Wave Number (cm-1)','fontsize',14);
% ylabel('Intensity','fontsize',14);
% legend('cTnI1','cTnI2','cTnI3','cTnI4');
% title('Change in concentration of cTnI in water and BSA
sample (30 sec. integration
time)','fontsize',14,'fontweight','b')
%
% axis tight;
% hold off


clear all
close all

Spectrum1 = xlsread('20mgpermLsample3.xls');
Spectrum2 = xlsread('20mgpermLsample4.xls');
Spectrum3 = xlsread('20mgpermLsample9.xls');
Spectrum4 = xlsread('20mgpermLsample10.xls');

%Spectrum5 = xlsread('nothing3.xls');
% Spectrum6 = xlsread('nothing4.xls');
% Spectrum7 = xlsread('nothing9.xls');
% Spectrum8 = xlsread('nothing10.xls');
%
Spectrum9 = xlsread('water3.xls');
Spectrum10 = xlsread('water4.xls');
Spectrum11 = xlsread('water9.xls');
Spectrum12 = xlsread('water10.xls');

Sample= (Spectrum1(1:446,2) + Spectrum2(1:446,2) +
Spectrum3(1:446,2) + Spectrum4(1:446,2))./4;

% Container= (Spectrum6(:,2) + Spectrum7(:,2) +
Spectrum8(:,2) )./3;

Water= (Spectrum9(1:446,2) + Spectrum10(1:446,2) +
Spectrum11(1:446,2) + Spectrum12(1:446,2))./4;

CtnI=Sample-Water;
```

```
x=xlsread('xx.xls');
xx=(x(:,1));

%water, BSA, cTnI

plot(xx,smooth(Sample, 8,'sgolay'),'r');
hold on
plot(xx,smooth(Water, 8,'sgolay'),'b:','LineWidth',1.5);
xlabel('Wave Number (cm-1)','fontsize',14);
ylabel('Intensity','fontsize',14);
legend('cTnI Sample','Water','fontsize',14);
title('cTnI and Watwer 2 Sec Integration
time','fontsize',14,'fontweight','b')
axis tight;
hold off

figure


plot(xx,smooth(CtnI, 4,'sgolay'),'k');
hold on
plot(xx, smooth(CtnI, 6,'sgolay'),'r');
hold on
plot(xx,smooth(CtnI, 8,'sgolay'),'b');
hold on
plot(xx,smooth(CtnI, 10,'sgolay'),'g');



xlabel('Wave Number (cm-1)','fontsize',14);
ylabel('Intensity','fontsize',14);
legend('cTnI "sgolay" smoothing 4','cTnI "sgolay" smoothing
6','cTnI "sgolay" smoothing 8','cTnI "sgolay" smoothing
10','fontsize',14);
title('Adjusted cTnI, 2 Sec integration time, change in
smoothing','fontsize',14,'fontweight','b')
axis tight;
hold off

figure
plot(xx(215:287,1),smooth(CtnI(215:287,1),
4,'sgolay'),'k');
hold on
```

```
plot(xx(215:287,1), smooth(CtnI(215:287,1),
6,'sgolay'),'r');
hold on
plot(xx(215:287,1),smooth(CtnI(215:287,1),
8,'sgolay'),'b');
hold on
plot(xx(215:287,1),smooth(CtnI(215:287,1),
10,'sgolay'),'g');

xlabel('Wave Number (cm-1)','fontsize',14);
ylabel('Intensity','fontsize',14);
legend('cTnI "sgolay" smoothing 4','cTnI "sgolay" smoothing
6','cTnI "sgolay" smoothing 8','cTnI "sgolay" smoothing
10','fontsize',14);
title('Adjusted cTnI, 2 Sec integration time, change in
smoothing','fontsize',14,'fontweight','b')
axis tight;
hold off

figure

plot(xx(215:287,1), smooth(CtnI(215:287,1),
6,'sgolay'),'b:','LineWidth',1.5);

xlabel('Wave Number (cm-1)','fontsize',14);
ylabel('Intensity','fontsize',14);
legend('cTnI "sgolay" smoothing 6','fontsize',14);
title('Adjusted cTnI
signiture','fontsize',14,'fontweight','b')
axis tight;
hold off

% figure
%
% plot(xx,smooth(CtnI, 6,'sgolay'),'g');
% xlabel('Wave Number (cm-1)','fontsize',14);
% ylabel('Intensity','fontsize',14);
% legend('cTnI Subtracted','fontsize',14);
% title('2 Sec Integration
time','fontsize',14,'fontweight','b')
% axis tight;
% hold off
```